



**A University of Sussex PhD thesis**

Available online via Sussex Research Online:

<http://sro.sussex.ac.uk/>

This thesis is protected by copyright which belongs to the author.

This thesis cannot be reproduced or quoted extensively from without first obtaining permission in writing from the Author

The content must not be changed in any way or sold commercially in any format or medium without the formal permission of the Author

When referring to this work, full bibliographic details including the author, title, awarding institution and date of the thesis must be given

Please visit Sussex Research Online for more information and further details

# Strongly Coupled Physics Beyond the Standard Model

Jack Setford

Submitted for the degree of Doctor of Philosophy  
University of Sussex  
March 2018

# Declaration

I hereby declare that this thesis has not been and will not be submitted in whole or in part to another University for the award of any other degree.

The work in this thesis was completed in collaboration with Veronica Sanz, Djuna Croon, Michele Papucci, Simon Knapen, and Hou Keong Lou, and is comprised of the following published papers:

- Veronica Sanz and Jack Setford, ‘Composite Higgs after Run 2’ [1], published in *Advances in High Energy Physics*, vol. 2018. The calculations and analysis were performed by myself, while the plots and fits were produced by Veronica Sanz.
- Djuna Croon, Veronica Sanz and Jack Setford, ‘Goldstone Inflation’ [2], published in *JHEP* 10 (2015) 020. The cosmological arguments and calculations were the work of Djuna Croon, while I performed the calculations relating to the inflaton potential.
- Veronica Sanz and Jack Setford, ‘Composite Higgses with seesaw EWSB’ [3], published in *JHEP* 12 (2015) 154. Original concept for the model presented in this paper was mine. Veronica Sanz produced the plots and oversaw the direction of the work.
- Simon Knapen, Hou Keong Lou, Michele Papucci and Jack Setford, ‘Tracking down Quirks at the Large Hadron Collider’ [4], published in *Phys. Rev. D* 96 (2017) no. 11, 115015. My role in this paper was to simulate the quirk trajectories and understand their dynamics.
- Jack Setford, ‘Composite Higgs models in disguise’ [5], published in *JHEP* 01 (2018) 092. All the work in this paper was my own.

Signature:

Jack Setford

UNIVERSITY OF SUSSEX

JACK SETFORD, DOCTOR OF PHILOSOPHY

STRONGLY COUPLED PHYSICS BEYOND THE STANDARD MODELSUMMARY

This thesis is concerned with strongly coupled extensions to the Standard Model. The majority of the thesis is dedicated to the study of Composite Higgs models, which are a proposed solution to the hierarchy problem of the electroweak scale. In these models the Higgs is a composite pseudo-Nambu Goldstone boson which forms a part of a new strongly interacting sector. There are many different variations on the basic Composite Higgs theme – the current status of some of these variations is assessed in light of results from the Large Hadron Collider. A new kind of Composite Higgs model is presented and studied, which features an alternative mechanism for the breaking of electroweak symmetry. A mechanism for deforming one model into another is also discussed, which might find application to the UV completion of Composite Higgs models.

The formalism used in the Composite Higgs literature is also applied to the study of inflation, where the inflaton is assumed to be a pseudo-Nambu Goldstone boson arising from strongly coupled dynamics. A study of the inflaton potential is performed and its cosmological implications discussed.

A different extension to the Standard Model with interesting phenomenological consequences is also studied. Quirks are strongly interacting particles whose masses are significantly higher than their confining scale. If produced in colliders, they leave unusual tracks which current searches are mostly blind to. A new search strategy for these hypothetical particles is proposed.

# Acknowledgements

PhDs are hard, and this one would have been impossible without the support of my friends and family.

My officemates, past and present: Niall, Wissarut, Tom St, Sonali, Chris F, Djuna, Alba, Luke, for helping and distracting me in equal measures. Anyone who has had the (mis)fortune of sharing a house with me during my PhD, in particular Matt R, Jack L, Dan H, Chris I, Orla, Tom T. And all the rest of my friends, especially the Decoders: Dan H, Dan M, Matt C and Tom Sh, in collaboration with whom I created and destroyed several universes. *Keust ei mecht!*

I would also like to thank the theoretical particle physics group at UC Berkeley / LBNL, in particular Simon Knapen and Michele Papucci, for making me very welcome during an enjoyable and productive four months spent there.

Veronica – a great physicist, fantastic supervisor and wonderful person.

Dan H, because he's already had two mentions and deserves another.

My family, who have never failed to support and encourage me, and who made all of this possible.

And Mia, who made it all worthwhile.

# Contents

<b>List of Tables</b>	<b>viii</b>
<b>List of Figures</b>	<b>x</b>
<b>1 Introduction</b>	<b>1</b>
1.1 Problems and solutions . . . . .	1
1.2 The hierarchy problem . . . . .	2
1.3 Solutions to the hierarchy problem . . . . .	4
1.4 Composite Higgs models . . . . .	5
1.4.1 The pNGB Higgs . . . . .	6
1.4.2 Couplings of the Higgs . . . . .	8
1.4.3 The Higgs potential . . . . .	11
1.4.4 Top partners . . . . .	12
1.4.5 UV completions? . . . . .	12
1.5 Outline of this thesis . . . . .	14
<b>2 Composite Higgs models after Run 2</b>	<b>16</b>
2.1 Introduction . . . . .	17
2.2 The non-linear Composite Higgs . . . . .	17
2.2.1 Gauge couplings . . . . .	18
2.2.2 Fermion couplings . . . . .	20
2.3 Tree-level effects . . . . .	22
2.4 Status after Run 2 . . . . .	25
2.5 Conclusions . . . . .	27
<b>3 Goldstone Inflation</b>	<b>29</b>
3.1 Introduction . . . . .	30
3.2 A successful Coleman-Weinberg potential . . . . .	32

3.3	Constraints from Inflation . . . . .	40
3.3.1	Fine-tuning . . . . .	43
3.3.2	Non-Gaussianity and its relation to Goldstone scattering . . . . .	44
3.4	Link to UV models . . . . .	47
3.5	Light resonance connection . . . . .	48
3.6	Discussion and conclusions . . . . .	51
<b>4</b>	<b>Composite Higgses with seesaw EWSB</b>	<b>57</b>
4.1	Intoduction . . . . .	58
4.2	Seesaw symmetry breaking . . . . .	59
4.3	$SO(6 \rightarrow 5 \rightarrow 4)$ . . . . .	61
4.4	Gauge couplings . . . . .	65
4.5	Quark masses and top partners . . . . .	66
4.6	Discussion and conclusions . . . . .	70
<b>5</b>	<b>Tracking down quirks at the Large Hadron Collider</b>	<b>74</b>
5.1	Introduction . . . . .	75
5.2	Quirk Dynamics . . . . .	76
5.3	Search strategy . . . . .	81
5.3.1	Signal simulation . . . . .	81
5.3.2	Trigger . . . . .	82
5.3.3	Plane finding Algorithm . . . . .	83
5.3.4	Backgrounds . . . . .	86
5.4	Results . . . . .	87
<b>6</b>	<b>Composite Higgs models in disguise</b>	<b>92</b>
6.1	Introduction . . . . .	93
6.2	Mechanism . . . . .	94
6.3	Two examples . . . . .	96
6.3.1	$SU(4)/Sp(4)$ . . . . .	97
6.3.2	$SU(5)/SO(5)$ . . . . .	99
6.4	Deforming with $t_R$ . . . . .	100
6.5	Conclusion . . . . .	102
<b>7</b>	<b>Conclusions</b>	<b>104</b>
7.1	Summary . . . . .	104

7.2	Directions for further study . . . . .	105
	<b>Bibliography</b>	<b>106</b>



# List of Tables

2.1	$\kappa_F$ in different models. . . . .	21
2.2	List of 13 TeV channels considered in the fit, with the corresponding $\kappa$ modifiers . . . . .	25
3.1	Trigonometric inflationary potentials, grouped by equivalence upon a rotation in parameter space . . . . .	41
3.2	Scaling of the form factors derived from an operator product expansion and symmetry restoration at high energies . . . . .	49
5.1	Breakdown of the signal efficiencies for two benchmarks, one for Drell-Yan production, and one for colored production . . . . .	89

# List of Figures

2.1	$\chi(f)^2 - \chi_{min}^2$ for the Run 1 and combination of Run 1 and 2 datasets . . .	24
2.2	$\chi(\xi)^2$ assuming a scenario where a deficit is found in $ttH$ production channels	27
3.1	Subgroups of a global $SO(N)$ symmetry . . . . .	35
3.2	Shape of the Goldstone inflaton potential . . . . .	42
3.3	Predictions for $n_s$ and $r$ plotted against Planck 2015 data . . . . .	43
3.4	Amount of tuning in the model . . . . .	44
3.5	Predictions for the speed of sound . . . . .	46
3.6	Goldstone quartic interactions . . . . .	55
4.1	Plots of the light Higgs potential for different combinations of model parameters . . . . .	65
4.2	$\kappa_V$ plotted against $\xi$ for different values of $\varepsilon$ . . . . .	67
5.1	Schematic event display of a pair of quirks with an ISR jet . . . . .	77
5.2	Angular momentum and the relative distance between the quirks, as a function of the radial distance of the center of mass to the interaction point for a representative event . . . . .	79
5.3	$\Delta\phi$ as a function of the radial distance of the center of mass to the origin for two representative benchmark events . . . . .	80
5.4	Hits for a sample signal event, projected onto the reconstructed plane . . .	84
5.5	Signal and background distributions for thickness and width of the strip . .	87
5.6	Contours of having 3 (5) events in the $m_Q$ vs $\Lambda$ plane for an integrated luminosity of $\int L dt = 300 \text{ fb}^{-1}$ , overlaid with (projected) HSCP and monojet limits . . . . .	90
5.7	Differential distribution of $dE/dx$ and $\beta\gamma$ for two signal benchmark points in our simulation of the ATLAS pixel detector . . . . .	91

6.1	Symmetry breaking patterns in the disguised $SU(4)/Sp(4)$ model . . . . .	97
-----	---	----

# Chapter 1

## Introduction

### 1.1 Problems and solutions

The Standard Model of particle physics is arguably the most successful scientific theory ever formulated – it is however, far from being a theory of everything. There are several problems with the Standard Model which still lack a satisfactory solution:

- It does not explain what dark matter is;
- It does not explain how there came to be a matter/anti-matter asymmetry in the universe;
- It does not explain how neutrinos acquire masses;
- It does not explain the mechanism behind cosmological inflation;
- It does not explain how gravity works at high energies;
- It does not explain why there is such a large hierarchy between the electroweak scale and the scale of gravity.

The last item on the list is known as the *hierarchy problem*. One might argue that it is different from the other problems in that it does not need an answer. It is a ‘why’ question and not a ‘how’ question, and there might not be a ‘why’. To be more precise, if this hierarchy turns out *not* to have any explanation, then the Standard Model would not have lost any predictive power. We understand electroweak physics very well – the hierarchy problem is not a barrier to our understanding of current experimental results.

The true appeal of the hierarchy problem is that it suggests the existence of new physics; in particular, new physics within the reach of current particle colliders. All of

the other problems on the list might be explained by physics which for the time being is experimentally out of reach. For instance, aside from its gravitational interactions, dark matter might be completely decoupled from the Standard Model, and neutrinos might acquire their masses from operators generated at the unification scale ( $\sim 10^{16}$  GeV). On the other hand, the hierarchy problem is best solved by new physics at the TeV scale, which could in principle be just around the corner.

The hierarchy problem is the main motivation for the work contained in this thesis. In particular, we shall be focusing on a specific solution to the problem, namely Composite Higgs models. In the following sections I shall describe in more detail the nature of the hierarchy problem and precisely how Composite Higgs models can solve it.

## 1.2 The hierarchy problem

The Higgs field is a crucial component of the Standard Model. It is a scalar field in the  $(\mathbf{1}, \mathbf{2})_1$  representation of the Standard Model (SM) gauge group  $SU(3)_c \times SU(2)_L \times U(1)_Y$ . It has couplings to gauge bosons via its covariant derivative

$$(D_\mu H^\dagger)(D^\mu H), \quad (1.1)$$

couplings to fermions via Yukawa couplings

$$\sum_{ij} y_{ij} \bar{\psi}_L^{(i)} H \psi_R^{(j)} + h.c. \quad (1.2)$$

and a potential

$$V(H) = -m_H^2 H^\dagger H + \lambda (H^\dagger H)^2. \quad (1.3)$$

For  $m_H^2, \lambda > 0$ , the potential is unstable at the origin and the Higgs acquires a vacuum expectation value (VEV):

$$\langle H^\dagger H \rangle = \frac{m_H^2}{2\lambda}. \quad (1.4)$$

We can use the  $SU(2)_L \times U(1)_Y$  gauge freedom to rotate the VEV into an arbitrary direction, and write:

$$\langle H \rangle = \begin{pmatrix} 0 \\ v \end{pmatrix}, \quad v = \sqrt{\frac{m_H^2}{2\lambda}}, \quad (1.5)$$

where  $v$  is real. This vacuum is not invariant under  $SU(2)_L \times U(1)_Y$ ; thus the electroweak symmetry of the Standard Model is spontaneously broken to  $U(1)_{em}$ . The VEV of the Higgs field, via the couplings in (1.1) and (1.2), gives masses to the fermions and the  $W$  and  $Z$  gauge bosons. This is the Higgs mechanism, and it is one of the cornerstones on

which the Standard Model is built [6–8]. In 2012 the Higgs boson was finally discovered, with a mass measured to be approximately 125 GeV [9, 10].

All of the massive particles in the Standard Model (possibly with the exception of the neutrinos) therefore have masses that are proportional to the electroweak scale  $v$ . As we have seen, the electroweak scale is proportional to  $m_H$ : the only mass scale, and indeed the only dimensionful parameter, in the Standard Model Lagrangian. The hierarchy problem concerns the extremely large hierarchy between this mass and the Planck mass  $m_P$  – the scale at which quantum gravity effects are expected to become important:

$$m_P/m_H \approx 10^{17}. \quad (1.6)$$

Why is this large hierarchy considered a problem? The problem concerns the notion of ‘technical naturalness’, as introduced by ’t Hooft in [11]. A small parameter is considered natural if setting it to zero restores a symmetry of the action. For instance, fermion masses are technically natural in the sense that setting them to zero restores the chiral symmetry under which their left- and right-handed components transform separately.

This means that, when quantum corrections to the fermion mass are computed, the corrections must be proportional to the bare parameter itself. Schematically:

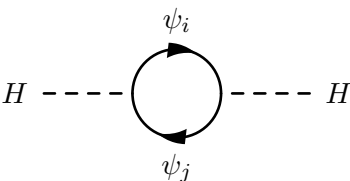
$$\delta m_f \propto m_f \log(\Lambda/m_f) + \dots \quad (1.7)$$

where  $\Lambda$  is the cutoff used to regularise the loop integrals. We expect this to be the case, because in the limit  $m_f \rightarrow 0$ , the chiral symmetry is restored and should remain exact, with  $\delta m = 0$ , to all orders in perturbation theory.

No such symmetry protects the Higgs mass, and quantum corrections to  $m_H$  may scale with the cutoff:

$$\delta m_H^2 \propto \Lambda^2 + \dots \quad (1.8)$$

Indeed, one-loop corrections to the Higgs mass from loops of fermions



$$H \text{ --- } \text{loop} \text{ --- } H \quad (1.9)$$

are given by [12]

$$\delta m_H^2 = \frac{y_{ij}^2}{8\pi^2} \Lambda^2 + \dots, \quad (1.10)$$

where  $\Lambda$  is the momentum cutoff in the loop integral. We can interpret  $\Lambda$  as the scale at which new physics appears that alters the high-energy behaviour of the theory. From an effective field theory point of view, *unless the Higgs mass is technically natural*, then it should scale with the mass of the heaviest degrees of freedom to which the Higgs couples. If  $\Lambda$  is equal to the Planck scale, then either some extremely finely-tuned cancellation occurs (tuned to the level of around 1 part in  $10^{34}$ ), or the Higgs mass, somehow, is a technically natural parameter which does not depend quadratically on the cutoff after all.

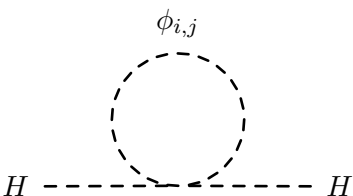
A solution would call for new physics, perhaps new fields and/or new symmetries. And crucially, to avoid the need for more cancellations and tuning, the scale of this new physics should not be too much higher than the electroweak scale.

### 1.3 Solutions to the hierarchy problem

Conventional solutions to the hierarchy problem generally involve introducing new fields with masses not too far above the electroweak scale. Some or all of these particles will couple to the Higgs and/or other Standard Model fields, opening up exciting possibilities for direct detection at particle colliders. New fields that couple to the Higgs have the potential to resolve the hierarchy problem, but they will typically only do so if there is some *symmetry* that ensures this.

One well studied and popular solution to the hierarchy problem is *supersymmetry* [12]. Supersymmetry (or SUSY) is a kind of symmetry that relates bosonic degrees of freedom to fermionic degrees of freedom. In a fully supersymmetric action, all states come with a superpartner, with the same mass and quantum numbers, but with opposite spin statistics. These states sit together in a representation of supersymmetry called a superfield, and interactions are introduced by writing down a superpotential which is a holomorphic function of these superfields.

It turns out that supersymmetry is sufficient to cancel out the quadratically divergent contributions to the Higgs mass. Take the fermion loops in (1.9): in a supersymmetric theory,  $\psi_i$  has the superpartner  $\phi_i$ , and the quadratic divergence is cancelled by the following diagrams



(1.11)

where  $\phi_{i,j}$  are the scalar superpartners of  $\psi_i$  and  $\psi_j$ .

Since we have not yet discovered any supersymmetric particles, they must exist at a scale not yet accessible to colliders. Thus, if supersymmetry is realised in our universe, it is clear that it must be a broken symmetry. One of the obstacles to constructing a viable supersymmetric model is ensuring that supersymmetry is broken in a way that does not reintroduce another hierarchy problem.

This is traditionally done via what are known as ‘soft’ breaking terms. These are breaking terms which are proportional to some mass scale, which we will label  $m_{soft}$ . If we break supersymmetry with soft terms, then the induced corrections to the Higgs mass must scale with

$$\delta m_H^2 \propto m_{soft}^2 \log(\Lambda/m_{soft}) + \dots \quad (1.12)$$

since the corrections must vanish in the limit  $m_{soft} \rightarrow 0$ . On the other hand, if we were to introduce some dimensionless SUSY-breaking parameter, then the corrections could scale with cutoff  $\sim \Lambda^2$ , and we would have reintroduced the hierarchy problem. This leads us to another obstacle facing supersymmetric theories: the origin of these soft supersymmetry breaking terms. Ultimately we need some mechanism for generating the scale associated with the breaking of supersymmetry, which is the scale that ultimately determines the electroweak scale. Of course, the literature on this problem is extensive, and beyond the scope of this thesis.

Supersymmetry can be considered a *weakly-coupled* solution to the hierarchy problem, in that all of the interactions are of order the strength of the Standard Model interactions, which, evaluated at the electroweak scale, are perturbative interactions. Composite Higgs models, which we shall discuss in the next section, are *strongly-coupled* models. Like SUSY, they also predict the existence of new states near the electroweak scale. But unlike SUSY, these states take part in non-perturbative interactions. In these models the Higgs, rather than being an elementary particle, is a composite bound state, allowing for a solution to the hierarchy problem of an altogether different kind.

## 1.4 Composite Higgs models

There are other scalar fields in the Standard Model besides the Higgs. The spectrum of bound states in QCD contains many scalar resonances, the lightest of which are the pions. We do not consider pion masses to be problematic: this is because their masses are not an input into the Standard Model Lagrangian, they are related to the confinement scale of QCD,  $\Lambda_{QCD}$ . This scale is generated by dimensional transmutation, and can be defined



as the scale at which QCD becomes strongly interacting (i.e. non-perturbative). This is determined by the RG running of the strong coupling constant:

$$\frac{\partial g_s}{\partial \log(\mu)} = -\frac{c}{16\pi^2}g_s^3 + \mathcal{O}(g_s^5), \quad (1.13)$$

where the value of  $c$  is dependent on the particle content of the Standard Model. The running is logarithmic with the energy scale  $\mu$ , meaning that a large hierarchy between  $\Lambda_{QCD}$  and the Planck scale can be easily generated. Hierarchies between scales generated in this way are considered natural since they arise without the need for any fine-tuning or cancellations.

Inspired by this, Composite Higgs models generate the electroweak scale via a similar mechanism. One can postulate the existence of a new gauge force which confines not far above the electroweak scale. If the Higgs is a bound state of this new strong dynamics, then its mass would be tied to this confining scale and would no longer be a fundamental input to the Standard Model Lagrangian.

The idea of generating the electroweak scale via dimensional transmutation is not unique to Composite Higgs models; in fact it was the main inspiration behind Technicolor models [13–15]. In Technicolor models, it is the confining vacuum of the new sector that breaks electroweak symmetry, rather than the VEV of the Higgs field; indeed, Technicolor theories do not require a Higgs field. Of course, now that the Higgs has been discovered, Technicolor theories are a less attractive possibility, notwithstanding the fact that they generally struggle to pass electroweak precision tests [16, 17].

#### 1.4.1 The pNGB Higgs

The first question one might ask is: if the Higgs is a composite formed from a new, strongly interacting sector, then why have we not yet seen any other resonances alongside the Higgs? QCD provides us with another clue: it is well known that in QCD the pions are *pseudo-Nambu Goldstone bosons* (pNGBs). They emerge from the spontaneous breaking of the approximate  $SU(2)_L \times SU(2)_R$  chiral symmetry of the up-down quark sector to its vectorial subgroup. If this chiral symmetry were exact – that is to say, if the up and down quarks were massless – then the pions would be exact, massless Goldstone bosons. In the Standard Model this chiral symmetry is broken by the small quark masses, allowing the pions to acquire mass. But they are the lightest QCD resonances nevertheless, and the ‘little hierarchy’ between their masses and the rest of the QCD resonances is explained by their pseudo-Goldstone nature.

Inspired by this, we can postulate that the Higgs is also a pNGB. Let us assume that the strong sector has a global symmetry, denoted by  $\mathcal{G}$ , which is spontaneously broken to a subgroup  $\mathcal{H} \in \mathcal{G}$ . This spontaneous symmetry breaking is, just like in QCD, assumed to be triggered by the appearance of a non-perturbative vacuum condensate. That is, some strong sector operator  $\mathcal{O}_{\mathcal{G}}$  gets a vacuum expectation value  $\langle \mathcal{O}_{\mathcal{G}} \rangle$  due to non-perturbative interactions which is invariant under  $\mathcal{H}$  transformations but not under the whole group  $\mathcal{G}$ . This spontaneous breaking will give rise to  $n = \dim(\mathcal{G}) - \dim(\mathcal{H})$  pNGB scalars. We need four pNGBs to account for the four real degrees of freedom in a complex doublet of  $SU(2)_L$ , so we need  $n \geq 4$ . The two minimal cosets that deliver exactly four pNGBs are

1.  $SU(3) \rightarrow SU(2) \times U(1)$ ,
2.  $SO(5) \rightarrow SO(4)$ .

However, in order to protect the Peskin-Takeuchi  $T$ -parameter<sup>1</sup> [18] from large corrections (coming mainly from the exchange of spin-1 composites), it is necessary to endow the strong sector with an unbroken custodial symmetry:

$$G_{cust} = SU(2)_L \times SU(2)_R, \quad (1.14)$$

where  $SU(2)_L$  is the electroweak gauge group (see the next section). This rules out option 1), since  $G_{cust}$  cannot be embedded in  $SU(2) \times U(1)$ . Therefore the minimal coset is  $SO(5)/SO(4)$ , where the unbroken  $SO(4)$  is identified exactly with  $G_{cust}$ , using the local isomorphism  $SO(4) \simeq SU(2) \times SU(2)$ . The model based on this coset is referred to as the Minimal Composite Higgs model (MCHM) [19].

We will be analysing Composite Higgs models in an effective field theory (EFT) framework. Generally speaking, our philosophy will be to be as agnostic as possible about the structure of the UV theory, and deal with an effective theory in which only the lightest resonances are kept as dynamical degrees of freedom. Without precise microscopic realisations of our models, we will not be able to make definite predictions; however, in a non-perturbative theory such predictions would prove difficult even if we did know the full structure of the theory. The formalism we will use for writing down an effective theory of the pNGB fields and their interactions is the CCWZ<sup>2</sup> formalism [20,21]. We introduce an object  $U$  which parametrises the pNGB fields:

$$U(x) = \exp(i\phi^a(x)X^a/f), \quad (1.15)$$

---

<sup>1</sup>The Peskin-Takeuchi  $S$ ,  $T$  and  $U$  parameters are a set of observables that parameterise new physics corrections to electroweak physics. They are all defined to be exactly zero in the Standard Model.

<sup>2</sup>CCWZ here stands for Callan, Coleman, Wess and Zumino, who coauthored the original papers on this formalism.

where  $\phi^a$  are the pNGB fields,  $X^a$  are the corresponding generators of the  $\mathcal{G}/\mathcal{H}$  coset, and  $f$  is a scale associated with the symmetry breaking  $\mathcal{G} \rightarrow \mathcal{H}$ . The Goldstone fields then parameterise the coset  $\mathcal{G}/\mathcal{H}$ . To find out how  $U$  transforms under a general group transformation  $g \in \mathcal{G}$ , let us first note that a general group element of  $\mathcal{G}$  can be written

$$g = \exp(i\chi^a X^a) \exp(i\theta^a T^a), \quad (1.16)$$

where  $T^a$  are the unbroken generators of  $\mathcal{H}$ . Thus  $U$  can be seen as a group element with  $\theta^a = 0$  and the parameters  $\chi^a$  being equal to the spacetime dependent fields  $\phi^a(x)/f$ . Therefore when we multiply  $U$  from the left with a general group element  $g$ , we should obtain another group element

$$g U(x) = \exp(i\tilde{\phi}^a(x) X^a) \exp(i\tilde{\theta}^a(x) T^a), \quad (1.17)$$

where we identify  $\tilde{\phi}^a$  as the transformed pNGB fields. In general now the parameters  $\tilde{\theta}^a$  will be spacetime dependent fields. We can multiply from the right by  $h^{-1}(x) = \exp(-i\tilde{\theta}(x) T^a)$  to obtain

$$\tilde{U} = g U h^{-1}(x) = \exp(i\tilde{\phi}^a(x) X^a), \quad (1.18)$$

which gives us the transformation properties of  $U$ . Notice that  $h(x)$  is a field-dependent transformation belonging to the unbroken subgroup  $\mathcal{H}$ . This means that transformations of  $U$  are *non-linear* in the sense that  $h(x)$  depends on the values of the fields themselves.

The task of writing down an effective theory for the pNGB fields will in practice be the task of writing down  $\mathcal{G}$ -invariant terms involving  $U$  and any *spurion* fields we introduce. The method of spurions will be covered in the next section.

#### 1.4.2 Couplings of the Higgs

The Lagrangian describing the interactions of exact Nambu Goldstone bosons should be invariant under the shift symmetry

$$\phi^a \rightarrow \phi^a + C^a, \quad (1.19)$$

for each NGB  $\phi^a$ . We know that the Higgs is not an exact Nambu Goldstone boson, since it has a potential and participates in interactions with other SM fields. Our first task is to describe the manner in which the strong sector couples to the rest of the Standard Model. To do so we will need to introduce couplings which will break  $\mathcal{G}$  explicitly.

## Gauge interactions

We can introduce gauge interactions by gauging a subgroup of the unbroken global symmetry  $\mathcal{H}$ . The Higgs transforms under the electroweak gauge group  $G_{ew} = SU(2)_L \times U(1)_Y$ , which means that we need to gauge a subgroup  $G_{ew} \in \mathcal{H}$ . Under the unbroken subgroup  $\mathcal{H}$  the transformations of  $U$  are *linear*:

$$U \rightarrow h U h^{-1}, \quad (1.20)$$

linear in the sense that  $h$  is no longer field-dependent. Gauge interactions are then introduced via the covariant derivative of  $U$ :

$$\mathcal{L}_{kinetic} = \frac{f^2}{4} \text{Tr}[D_\mu U^\dagger D^\mu U]. \quad (1.21)$$

Note that gauging a subgroup of the global symmetry breaks it explicitly.

## Fermion interactions

We are now faced with the question of how to couple fermions to the strong sector. One way of doing this, inspired by technicolor models, is to couple the left and right handed quarks directly to an operator  $\mathcal{O}$  as follows:

$$\mathcal{L} \supset \lambda \bar{q}_L q_R \mathcal{O} + h.c. \quad (1.22)$$

The operator  $\mathcal{O}$  thus has the same quantum numbers as the Higgs. It turns out that this procedure is problematic, and has difficulties reproducing a large enough top Yukawa coupling while at the same time evading flavour constraints.

An alternative, more successful approach is the *partial compositeness* paradigm [22–24]. The idea in this case is that the strong sector contains operators with the same quantum numbers as the SM quarks, with which the quarks have linear mixings, schematically given by

$$\mathcal{L} \supset y_L \bar{q}_L \mathcal{O}_L + y_R \bar{q}_R \mathcal{O}_R + h.c. \quad (1.23)$$

Since the operators  $\mathcal{O}_{L,R}$  come in representations of  $\mathcal{G}$ , the interactions in (1.23) also explicitly break the global symmetry. To write down operators encoding the interactions of the quarks and the pNGBs, we can embed the quarks in ‘spurionic’ representations of  $\mathcal{G}$ :

$$q \rightarrow \Psi_q, \quad (1.24)$$

where  $\Psi_q$  formally transforms in the same representation as the operator  $\mathcal{O}_q$ . Then we can write down effective operators involving  $U$  and the  $\Psi_q$ , invariant under  $\mathcal{G}$ , which encode all the interactions of the pNGBs with the SM fermions.

### An example

To see how this works in practice, let us look at the MCHM, which, as we already discussed, involves the coset  $SO(5)/SO(4)$ . To accommodate the  $U(1)_Y$  hypercharge gauge group we must actually extend the global symmetry by an extra unbroken  $U(1)_X$ , so that  $\mathcal{G} = SO(5) \times U(1)_X$ , and hypercharge is realised as  $Y = T_R^3 + X$ , with  $T_R^3$  the diagonal generator of the  $SU(2)_R \in SO(4)$ .

We can break  $SO(5)$  to  $SO(4)$  if an operator in the vectorial  $\mathbf{5}$  of  $SO(5)$  gets a VEV. We will take this VEV to be proportional to

$$\langle \mathbf{5} \rangle \propto (0, 0, 0, 0, 1). \quad (1.25)$$

Then the broken  $SO(5)/SO(4)$  generators can be taken to be

$$X_{ij}^a = -\frac{i}{\sqrt{2}} (\delta_i^a \delta_j^5 - \delta_j^a \delta_i^5), \quad (1.26)$$

with  $i, j = 1, \dots, 5$  and  $a = 1, \dots, 4$ . We can construct a linearly transforming object, labeled by  $\Sigma$ , by noticing that  $h\langle \mathbf{5} \rangle = \langle \mathbf{5} \rangle$ , for  $h \in \mathcal{H}$ . This is just the trivial statement that the vacuum is invariant under the unbroken group  $\mathcal{H}$ . Thus

$$\Sigma = U\langle \mathbf{5} \rangle \quad (1.27)$$

transforms as  $\Sigma \rightarrow gUh^{-1}\langle \mathbf{5} \rangle = gU\langle \mathbf{5} \rangle = g\Sigma$ , and we have removed the non-linear dependence on the fields. The object  $\Sigma$  is therefore a more convenient object for constructing invariants involving the pNGB fields, and is given explicitly by

$$\Sigma = \frac{\sin(\tilde{h}/f)}{\tilde{h}} (h^1, h^2, h^3, h^4, \tilde{h} \cot(\tilde{h}/f)), \quad (1.28)$$

where  $h^a$  are the four pNGB fields and  $\tilde{h} = \sqrt{h^a h^a}$ .

The Standard Model fermions must be embedded in representations of the group  $\mathcal{H}$ . In principle there are many options: the smallest irreducible representations of  $SO(5)$  are the  $\mathbf{1}, \mathbf{4}, \mathbf{5}, \mathbf{10}, \mathbf{14}$ , and without knowledge of the full theory the representation is essentially a free choice of the model. There is, however, a theorem which states that the left-handed quark doublet  $q_L = (t_L, b_L)$  must be embedded in a  $(\mathbf{2}, \mathbf{2})$  bidoublet of the  $SU(2)_L \times SU(2)_R$  custodial symmetry, if the  $Zb\bar{b}$  coupling is not to receive unacceptably large corrections [25]. The smallest representation that fulfills this criterion is the  $\mathbf{5}$ , decomposing as  $(\mathbf{2}, \mathbf{2}) \oplus (\mathbf{1}, \mathbf{1})$  under  $\mathcal{H}$ . We can embed  $q_L$  in the  $(\mathbf{2}, \mathbf{2})$ , and the right-

handed  $t_R, b_R$  in the singlet  $(\mathbf{1}, \mathbf{1})$ , like so

$$\begin{aligned}\Psi_q &= (b_L, ib_L, t_L, -it_L, 0)/\sqrt{2}, \\ \Psi_t &= (0, 0, 0, 0, t_R), \\ \Psi_b &= (0, 0, 0, 0, b_R).\end{aligned}\tag{1.29}$$

We can build our EFT for the Higgs-fermion interactions out of these objects and  $\Sigma$ , all of which transform in the vector representation. For instance, the top Yukawa coupling can be recovered from the operator

$$M_t(p)(\bar{\Psi}_q \cdot \Sigma)(\Sigma \cdot \Psi_t) + h.c.\tag{1.30}$$

where  $M_t(p)$  is a momentum-dependent form factor, encoding the integrated-out dynamics of the strong sector. This gives a term of the form

$$M_t(p) \bar{t}_L H t_R \frac{\sin(\tilde{h}/f) \cos(\tilde{h}/f)}{\tilde{h}} + h.c.\tag{1.31}$$

from which the top Yukawa coupling can be extracted. Note however that there are also form factor corrections to the fermion kinetic terms:

$$\mathcal{L} \supset \Pi_q(p) \bar{\Psi}_q \not{p} \Psi_q + \Pi_t(p) \bar{\Psi}_t \not{p} \Psi_t,\tag{1.32}$$

so that fields must be canonically normalised before the Yukawa coupling itself can be extracted.

### 1.4.3 The Higgs potential

The couplings of the Higgs to the SM fields lead to a Coleman-Weinberg potential for the Higgs at one-loop [26]. The potential is expected to be dominated by the gauge bosons and by the third generation quarks, since these have the largest couplings to the Higgs. We will delay a detailed explanation of this mechanism until Chapter 3, where we consider general Coleman-Weinberg contributions to the inflaton potential.

For the time being it is sufficient to say that the Higgs potential (and that of the other pNGBs, if there are any) will generally be a trigonometric function of the scalars. In the MCHM, with fermions in the  $\mathbf{5}$ , the potential is given to leading order by

$$V(h) = \alpha \sin^2(h/f) - \beta \sin^2(h/f) \cos^2(h/f),\tag{1.33}$$

where  $\alpha$  and  $\beta$  are given by integrals over form factors. Loops of gauge bosons contribute only to the first term, and their contribution to  $\alpha$  is guaranteed to be positive. Therefore the fermionic contribution, coming primarily from the top quark, is necessary for a negative

Higgs mass-squared and electroweak symmetry breaking to occur. We also need some tuning between  $\alpha$  and  $\beta$  to ensure that the VEV of the Higgs field is significantly lower than the scale  $f$ . If we have  $\langle h \rangle \sim f$ , then corrections to the SM couplings of the Higgs will be unacceptably large, as will be contributions to the Peskin-Takeuchi  $S$ -parameter [24].

#### 1.4.4 Top partners

One of the consequences of the partial compositeness mechanism described in Section 1.4.2 is the existence of bound states with the same quantum numbers as the SM fermions. As we will show in Chapter 4, an important phenomenological prediction of Composite Higgs models is that the lightest of these states are expected to be the top partners. Diagonalisation of the mixing terms in (1.23) leads to mass eigenstates which are a linear superposition of elementary and composite states:

$$\begin{aligned} |\tilde{t}\rangle &= \cos\theta |t\rangle - \sin\theta |T\rangle \\ |\tilde{T}\rangle &= \cos\theta |T\rangle + \sin\theta |t\rangle, \end{aligned} \tag{1.34}$$

where  $\tilde{T}, \tilde{t}$  represent the physical, partially-composite mass eigenstates and  $\theta$  is the mixing angle. There will generally be a separate partner for the left and right handed components of the top, and these could in principle be embedded in different representations of  $\mathcal{G}$ .

As we demonstrate in Chapter 4, one can derive strong relations between the mass of the Higgs and the mass of the lightest top partner. Generally one finds relations of the form:

$$m_H \sim \frac{\sqrt{N_c}}{\pi} \frac{m_t m_T}{f}, \tag{1.35}$$

where  $N_c = 3$  is the number of QCD colours. One therefore expects top partners with masses around the scale  $f$ , and the higher the scale  $f$ , the more tuning necessary to obtain a light Higgs.

New states charged under QCD are an obvious search candidate at the LHC, and a number of dedicated searches have been performed. Current bounds are at around 1 – 1.2 TeV for the mass of the lightest top partner, which already implies an uncomfortable degree of tuning [27]. Precise bounds will depend on the model in question. Models can vary both in the choice of symmetry coset  $\mathcal{G}/\mathcal{H}$ , and the representation that the left and right handed top partners come in.

#### 1.4.5 UV completions?

We have treated the symmetry coset and the top partner representations as free choices, but in principle they should depend on the UV completion of the theory. By ‘UV comple-

tion’ I mean a description of the strongly coupled theory out of which the composite Higgs emerges.<sup>3</sup> There are, however, many challenges involved in constructing a phenomenologically viable UV completion of a Composite Higgs model.

The most straightforward way to UV-complete a Composite Higgs model would be in the form of a fermion-gauge theory; that is, a theory with a set of new fermions  $\psi$  charged under a new strongly interacting gauge group. In general, one can have  $n_i$  fermions in each representation  $R_i$  of this gauge group. Then the global symmetry of the theory will be a product of  $SU(N)$  and  $U(1)$  factors:

$$\mathcal{G} = SU(n_1) \times \cdots \times SU(n_p) \times U(1)^{p-1}, \quad (1.36)$$

where  $p$  is the number of different irreducible representations in the model.

Immediately we can see that the Minimal Composite Higgs model  $SO(5)/SO(4)$  will not be straightforward to embed in a UV-complete model, since  $SO(5)$  cannot be written as a product of  $SU(N)$  factors. On the other hand, the *next-to-minimal* Composite Higgs model [28] is based on the coset  $SO(6)/SO(5)$ , and is UV-completable thanks to the local isomorphism  $SO(6) \simeq SU(4)$ . The  $SO(6)/SO(5)$  model has 5 pNGB fields, leading to a doublet and a singlet under  $SU(2)_L$ .

### Symmetry breaking

In QCD, the global chiral symmetry is broken by the vacuum expectation value of the condensate

$$\langle \bar{q}_L q_R \rangle, \quad (1.37)$$

which is invariant only under vectorial  $SU(N)_V \in SU(N)_L \times SU(N)_R$  transformations:

$$q_L \rightarrow V q_L, \quad q_R \rightarrow V q_R. \quad (1.38)$$

Similarly we can argue that the strongly interacting fermions  $\psi$  will form vacuum condensates that will break the global symmetry  $\mathcal{G}$  to some subgroup  $\mathcal{H}$ . There are a few different possibilities [29–31]:

1.  $SU(N)_1 \times SU(N)_2 \rightarrow SU(N)_D$  – this is the ‘QCD-like’ case, and can be achieved with two sets of fermions,  $\psi_1$  in representation  $R$  of the new gauge group, and  $\psi_2$  in representation  $\bar{R}$ , with  $\bar{R}$  the conjugate representation of  $R$ . The condensate

$$\langle \psi_1^i \psi_2^j \rangle \quad (1.39)$$

---

<sup>3</sup>This description itself might not be truly ‘UV-complete’ in the sense that it might contain non-renormalisable operators.



will be invariant under the diagonal subgroup of the two  $SU(N)$ s.

2.  $SU(N) \rightarrow SO(N)$  – this can be achieved with a single fermion  $\psi$  in a *real* representation of the gauge group. The condensate

$$\langle \psi^i \psi^j \rangle \tag{1.40}$$

turns out to be symmetric in  $i \leftrightarrow j$  and invariant under the  $SO(N)$  subgroup of  $SU(N)$ .

3.  $SU(N) \rightarrow Sp(N)$  – this can be achieved with a single fermion  $\psi$  in a *pseudo-real* representation of the gauge group. The condensate

$$\langle \psi^i \psi^j \rangle \tag{1.41}$$

turns out to be antisymmetric in  $i \leftrightarrow j$  and invariant under the  $Sp(N)$  subgroup of  $SU(N)$ .

The most minimal examples, in terms of number of pNGB fields, in each category are<sup>4</sup> [29–31]

- $SU(4) \times SU(4) \rightarrow SU(4)$ ,
- $SU(5) \rightarrow SO(5)$ ,
- $SU(4) \rightarrow Sp(4)$ .

We will consider the latter two models in Chapter 6, where we will also discuss how the cosets might be deformed by strong external couplings so that their phenomenology could resemble different models.

## 1.5 Outline of this thesis

This thesis features five papers that were published during the course of my PhD, and is structured as follows:

- Chapter 2 – *Composite Higgs models after Run 2* [1]. In this paper we assess the status of various Composite Higgs models in the light of the latest Run 2 LHC data at 13 TeV. We focus on the measurements of the Higgs couplings and introduce a

---

<sup>4</sup>The reader may ask why the coset  $SU(4)/SO(4)$  does not appear in this list. The reason is that when  $SU(4)$  is broken to  $SO(4)$  by a fermion condensate of the form (1.40), the 9 pNGBs come in the  $(\mathbf{3}, \mathbf{3})$  representation of  $SU(2)_L \times SU(R)$ , so we do not recover the necessary Higgs doublet.

classification of different models depending on how the couplings of the Higgs are modified. We also consider various scenarios in which the Higgs might mix with an extra singlet or doublet field, and how this will affect the couplings.

- Chapter 3 – *Goldstone Inflation* [2]. In this paper we apply some of the formalism developed in the Composite Higgs literature to the study of inflation. The problems that models with a scalar inflaton face are in many ways comparable to the problem of generating a natural electroweak scale, so we find that this approach is useful and can ameliorate issues with trans-Planckian decay constants in models of Natural Inflation.
- Chapter 4 – *Composite Higgses with seesaw EWSB* [3]. In this paper we present an original model in which the pNGB coset consists of two doublets that acquire a mixing term. This mixing term can contribute to the misalignment of the vacuum and electroweak symmetry breaking. We perform a thorough analysis of this model, including a discussion of tuning and the modifications of the Higgs couplings.
- Chapter 5 – *Tracking down Quirks at the Large Hadron Collider* [4]. This paper can be considered an ‘interlude’, in which we move away from Composite Higgs and focus on another strongly-coupled extension of the Standard Model. In this paper we focus on *quirks*, which are heavy states charged under a new confining gauge group. The key feature of quirks is that their mass is assumed to be considerably higher than the confining scale of the new gauge group, so that these particles do not confine and instead interact over macroscopic distances. We present a novel detection strategy that could be implemented at the LHC, utilising the fact that quirk trajectories are constrained to lie within a plane.
- Chapter 6 – *Composite Higgs models in disguise* [5]. Returning to Composite Higgs, in the final chapter we present a mechanism that could disguise one Composite Higgs model as another. Strong couplings between the strong sector and an external sector can deform the symmetry group so that, at low energies, the model has the same phenomenology as a different model. Any extra resonances acquire large masses and remain hidden. This mechanism could be of interest especially if one is concerned with models that have a viable UV completion; in particular, we show that two such models can be ‘disguised’ as the Minimal Composite Higgs model  $SO(5)/SO(4)$  if the correct external couplings are introduced.

## Chapter 2

# Composite Higgs models after Run 2

### Abstract

We assess the status of models in which the Higgs is a composite pseudo-Nambu Goldstone boson, in the light of the latest 13 TeV Run 2 Higgs data. Drawing from the extensive Composite Higgs literature, we collect together predictions for the modified couplings of the Higgs, in particular examining the different predictions for  $\kappa_V$  and  $\kappa_F$ . Despite the variety and increasing complexity of models on the market, we point out that many independent models make identical predictions for these couplings. We then look into further corrections induced by tree-level effects such as mass-mixing and singlet VEVs. We then investigate the compatibility of different models with the data, combining the Run 1 and recent Run 2 LHC data. We obtain a robust limit on the scale  $f$  of 600 GeV, with stronger limits for different choices of fermion embeddings. We also discuss how a deficit in a Higgs channel could pinpoint the type of Composite Higgs model responsible for it.

## 2.1 Introduction

Composite Higgs models [19, 32, 33] offer an elegant solution to the hierarchy problem of Higgs physics. They postulate the existence of a new strongly interacting sector which confines not far above the electroweak scale. In recent years there has been significant interest in a specific class of these models – models in which the Higgs emerges as a pseudo-Nambu Goldstone boson of the strong sector. This sector is taken to be endowed with a global symmetry which is spontaneously broken in the confining phase, protecting the Higgs mass from corrections above the compositeness scale. Although the idea is reasonably straightforward, there are, as with most theories Beyond the Standard Model, many possibilities for its realisation.

Although this plethora of models offers a variety of unique and interesting predictions, those that are most immediately testable are the modifications of the Higgs couplings to the rest of the Standard Model fields. Of particular interest are the values of the coupling modifiers  $\kappa_V$  and  $\kappa_F$ , as defined in [34].

In this paper we summarise the predictions for these couplings in Composite Higgs (CH) models. We make the case that, despite the diversity of models in the literature, these predictions have very generic structures, and we attempt to provide some intuition for this fact.

We then investigate some simple cases in which tree-level effects can modify these generic structures. These can occur, for instance, in models with extra singlets that get vacuum expectation values (VEVs), or models with an extra  $SU(2)_L$  doublet that mixes with the Higgs. We point out that to leading order the modifications to  $\kappa_V$  and  $\kappa_F$  are precisely as one would expect in corresponding models where all the scalars are elementary, plus the usual CH corrections.

Taking the generic structures we have identified, we then perform a  $\chi^2$  fit to the data, allowing for the possibility that different fermions couple in different ways. We place bounds on the compositeness scale  $f$ , and identify the classes of models that are most constrained.

## 2.2 The non-linear Composite Higgs

In Composite Higgs models, the Higgs is realised as a pseudo-Nambu Goldstone boson (pNGB) of a broken global symmetry. This symmetry is a symmetry of a *new* strongly interacting sector, out of which the Higgs emerges as a composite.

Let the global symmetry be denoted  $\mathcal{G}$  and the subgroup to which it spontaneously breaks be denoted  $\mathcal{H}$ . Then the Higgs and the other pNGBs (denoted collectively by  $\phi^a$ , one for each broken generator  $X^a$ ), are parametrised via

$$U = \exp(i\phi^a X^a / f), \quad (2.1)$$

where  $f$  is an energy scale associated with the spontaneous symmetry breaking.  $U$  transforms non-linearly under the global symmetry  $\mathcal{G}$ :

$$U \rightarrow gUh^{-1}, \quad (2.2)$$

where  $g \in \mathcal{G}$  and  $h \in \mathcal{H}$ . By non-linear we mean that the transformation  $h$  is field-dependent:  $h = h(g, \phi^a)$ .

In cases where the coset  $\mathcal{G}/\mathcal{H}$  is symmetric<sup>1</sup> we are allowed to construct an object (which we will label  $\Sigma$ ) whose transformation under  $\mathcal{G}$  is *linear*. In all the models considered here [3, 19, 24, 28–30, 35–47], and in the vast majority of models in the literature,  $\mathcal{G}/\mathcal{H}$  will be symmetric. This reduces the task of writing down a low-energy effective theory for the pNGBs to a relatively trivial search for invariant combinations of  $\Sigma$  and the other relevant fields.

We will assume that the Higgs boson is a doublet under  $SU(2)_L$ , which, along with  $U(1)_Y$ , must be embedded as an unbroken subgroup of  $\mathcal{G}$ . Although data strongly supports the doublet scenario (e.g. see LHC constraints on the ratio of couplings to  $W$  and  $Z$  bosons [34]), non-linear models have been studied in which the four scalar fields are actually a singlet and a triplet under  $SU(2)_L$  [48–51].<sup>2</sup>

### 2.2.1 Gauge couplings

The couplings of the Higgs to the gauge bosons come from the kinetic term for  $\Sigma$ , which in the CCWZ prescription [21] is:

$$\mathcal{L}_{kinetic} = \frac{f^2}{4} \text{Tr}[D_\mu \Sigma^\dagger D^\mu \Sigma], \quad (2.3)$$

where  $D_\mu = \partial_\mu - igA_\mu$ , with  $A_\mu = A_\mu^a T^a$  for each gauged generator  $T^a$ . We assume that the Higgs is embedded in a bidoublet  $(\mathbf{2}, \mathbf{2})$  of a custodial  $SO(4) \simeq SU(2)_L \times SU(2)_R \in \mathcal{H}$

---

<sup>1</sup>If  $T^a$  and  $X^a$  are the unbroken and broken generators respectively, then the Lie algebra of a symmetric coset obeys the schematic relations

$$[T, T] \sim T, \quad [X, X] \sim T, \quad [T, X] \sim X.$$

<sup>2</sup>Note, though, that one could assume a custodially symmetric strong sector as in Ref. [52, 53].

– this is necessary in order to protect the  $\rho$  parameter from unwanted corrections [54]. Note that this imposes the non-trivial requirement that  $\mathcal{H}$  must contain an unbroken factor of  $SO(4)$ .

Since we are interested in the couplings of the physical Higgs boson to SM fields, we will expand  $\Sigma$  along the direction in which the Higgs will get a VEV, and set all other pNGB fields to zero. The term in (2.3) will generically<sup>3</sup> lead to a Higgs-gauge coupling of the form:

$$g^2 f^2 A_\mu A^\mu \sin^2(H/f), \quad (2.4)$$

which is valid as a series expansion around  $H/f$ .

Expanding around the Higgs VEV  $H \rightarrow \langle H \rangle + h$  (where  $h$  is the physical excitation of the Higgs field) we find the gauge boson masses and couplings:

$$\begin{aligned} \mathcal{L}_{gauge} \supset \frac{1}{8} g^2 f^2 \sin^2 \left( \frac{\langle H \rangle}{f} \right) W_\mu^a W^{a\mu} \\ + \frac{1}{8} g^2 f \sin \left( \frac{2\langle H \rangle}{f} \right) W_\mu^a W^{a\mu} h \\ + \frac{1}{8} g^2 \cos \left( \frac{2\langle H \rangle}{f} \right) W_\mu^a W^{a\mu} h^2. \end{aligned} \quad (2.5)$$

Identifying<sup>4</sup>  $v = f \sin(\langle H \rangle/f)$  and defining  $\xi = v^2/f^2$ , we find

$$\mathcal{L}_{gauge} \supset \frac{1}{8} g^2 v^2 W_\mu^a W^{a\mu} + \frac{1}{4} g^2 v \sqrt{1-\xi} W_\mu^a W^{a\mu} h + \frac{1}{8} g^2 (1-2\xi) W_\mu^a W^{a\mu} h^2. \quad (2.6)$$

Thus

$$\begin{aligned} g_{WWh} &= \sqrt{1-\xi} g_{WWh}^{SM} \\ g_{WWhh} &= (1-2\xi) g_{WWhh}^{SM}. \end{aligned} \quad (2.7)$$

Since  $\kappa_V$  is defined as  $g_{WWh}/g_{WWh}^{SM}$ , we find

$$\kappa_V = \sqrt{1-\xi} \approx 1 - \frac{1}{2}\xi \quad (2.8)$$

Since the structure of (2.3) is generic, so too is this result, at leading order, across almost all Composite Higgs models.<sup>5</sup>

---

<sup>3</sup>In unusual cases the coupling may be proportional instead to  $\sin^2(H/(2f))$ , but all this amounts to is a redefinition of  $\xi$  and an effective rescaling of  $f$ .

<sup>4</sup>Here  $v$  is defined as  $4M_W^2/g^2$ , as in the Standard Model

<sup>5</sup>This discussion has assumed that we can only write down one kinetic term for the pNGBs; in cases where there exist more than one possible kinetic term, these conclusions will be modified.

### 2.2.2 Fermion couplings

In Composite Higgs models the SM fermions usually couple to the strong sector via the *partial compositeness* mechanism [22–24]. As far as this mechanism pertains to the construction of the low energy effective theory, it involves embedding the SM fermions in representations of the global symmetry  $\mathcal{G}$ , and then constructing  $\mathcal{G}$  invariant operators out of these multiplets and  $\Sigma$ . Such an embedding is sometimes called a spurion – the term spurion refers to the ‘missing’ elements of the multiplet, since after all, the SM particles do not come in full multiplets of the new symmetry  $\mathcal{G}$ . The incompleteness of these spurious multiplets contributes to the explicit breaking of  $\mathcal{G}$  and allows the Higgs to acquire a potential via loops of SM fermions.

The appropriate representation in which to embed the SM particles would, in principle, depend on the UV completion of the model. Some attempts towards UV completions of Composite Higgs models have been made (see, for example [29, 30, 35]), however for the purposes of most model building the choice of representation is a ‘free parameter’ of the model. There is, however, good cause to restrict the choice of representation into which the  $SU(2)_L$  quark doublet is embedded. As shown in [25], embedding  $q_L$  into a bidoublet  $(\mathbf{2}, \mathbf{2})$  of the custodial  $SO(4) \simeq SU(2)_L \times SU(2)_R$  can prevent anomalous contributions to the  $Z \rightarrow b\bar{b}$  coupling. This restriction forces one to choose representations that contain a bidoublet in their decomposition under the custodial  $SO(4)$  subgroup of  $\mathcal{G}$ .

To treat the EFT in full generality, one should embed  $q_L$ ,  $t_R$  and  $b_R$  into different multiplets  $\Psi_q$ ,  $\Psi_t$  and  $\Psi_b$ . The kind of representation that the three quarks are embedded into need not be the same. Thus, even for each coset  $\mathcal{G}/\mathcal{H}$ , there are a bewildering number of possibilities. However, for the vast majority of models the form of  $\kappa_F$  is actually quite restricted. We tabulate a few examples in Table 2.1.

It might seem strange that so many distinct models lead to so few possibilities for  $\kappa_F$ . In fact, when one examines the structure of the allowed terms in the effective Lagrangian, a general pattern emerges: the lowest order coupling of the Higgs to fermions will generally contain either one or two factors of  $\Sigma$ . For example, in the Minimal Composite Higgs Model (MCHM), the coset group is  $SO(5)/SO(4)$ , and one can define a linearly transforming  $\Sigma$  in the  $\mathbf{5}$  of  $SO(5)$ , which, expanded along the  $H$  direction can be expressed as

$$\Sigma(h) = (0, 0, 0, \sin(H/f), \cos(H/f)). \quad (2.9)$$

With  $q_L$  and  $t_L$  embedded in the  $\mathbf{5}$ , Yukawa couplings come from the  $SO(5)$  invariant effective operator

$$(\bar{\Psi}_q^5 \cdot \Sigma)(\Sigma \cdot \Psi_t^5), \quad (2.10)$$

$\kappa_F$	Models
$\kappa_F^A = \sqrt{1-\xi}$	$SO(5)/SO(4) - [19, 37]$
	$SO(6)/SO(4) \times SO(2) - [40-42]$
	$SU(5)/SU(4) - [43]$
	$SO(8)/SO(7) - [46, 47]$
$\kappa_F^B = \frac{1-2\xi}{\sqrt{1-\xi}}$	$SO(5)/SO(4) - [37-39, 45]$
	$SU(4)/Sp(4) - [28]$
	$SU(5)/SO(5) - [30]$
	$SO(6)/SO(4) \times SO(2) - [40-42]$

Table 2.1:  $\kappa_F$  in different models.

leading to a term proportional to  $\sin(H/f)\cos(H/f)$ . Alternatively one could embed  $q_L$  into a **10**, the  $t_R$  into a **5** – in this case the Yukawa term originates from an operator like

$$\Sigma^T \bar{\Psi}_q^{\mathbf{10}} \Psi_t^{\mathbf{5}}, \quad (2.11)$$

and the interaction is proportional to  $\sin(H/f)$ .<sup>6</sup>

In general the structure must be such that the leading term in the trigonometric expansion is  $H/f$ . In almost all cases the relevant term will be proportional to either  $\sin(H/f)$  or  $\sin(H/f)\cos(H/f)$ . This argument is certainly not intended to be rigorous – we merely hope to provide some intuition for the fact the non-linear nature of a pNGB Higgs boson leads to repeated structures even across different models and choices of representations.<sup>7</sup>

Following the same procedure as in equation (2.5), we can expand around the Higgs VEV to find the expression for  $\kappa_F$ , defined by  $yv/m_F$ . A coupling of the form  $\bar{\psi}\psi\sin(H/f)$  leads to

$$\kappa_F = \sqrt{1-\xi} \approx 1 - \frac{1}{2}\xi, \quad (2.12)$$

while a coupling of the form  $\bar{\psi}\psi\sin(H/f)\cos(H/f)$  leads to

$$\kappa_F = \frac{1-2\xi}{\sqrt{1-\xi}} \approx 1 - \frac{3}{2}\xi. \quad (2.13)$$

As we stated above, the representation into which we embed  $t_R$  and  $b_R$  might not be the same – in this case it is quite possible (depending on the details of the model) that

---

<sup>6</sup>Note that this structure of couplings also depends on the assumption that the Higgs forms part of a doublet, whereas other forms of the effective coupling could be possible in a singlet case, see e.g. the generic forms of the potential in Ref. [2].

<sup>7</sup>See also [55] for a comprehensive review of different Composite Higgs models, and an especially detailed look at the constraints on the  $SO(5)/SO(4)$  coset with Run 1 data.



the top and bottom couplings to the Higgs have different structures. For instance, in the second example above, although the  $t_R$  is embedded into a **5**, the  $b_R$  might be embedded into a **10**. As a result the top coupling would scale with  $1 - \frac{1}{2}\xi$  while the bottom coupling would scale with  $1 - \frac{3}{2}\xi$ .

There are (as always) some interesting exceptions. For example, in [44], with  $q_L$  in a **5** and  $t_R$  in a **14**, one can derive  $\kappa_F \approx 1 - 3\xi$ , see also Ref. [56]. In some models (for some examples, see [37, 44]) more than one operator can be constructed which contributes to the same Yukawa coupling. The degree to which each operator contributes will, in such cases, be a free parameter and will lead to more complex expressions for  $\kappa_F$ . Such models are interesting insofar as they are exceptions – however more minimal scenarios will follow the structure we have outlined above.

No mention has been made so far of the leptonic sector. In theory the lepton Yukawas can also be generated via the partial compositeness mechanism (see for instance [38]). This means that  $\kappa_\tau$  (for instance) would also receive corrections, and in minimal scenarios would depend on  $\xi$  like  $\kappa_F^A$  or  $\kappa_F^B$ , as defined in Table 2.1.

## 2.3 Tree-level effects

In this section we will briefly look at two interesting scenarios that can lead to tree-level corrections to  $\kappa_V$  and  $\kappa_F$  from the integrating-out of heavier states. We will describe these corrections as leading to a new effective  $\xi_{eff}$  to be compared with the vanilla prediction for  $\xi$ .

The first possibility is that in models with an extra singlet pNGB (such as the  $SU(4)/Sp(4)$  and  $SU(5)/SO(5)$  cosets), the pNGB potential could induce a VEV for the singlet. This can modify  $\kappa_F$  and  $\kappa_V$  in two ways – firstly a VEV for the singlet  $\eta$  will induce singlet-doublet mixing between  $\eta$  and  $H$ . Singlet-doublet mixing (in the elementary case) and its effect on Higgs couplings was studied in detail in [57]. The fact that the  $H$  mixes with another scalar means that the couplings will be modified by a factor of  $\cos \theta$ , where  $\theta$  is the mixing angle between  $H$  and  $\eta$ . For small mixing angles:

$$\kappa_V \approx 1 - \frac{1}{2}\theta^2. \quad (2.14)$$

In this and in the following we are assuming that the singlet is heavier than the Higgs and that it makes sense to integrate it out. Generally, in the absence of further tuning, one expects the extra pNGBs to be heavier than the Higgs by a factor of  $\xi = v^2/f^2$ , since this is the amount by which the mass of the Higgs has to be tuned to satisfy electroweak

precision test [58]. Thus, in models with around 10% tuning, values for the extra pNGB masses of around 300 – 500 GeV are not unreasonable.

There could also be effects similar to those studied above, arising from higher-dimensional terms in the non-linear effective theory. As an example we will look at the  $SU(4)/Sp(4)$  model. The gauge boson coupling to the Higgs and  $\eta$  (the equivalent of equation (2.4)) will be (neglecting hypercharge)

$$\frac{H^2}{H^2 + \eta^2} \sin^2 \left( \frac{\sqrt{H^2 + \eta^2}}{f} \right) W_\mu^a W^{a\mu}. \quad (2.15)$$

As expected, there is no dimension-4 coupling of  $\eta$  to the  $SU(2)_L$  gauge bosons, but there are higher order terms involving  $\eta$  which could modify the  $hWW$  coupling if  $\eta$  gets a VEV. However one should also note that the kinetic term in (2.3) corrects the Higgs kinetic term:

$$\mathcal{L}_{kinetic} = \frac{\sin^2(v_\eta/f)}{v_\eta^2/f^2} (\partial_\mu H)^2 \approx (1 - \frac{1}{3}\xi_\eta) (\partial_\mu H)^2. \quad (2.16)$$

After canonically normalising the Higgs field and expanding around small values of  $\xi_\eta = v_\eta^2/f^2$  we find that the  $\mathcal{O}(\xi_\eta)$  correction to  $\kappa_V$  actually cancels. To leading order in  $\xi, \xi_\eta$  and  $\theta$  we have:

$$\kappa_V \approx 1 - \frac{1}{2}\xi - \frac{1}{2}\theta^2. \quad (2.17)$$

The correction due to the singlet VEV thus neatly “factorises” into the mass-mixing correction  $\mathcal{O}(\theta^2)$  plus the usual compositeness correction  $\mathcal{O}(\xi)$ . We can thus define a  $\xi_{eff} = \xi + \theta^2$ , such that  $\kappa_V \approx 1 - \xi_{eff}/2$ .

One finds a similar result for  $\kappa_F$ . The singlet VEV modifies  $\kappa_F$  from  $\approx 1 - \frac{3}{2}\xi$  to

$$\kappa_F \approx 1 - \frac{3}{2}\xi - \frac{1}{2}\theta^2, \quad (2.18)$$

and in this case our effective  $\xi_{eff} = \xi + \frac{1}{3}\theta^2$ .

In the regime where  $m_\eta$  and  $v_\eta$  are both  $\gg v$ , the mixing will be small and will scale approximately as

$$\theta^2 \sim \frac{v^2 v_\eta^2}{m_\eta^4} = \frac{1}{g_\eta^4} \xi \xi_\eta, \quad (2.19)$$

where we have related  $m_\eta$  to  $f$  via some coupling:  $m_\eta = g_\eta f$ .

The amount of tuning present in such a model was analysed in [59]. This coset was also investigated in a cosmological setting in [2, 60], where the singlet  $\eta$  plays the role of the inflaton. In such a scenario the size of the singlet VEV has important implications for the scale of inflation, and the mass-mixing of the inflaton would be important also for the process of reheating. Moreover, the singlet  $\eta$  and a non-zero value of  $\xi_\eta$  could be a key component of a solution to the matter-antimatter asymmetry in the Universe [61].

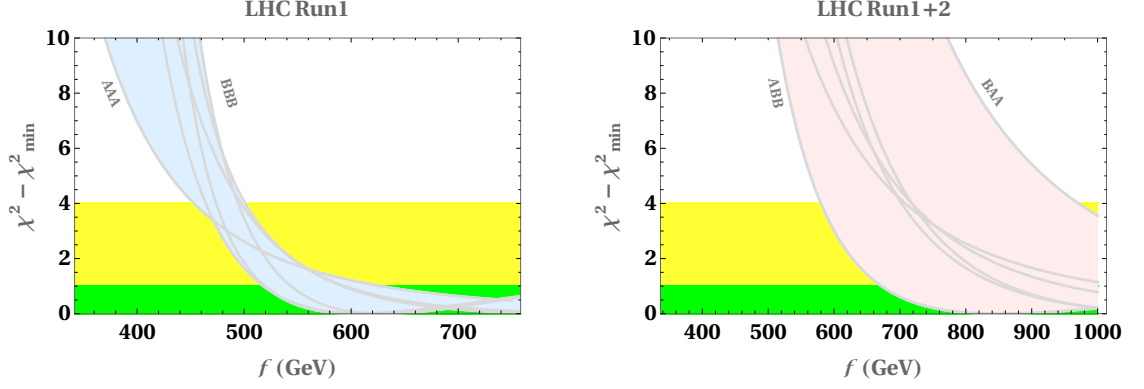


Figure 2.1:  $\chi(f)^2 - \chi_{\min}^2$  for the Run 1 (left) and combination of Run 1 and 2 (right) datasets. The lines correspond to different choices of fermion couplings  $\kappa_F^{A,B}$  for  $(\kappa_t, \kappa_b, \kappa_\tau)$ . For example, AAA indicates  $\kappa_t = \kappa_b = \kappa_\tau = \kappa_F^A$ .

If the value of  $\xi_{\text{eff}}$  were the same for all couplings (i.e. the modifications to  $\kappa_V$  and  $\kappa_{F_i}$  were the same), then the theory would resemble a CH model without any mixing, only with an apparent rescaling of  $f$ . However it is interesting to note that in the above case the inferred values of  $\xi_{\text{eff}}$  from the measurements of  $\kappa_V$  and  $\kappa_F$  are different, which would in principle allow us to experimentally distinguish between these two scenarios.

Another possibility is that the spontaneous breaking leads to another pNGB doublet of  $SU(2)_L$  (a composite two Higgs doublet model). In principle, explicit breaking effects could lead to a mixing between the two doublets. This possibility is discussed in [40, 41], and in a different context in [3], in which the two doublets appear from two different spontaneous breakings at different scales.

In this case we will obtain similar results to our expressions above for  $\xi_{\text{eff}}$ , with a correction from the mass-mixing at  $\mathcal{O}(\theta^2)$  that will be present in the elementary case, and the usual correction at  $\mathcal{O}(\xi)$  coming from higher dimensional operators (see [62] for a review of the elementary two Higgs doublet model, and [57] for an analysis of the Higgs EFT in such a scenario).

Since we have looked at tree-level corrections to  $\kappa_V$  and  $\kappa_F$  coming from new states in the composite sector, one should also talk about loop level modifications. In principle loops of scalar, fermionic and vector resonances of the strong sector can modify the Higgs couplings. These will arise from higher dimensional ( $d \geq 6$ ) operators in the effective theory, suppressed by factors of  $f^{4-d}$ .

## 2.4 Status after Run 2

In this section we study the impact of Run 1 LHC data on Composite Higgs models, as well as the improvement which results when adding the 13 TeV results recently released by the collaborations. In Table 3.1 we summarize the channels considered in the combination of Run 1 and 2 data from ATLAS and CMS, as well as indicate the coupling modifiers that one would obtain in Composite Higgs models, as discussed previously.

Channel	Refs.	$\kappa$ -factors
$ttH$ ( $H \rightarrow \gamma\gamma$ )	[63–65]	$\frac{\kappa_t^2 \kappa_\gamma^2}{\kappa_H^2}$
$ttH$ ( $H \rightarrow b\bar{b}$ )	[63]	$\frac{\kappa_t^2 \kappa_b^2}{\kappa_H^2}$
$ttH$ ( $H \rightarrow \tau^+ \tau^-$ )	[63]	$\frac{\kappa_t^2 \kappa_\tau^2}{\kappa_H^2}$
$ttH$ ( $H \rightarrow WW^*, H \rightarrow ZZ^*$ )	[63]	$\frac{\kappa_t^2 \kappa_V^2}{\kappa_H^2}$
$ggF$ ( $H \rightarrow \gamma\gamma$ )	[64, 65]	$\frac{\kappa_g^2 \kappa_\gamma^2}{\kappa_H^2}$
$ggF$ ( $H \rightarrow \tau^+ \tau^-$ )	[66]	$\frac{\kappa_g^2 \kappa_\tau^2}{\kappa_H^2}$
$ggF$ ( $H \rightarrow WW^*, H \rightarrow ZZ^*$ )	[67–69]	$\frac{\kappa_g^2 \kappa_Z^2}{\kappa_H^2}$
$HV$ ( $H \rightarrow b\bar{b}$ )	[70, 71]	$\frac{\kappa_V^2 \kappa_b^2}{\kappa_H^2}$
$VBF, HV$ ( $H \rightarrow \gamma\gamma$ )	[64, 65]	$\frac{\kappa_V^2 \kappa_\gamma^2}{\kappa_H^2}$
$VBF, HV$ ( $H \rightarrow WW^*, H \rightarrow ZZ^*$ )	[67, 69, 72]	$\frac{\kappa_V^4}{\kappa_H^2}$

Table 2.2: List of 13 TeV channels considered in the fit, with the corresponding  $\kappa$  modifiers. Note that the 7+8 TeV Run 1 data was included using the results of the combination of ATLAS and CMS data in Ref. [34].

The couplings of the Composite Higgs to gluons and photons,  $\kappa_g$  and  $\kappa_\gamma$ , are functions of the modifications of the couplings to fermions and gauge bosons, which appear at one-loop order, i.e.  $\kappa_g^2 = 1.06\kappa_t^2 + 0.01\kappa_b^2 - 0.07\kappa_b\kappa_t$  and  $\kappa_\gamma^2 = 1.59\kappa_V^2 + 0.07\kappa_t^2 - 0.66\kappa_V\kappa_t$  [34, 73]. The modification of the Higgs width,  $\kappa_H$  is also a function of the coupling modifiers,  $\kappa_H^2 \approx 0.57\kappa_b^2 + 0.25\kappa_V^2 + 0.09\kappa_g^2$ , see e.g. Ref. [34].

We then perform a  $\chi^2$  fit to the ATLAS and CMS data<sup>8</sup>, with the restriction  $\xi > 0$ .

The dependence of the  $\chi^2$  function with the scale of new physics  $f$  is shown in Fig. 2.1. The green and yellow bands correspond to the one- and two-sigma regions of the fit, and

<sup>8</sup>When two measurements of the same channel were available, we discarded the worse measurement, or kept both if they were of similar significance. Results from [74, 75] were considered but not included in the fit.

the left and right panels correspond to Run 1 and the combination of Run 1 and Run 2, respectively. Different choices of fermion representations  $\kappa_F^{A,B}$  (as shown in Table 2.1) lead to different  $\chi^2$  dependences.

The model-independent limit on  $f$  improves from 450 GeV (Run 1) to 600 GeV (Run 1+2) at 95% CL, and we see that the most constrained scenario is  $\kappa_t = \kappa_F^A$ ,  $\kappa_b = \kappa_\tau = \kappa_F^B$ . Moreover, one can see that the spread of limits on the scale  $f$  due to these fermion choices increases with the addition of more data. This is a signal that the data is increasingly sensitive to these choices, due to better determination of the Higgs couplings to the heavy fermions. To illustrate this point, assume that at some point in the future a deficit in one channel is observed, whereas other channels remain consistent with the SM. For example, assume that the signal strength of the  $ttH$  processes was found to be a third of the SM rate, whereas other processes involving the coupling of the Higgs to vector bosons remained consistent with the SM. In this case, certain representations for fermion embeddings of the top and bottom quarks would be preferred by data, see Fig. 2.2.

These limits on  $f$  should be compared with the limits of direct searches for new resonances. One would typically expect a set of new resonances, e.g. new massive  $W'$  and  $Z'$ , to appear at some scale related to  $f$ ,  $m_{W'} = g_\rho f$ , with  $g_\rho \lesssim \mathcal{O}(4\pi)$ . The value of  $g_\rho$  is an input to the effective theory, but can be obtained by performing a lattice simulation of the theory and investigating the spectrum of resonances. Its value depends on the specific pattern of breaking as well as the possible electroweak effects. As an indicator of the value of  $g_\rho$  in these kind of models, we draw attention to the work done in the coset  $SO(6)/SO(5)$  [76], and in others scenarios [77], where  $g_\rho$  was found to be  $\mathcal{O}(10)$ . In this case, a limit on  $f \sim 600$  GeV, would correspond to a  $Z'$  and  $W'$  in the multi-TeV scale, certainly competitive with direct searches for these resonances.

Besides vector resonances, one would expect a tower of fermion resonances, or techni-baryons. Typically, these techni-baryons are heavier than the vector bound states by a factor of  $N_{TC}$ , with  $N_{TC}$  the number of colours in the new strongly coupled sector [78, 79]. Hence, naively one would expect fermion resonances again in the multi-TeV scale. Yet, in most Composite Higgs models the mechanism of electroweak symmetry breaking depends on the existence of light techni-baryons (*top partners*) with masses of the order of  $f$ , contrary to the large- $N$  expectation. This mechanism is being tested by direct searches of heavy partners of the top, with recent Run 2 results already sensitive to the 1.2 TeV region [27], clearly more competitive than the indirect searches in Higgs data if one believed this is the correct mechanism in place. Note, though, that the mass of the top partner

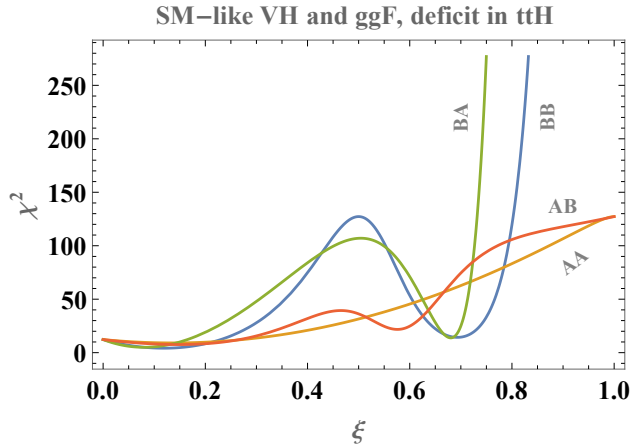


Figure 2.2:  $\chi(\xi)^2$  assuming a scenario where a deficit is found in  $ttH$  production channels, while other channels remain consistent with the SM. The labels correspond to different hypothesis of  $\kappa_F^{A,B}$  for  $(\kappa_t, \kappa_b)$ . In this case, the choice  $\kappa_t = \kappa_b = \kappa_F^B$  would be preferred by data. We assume a 20% uncertainty in these channels, except in  $gg \rightarrow H \rightarrow \gamma\gamma$  where a 10% accuracy is assumed.

is also linked to the amount of fine-tuning in these models. From this point of view the strong limits in top partners may lead one to consider alternative constructions, such as Composite Twin Higgs models [46, 47, 80, 81], or models involving the see-saw mechanism developed in [3]. In such models the top partners can be significantly heavier without introducing more fine-tuning.

## 2.5 Conclusions

In this paper we have summarised the structure of the Higgs couplings (parameterised by  $\kappa_V$  and  $\kappa_F$ ) in Composite Higgs models. Although different CH models have very different predictions for the UV theory and the spectrum of higher mass resonances, we have identified generic forms for  $\kappa_V$  and  $\kappa_F$  which hold for many different choices of the coset group and fermion representations.

We have also looked into tree level effects on these couplings coming from extra states. In particular we studied the interesting possibility that an extra singlet pNGB may acquire a VEV. The modifications to  $\kappa_V$  and  $\kappa_F$  are to leading order just a sum of the corrections in elementary singlet + doublet models, and the usual correction expected in composite models. The same can be said for the case in which the Higgs mixes with an extra doublet.

We combined the Run 1 and recent Run 2 LHC data to set limits on CH models, finding that different choices for fermion representations lead to a spread of limits but a lower bound on the scale  $f$  can be set to 600 GeV. We also discussed how an observed

deficit in a Higgs channel such as  $t\bar{t}H$  could pinpoint the type of CH model responsible for it.

## Acknowledgements

This work is supported by the Science Technology and Facilities Council (STFC) under grant number ST/J000477/1.

## Chapter 3

# Goldstone Inflation

### Abstract

Identifying the inflaton with a pseudo-Goldstone boson explains the flatness of its potential. Successful Goldstone Inflation should also be robust against UV corrections, such as from quantum gravity: in the language of the effective field theory this implies that all scales are sub-Planckian. In this paper we present scenarios which realise both requirements by examining the structure of Goldstone potentials arising from Coleman-Weinberg contributions. We focus on single-field models, for which we notice that both bosonic and fermionic contributions are required and that spinorial fermion representations can generate the right potential shape. We then evaluate the constraints on non-Gaussianity from higher-derivative interactions, finding that axiomatic constraints on Goldstone boson scattering prevail over the current CMB measurements. The fit to CMB data can be connected to the UV completions for Goldstone Inflation, finding relations in the spectrum of new resonances. Finally, we show how hybrid inflation can be realised in the same context, where both the inflaton and the waterfall fields share a common origin as Goldstones.



### 3.1 Introduction

The empirically well supported paradigm of cosmic inflation [82] has a hierarchy problem from the perspective of particle physics. Parameterised in terms of a slowly rolling scalar field, the scale of inflation (from CMB data [83]) is exceeded by the field excursion (given by the Lyth bound [84, 85]) by roughly two orders of magnitude:

$$\Lambda^4 = (1.88 \times 10^{16} \text{ GeV})^4 \left( \frac{r}{.10} \right) \quad \text{and} \quad \Delta\phi \geq M_p \sqrt{\frac{r}{4\pi}} \quad (3.1)$$

where  $r$  is the ratio of the tensor to the scalar power spectrum, and where  $M_p = 2.435 \times 10^{18} \text{ GeV}$  is the reduced Planck mass. Meeting both these conditions implies an exceptionally flat potential for the inflaton, which generically is radiatively unstable.

Natural Inflation (NI) [86, 87] offers a solution to this hierarchy problem by imposing a symmetry on the inflaton: the inflaton potential exhibits a shift symmetry  $\phi \rightarrow \phi + C$  with  $C$  a constant, and therefore could be protected from higher order corrections. The shift symmetry is realised by identifying the inflaton with the Goldstone boson (GB)  $\phi$  of a broken global symmetry  $G$  to its subgroup  $H$  ( $\phi \in G/H$ ). In turn, the GB obtains a potential through effects that render  $G$  inexact. The resulting degree of freedom is therefore not an exact Goldstone boson, but a *pseudo-Goldstone boson* (pGB). Different effects can lead to an inexact global symmetry; we reviewed the relevant mechanism in [88].

The original and most popular NI model has an axion as the inflaton, the GB of spontaneously broken Peccei-Quinn symmetry [86, 87]. The axion gets a potential through non-perturbative (instanton) effects. As shown in Ref. [89] these effects lead to the characteristic  $\cos(\phi/f)$  potential across models, where  $f$  is the scale at which  $G$  is broken. To obtain the famous NI model one adds a cosmological constant term to impose the phenomenological constraint  $V(\phi_{min}) = 0$ , to obtain,

$$V(\phi) = \Lambda^4 (1 + \cos \phi/f) \quad (3.2)$$

Alas, the original NI model can only be successfully reconciled with the data from CMB missions for superplanckian scales of the decay constant:  $f = \mathcal{O}(10M_p)$ . This is evidently a problem, because above the Planck scale one should expect a theory of Quantum Gravity (QG), and it is known that theories of QG in general do not conserve global symmetries [90]. Therefore one generically expects large contributions to the simple potential (3.2), as was shown recently in [91]. Thus, one may conclude that vanilla NI is not a good effective theory.<sup>1</sup>

---

<sup>1</sup>It is found that it is only possible to maintain control over the backreaction in very specific configurations, such as [92].

Different proposals have been made to explain the super-Planckian decay constant while maintaining the simple potential (3.2) and the explanatory power of the model. Among these are Extra-Natural inflation [93], hybrid axion models [94, 95], N-flation [96–98], axion monodromy [99] and other pseudo-natural inflation models in Supersymmetry [100]. These proposals usually focus on generating an effective decay constant  $f_{\text{eff}}$  in terms of model parameters, such that  $f_{\text{eff}} = \mathcal{O}(10M_p)$  is no longer problematic. Some of these models rely on a large amount of tuning or on the existence of extra dimensions, as 4D dual theories suffer from the same problems as the vanilla model.

In [88] we recognised that pGB inflation does not have to have an axion as the inflaton. There are other models which generate a natural inflaton potential, protected from radiative corrections by the same mechanism. In particular, we focussed on compact group structures and showed that one can find models<sup>2</sup> that fit the CMB constraints for a sub-Planckian symmetry breaking scale  $f$ .

For example, if the pGB field is coupled to external gauge bosons and fermions, a Coleman-Weinberg potential is generated for the inflaton. We demonstrated the general mechanism and gave a specific successful example inspired by the minimal Composite Higgs model MCHM<sub>5</sub> [102].

Here we develop a comprehensive approach to Goldstone Inflaton. In Sec. 3.2, we give a full analysis of the potentials that can be generated, and motivate that the potential that is uniquely expected to give successful single-field inflation is given by

$$V(\phi) = \Lambda^4 (C_\Lambda + \alpha \cos(\phi/f) + \beta \sin^2(\phi/f)). \quad (3.3)$$

In Sec. 3.3, we compare its predictions against the CMB data and find that the latter singles out a specific region in the parameter space. We comment on the fine-tuning necessary and show that one obtains a successful model with  $f < M_p$  at marginal tuning.

As the Goldstone inflaton is expected to have non-canonical kinetic terms, we give an analysis of the non-Gaussianity predictions. We show that the current bounds are comfortably evaded.

In Sec. 3.4, we further explore the region of parameter space that leads to successful inflation. The relations that we find by comparison with the Planck data give information about the form factors that parameterise the UV-theory. We comment on the scaling with momentum we expect from theoretical considerations. We finish with an analysis of the

---

<sup>2</sup>One can also consider non-compact groups such as space time symmetries. In [101] the authors consider broken conformal symmetry and showed that a dilaton inflaton can generate inflation with strictly sub-Planckian scales.

UV theory, in which we use QCD-tools to compute the relevant parameters and give a specific example in the approximation of light resonance dominance in Sec. 3.5. Finally, in the Appendices we give specific examples of single-field and hybrid inflation coming from Goldstone Inflation.

### 3.2 A successful Coleman-Weinberg potential

Our starting assumption is that the inflaton is a Goldstone boson, coming from the breaking of some global symmetry  $G \rightarrow H$ . We parameterise the Goldstone bosons using a non-linear sigma model

$$\Sigma(x) = \exp(iT^{\hat{a}}\phi^{\hat{a}}(x)/f), \quad (3.4)$$

where  $T^{\hat{a}}$  are the broken  $G/H$  generators,  $\phi^a(x)$  are the Goldstone fields, and  $f$  is the scale of spontaneous symmetry breaking<sup>3</sup> [21]. Under a  $G/H$  symmetry transformation the Goldstone bosons transform via a shift  $\phi^a(x) \rightarrow \phi^a + f\alpha^a$ , for some transformation parameters  $\alpha^a$ . This non-linear shift symmetry prevents the Goldstone fields from acquiring a tree-level potential. The inflaton can only get a potential if there are sources of explicit symmetry-breaking that will render  $G$  inexact. We list two possibilities:

1. If the inflaton is a composite object formed of strongly-interacting UV fermions, then explicit fermion mass terms could break the symmetry and give the inflaton a non-zero mass. This would be analogous to the pions of QCD, which acquire a mass from the explicit breaking of chiral symmetry due to the small up and down quark masses.
2. If the inflaton sector has couplings to particles that do not form complete representations of  $G$ , then loops of these ‘external’ particles will generate a Coleman-Weinberg potential for the inflaton.

Although 1. is an interesting possibility, in this paper we will explore 2., since the Coleman-Weinberg potential can be computed perturbatively (up to coefficients determined by strongly interacting dynamics).

A point worth noting is that, as of yet, we have not fixed the scale at which inflation occurs. The ‘external’ particles relevant to our calculation are those with masses close to, but below the scale of symmetry breaking  $\sim f$ . If inflation occurs near the TeV scale, we

---

<sup>3</sup>Here we assume the CCZW formalism. A different proposal relying on quark seesaw has been made recently (see for instance [103] and references therein); however, in this setup the periodicity of the Goldstone field is disguised and therefore we will stick to CCWZ.

would have to embed the SM gauge group and the heavy quarks into representations of  $G$ , since these particles would be expected to have the greatest contributions to the inflaton potential (just as in Composite Higgs models). If inflation occurs at the GUT scale  $\sim 10^{16}$  GeV, then our lack of knowledge of the high-scale particle spectrum means we can be more open-minded. In the following treatment we leave this question open, considering generic possibilities for the particle content.

That said, we will not consider the contribution from elementary scalars, our prime motivation being the unnaturalness of scalar masses much below the Planck scale. The only scalars appearing in our model will be those coming from the  $G/H$  breaking, with masses protected by the non-linear Goldstone symmetry.

We will work through in detail a scenario in which the strong sector has a global  $SO(N)$  symmetry which breaks to  $SO(N-1)$ .<sup>4</sup> This symmetry breaking gives rise to  $N-1$  massless Goldstone fields, one linear combination of which will play the role of the inflaton. We will assume that the symmetry-breaking VEV is in the fundamental representation:

$$\Sigma_0 = \langle \Sigma \rangle = \begin{pmatrix} 0 \\ 0 \\ \vdots \\ 1 \end{pmatrix}, \quad (3.5)$$

so that

$$\Sigma(x) = \exp(iT^{\hat{a}}\phi^{\hat{a}}(x)/f)\Sigma_0, \quad (3.6)$$

transforms as a fundamental of  $SO(N)$ .

If we take the unbroken symmetry  $SO(N-1)$  to be a gauge symmetry, we can gauge away  $N-2$  of the Goldstone fields (they give mass to  $N-2$  gauge bosons once the vacuum is misaligned), as we show pictorially in Fig. 3.1. This will leave us with one physical Goldstone field, which we identify with the inflaton. The same mechanism gives masses to the  $W^\pm$  and  $Z$  bosons in Composite Higgs models (see for example [19,28]). We can gauge a smaller subgroup of  $SO(N)$ , although this will leave more than one Goldstone degree of freedom. Some possibilities are explored in Appendix 3.6.

We now attempt to write down an effective Lagrangian containing couplings of the Goldstone fields to the  $SO(N-1)$  gauge bosons. A useful trick is to take the whole  $SO(N)$  global symmetry to be gauged, and only at the end of the calculation setting the unphysical  $SO(N)/SO(N-1)$  gauge fields to zero [24,55]. The most general effective

---

<sup>4</sup>Many of the results of this section generalise straightforwardly to  $SU(N) \rightarrow SU(N-1)$ .

Lagrangian involving couplings between  $\Sigma$  and  $SO(N)$  gauge bosons, in momentum space and up to quadratic order in the gauge fields, is

$$\mathcal{L}_{eff} = \frac{1}{2}(P_T)^{\mu\nu} [\Pi_0^A(p^2) \text{Tr}\{A_\mu A_\nu\} + \Pi_1^A(p^2) \Sigma^T A_\mu A_\nu \Sigma], \quad (3.7)$$

where  $A_\mu = A_\mu^a T^a$  ( $a = 1, \dots, N$ ) are the  $SO(N)$  gauge fields,  $P_T^{\mu\nu} = \eta^{\mu\nu} - q^\mu q^\nu / q^2$  is the transverse projector, and  $\Pi_{0,1}^A(p^2)$  are scale-dependent form factors, parameterising the integrated-out dynamics of the strong sector.

Taking an appropriate choice for the  $SO(N)$  generators and expanding out the matrix exponential in (3.6), we obtain:

$$\Sigma = \frac{1}{\phi} \begin{pmatrix} \phi^1 \sin(\phi/f) \\ \vdots \\ \phi^{N-1} \sin(\phi/f) \\ \phi \cos(\phi/f) \end{pmatrix}, \quad (3.8)$$

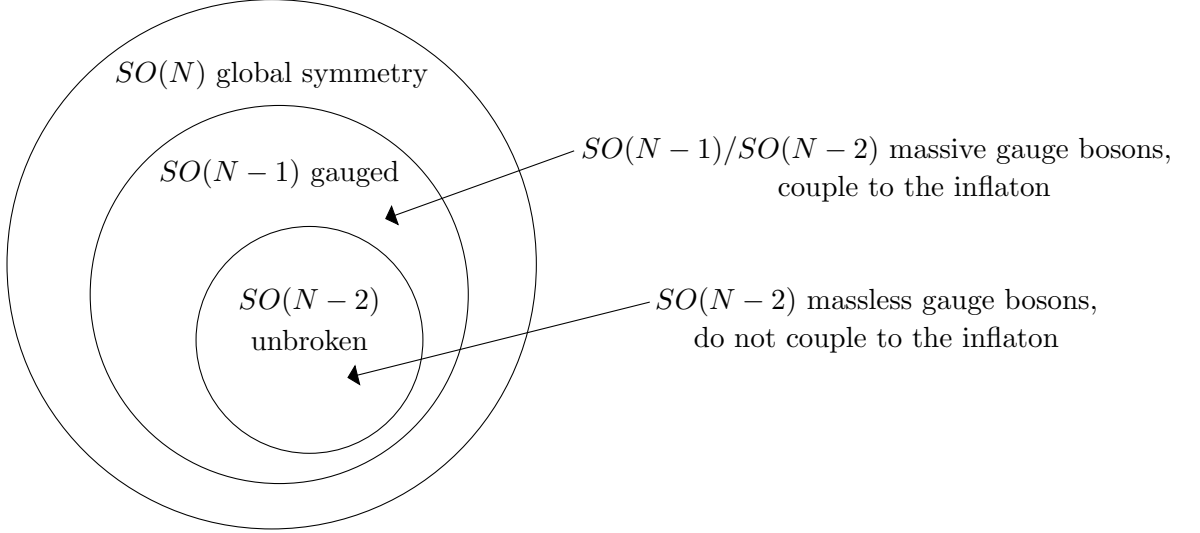
where  $\phi = \sqrt{\phi^{\hat{a}} \phi^{\hat{a}}}$ . With an  $SO(N-1)$  gauge transformation we can rotate the  $\phi^{\hat{a}}$  fields along the  $\phi^1$  direction, so that

$$\Sigma = \begin{pmatrix} \sin(\phi/f) \\ \vdots \\ 0 \\ \cos(\phi/f) \end{pmatrix}. \quad (3.9)$$

The remaining  $N-2$  degrees of freedom give masses to as many gauge bosons. Expanding out all the terms in (3.7) and setting the  $SO(N)/SO(N-1)$  gauge fields to zero as promised, we obtain:

$$\mathcal{L}_{eff} = \frac{1}{2}(P_T)^{\mu\nu} \left[ \Pi_0^A(p^2) + \frac{1}{2} \Pi_1^A(p^2) \sin^2(\phi/f) \right] A_\mu^{\tilde{a}} A_\nu^{\tilde{a}}, \quad (3.10)$$

where  $A_\mu^{\tilde{a}}$  are the  $SO(N-1)/SO(N-2)$  gauge fields. The remaining (massless)  $SO(N-2)$  gauge fields do not couple to the inflaton (See Fig. 3.1).

Figure 3.1: Subgroups of the global  $SO(N)$  symmetry.

Using this Lagrangian we can derive a Coleman-Weinberg potential for the inflaton [26]:

$$V = \frac{3(N-2)}{2} \int \frac{d^4 p_E}{(2\pi)^4} \log \left[ 1 + \frac{1}{2} \frac{\Pi_1^A}{\Pi_0^A} \sin^2(\phi/f) \right], \quad (3.11)$$

where  $p_E^2 = -p^2$  is the Wick-rotated Euclidean momentum. This result can be understood as the sum over the series of diagrams:

in which the inflaton field is treated as a constant, classical background. The factor of  $3(N-2)$  comes from the 3 degrees of freedom of each of the massive  $SO(N-1)/SO(N-2)$  gauge bosons, any of which may propagate around the loop.

As discussed in [24, 55],  $\Pi_1$  can be thought of as an order parameter, which goes to zero in the symmetry-preserving phase at high momenta. Provided the ratio  $\Pi_1^A/\Pi_0^A$  decreases fast enough, the integral in (3.11) will converge. We can approximate the potential by expanding the logarithm at leading order. This approximation is equivalent to assuming the dominant contribution comes from diagrams with one vertex, and that higher order

diagrams are suppressed.<sup>5</sup> This gives

$$V(\phi) = \gamma \sin^2(\phi/f), \quad (3.14)$$

where

$$\gamma = \frac{3(N-2)}{4} \int \frac{d^4 p_E}{(2\pi)^4} \left( \frac{\Pi_1^A}{\Pi_0^A} \right). \quad (3.15)$$

It is worth pointing out that gauge contributions generically lead to a  $\sin^2$  type potential at leading order. A  $\sin^2$  potential suffers from the same problems as the cosine of Natural Inflation – it is only flat enough for superplanckian values of  $f$ .

However, we should also include contributions from external fermions. Just as with the gauge case, the easiest way to write down a general effective Lagrangian is to assume that the fermions are embedded within representations of the full symmetry group  $SO(N)$ . First we try embedding two Dirac fermions (one left and one right handed) in fundamental  $SO(N)$  representations:

$$\Psi_L = \begin{pmatrix} \psi_L \\ \vdots \\ 0 \end{pmatrix}, \quad \Psi_R = \begin{pmatrix} 0 \\ \vdots \\ \psi_R \end{pmatrix}. \quad (3.16)$$

The reader will note that fermions placed anywhere other than the first and  $N^{th}$  entries of these fundamentals will not contribute to the inflaton potential, since they will not couple to the rotated  $\Sigma$  (3.9). We place  $\psi_L$  and  $\psi_R$  in two separate fundamentals for the sake of generality – this arrangement will avoid cancellations between terms that would occur if we used the embedding

$$\begin{pmatrix} \psi_L \\ \vdots \\ \psi_R \end{pmatrix}. \quad (3.17)$$

The most general  $SO(N)$  invariant effective Lagrangian we can write down, up to quadratic order in the fermion fields, is

$$\mathcal{L}_{eff} = \sum_{r=L,R} \bar{\Psi}_r^i \not{p} [\Pi_0^r(p) \delta_{ij} + \Pi_1^r(p) \Sigma_i \Sigma_j] \Psi_r^j + M(p) \bar{\Psi}_L^i \Sigma_i \Sigma_j \Psi_R^j + h.c., \quad (3.18)$$

which can be rewritten:

$$\begin{aligned} \mathcal{L}_{eff} = & \bar{\psi}_L \not{p} [\Pi_0^L(p) + \Pi_1^L(p) \sin^2(\phi/f)] \psi_L + \bar{\psi}_R \not{p} [\Pi_0^R(p) + \Pi_1^R(p) \cos^2(\phi/f)] \psi_R \\ & + M(p) \sin(\phi/f) \cos(\phi/f) \bar{\psi}_L \psi_R + h.c. \end{aligned} \quad (3.19)$$

---

<sup>5</sup>Equivalently

$$\int \frac{d^4 p_E}{(2\pi)^4} \left( \frac{\Pi_1^A}{\Pi_0^A} \right) \gg \int \frac{d^4 p_E}{(2\pi)^4} \frac{1}{2} \left( \frac{\Pi_1^A}{\Pi_0^A} \right)^2 \gg \int \frac{d^4 p_E}{(2\pi)^4} \frac{1}{3} \left( \frac{\Pi_1^A}{\Pi_0^A} \right)^3 \gg \dots \quad (3.13)$$

If the form factors behave as described in Section 3.5, then this is a reasonable approximation.

We can derive the Coleman-Weinberg potential using the formula

$$V = -\frac{1}{2}N_c \int \frac{d^4 p_E}{(2\pi)^4} \text{Tr} \left[ \log \left( \mathcal{M} \mathcal{M}^\dagger \right) \right], \quad (3.20)$$

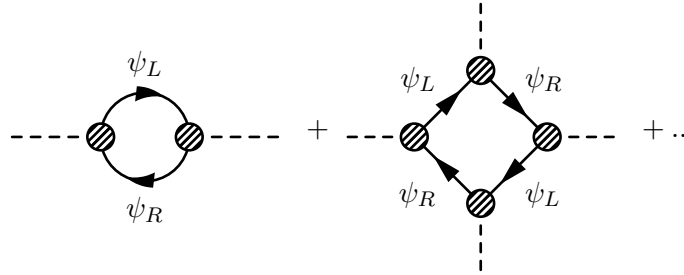
which is correct up to terms independent of  $\phi$ . Here  $N_c$  is the number of fermion colours and

$$\mathcal{M}_{ij} = \frac{\partial^2 \mathcal{L}}{\partial \psi^i \partial \bar{\psi}^j}, \quad (3.21)$$

for all fermions  $\psi^i$ . We obtain, up to terms independent of  $\phi$ :

$$V = -2N_c \int \frac{d^4 p_E}{(2\pi)^4} \log \left[ 1 + \frac{\Pi_1^L}{\Pi_0^L} \sin^2(\phi/f) + \frac{\Pi_1^R}{\Pi_0^R} \cos^2(\phi/f) + \frac{\Pi_1^L}{\Pi_0^L} \frac{\Pi_1^R}{\Pi_0^R} \sin^2(\phi/f) \cos^2(\phi/f) + \frac{M^2}{p_E^2 \Pi_0^L \Pi_0^R} \sin^2(\phi/f) \cos^2(\phi/f) \right]. \quad (3.22)$$

The presence of the  $\sin^2 \cos^2$  function inside the logarithm is essentially due to the fact that there are loops in which both  $\psi_L$  and  $\psi_R$  propagate. We have, among other diagrams, the series:



$$+ \dots \quad (3.23)$$

This series includes diagrams with  $2n$  vertices (compare to (3.12), which sums over diagrams with  $n$  vertices). Thus the resummation leads to a higher order term in the argument of the log. Again we can expand the logarithm at first order to get a potential of the form:

$$V(\phi) = \alpha \sin^2(\phi/f) + \beta \sin^2(\phi/f) \cos^2(\phi/f). \quad (3.24)$$

This potential has a very flat region for  $\alpha \simeq \beta$ , the flat region being a maximum (minimum) for  $\beta > 0$  ( $\beta < 0$ ). For realistic inflation we require the flat region to be a local maximum, so that the inflaton can roll slowly down the potential. However, since we expect the  $\Pi_0$  form factors to be positive (see, for example [104]), the expansion of the  $\log^6$  gives a *negative* value for  $\beta$ . The gauge contribution – being of the form  $\sin^2(\phi/f)$  – will not help matters.

Therefore we turn to the next simplest option: embedding the fermions in *spinorial* representations of  $SO(N)$ . Spinors of  $SO(N)$ , for odd  $N$ , have the same number of

---

<sup>6</sup>Note that the  $(\Pi_1^L \Pi_1^R)/(\Pi_0^L \Pi_0^R)$  term cancels other terms at next order in the expansion, so does not contribute to the potential.



components as spinors of  $SO(N-1)$ . The extra gamma matrix  $\Gamma^N$  is the chiral matrix, which in the Weyl representation is the only diagonal gamma matrix. Spinors of  $SO(N)$  are built from two spinors of  $SO(N-2)$  in the same way that Dirac spinors are constructed using two Weyl spinors. We denote these  $SO(N-2)$  spinors  $\chi_{L,R}$ , and embed the fermions as follows:

$$\chi_{L,R} = \begin{pmatrix} \psi_{L,R} \\ 0 \\ \vdots \end{pmatrix}, \quad (3.25)$$

and construct the full  $SO(N)$  spinors thus:

$$\Psi_L = \begin{pmatrix} \chi_L \\ 0 \end{pmatrix}, \quad \Psi_R = \begin{pmatrix} 0 \\ \chi_R \end{pmatrix}. \quad (3.26)$$

This embedding is chosen so as to ultimately give a coupling between  $\psi_L$  and  $\psi_R$  – other embeddings that achieve this will lead to the same eventual result. The  $SO(N)$  invariant effective Lagrangian takes the form

$$\mathcal{L}_{eff} = \sum_{r=L,R} \bar{\Psi}_r^i \not{p} [\Pi_0^r(p) \delta_{ij} + \Pi_1^r(p) \Gamma_{ij}^a \Sigma^a] \Psi_r^j + M(p) \bar{\Psi}_L^i \Gamma_{ij}^a \Sigma^a \Psi_R^j + h.c., \quad (3.27)$$

where  $\Gamma^a$  are the Gamma matrices of  $SO(N)$ . If we take

$$\Gamma^1 = \begin{pmatrix} 0 & I \\ I & 0 \end{pmatrix}, \quad \Gamma^N = \begin{pmatrix} I & 0 \\ 0 & -I \end{pmatrix} \quad (3.28)$$

this can be expanded to give:

$$\begin{aligned} \mathcal{L}_{eff} = & \bar{\psi}_L \not{p} [\Pi_0^L(p) + \Pi_1^L(p) \cos(\phi/f)] \psi_L + \bar{\psi}_R \not{p} [\Pi_0^R(p) - \Pi_1^R(p) \cos(\phi/f)] \psi_R \\ & + M(p) \sin(\phi/f) \bar{\psi}_L \psi_R + h.c. \end{aligned} \quad (3.29)$$

Combined with the gauge contribution, this will lead to the potential:

$$V(\phi) = \alpha \cos(\phi/f) + \beta \sin^2(\phi/f), \quad (3.30)$$

where

$$\alpha = -2N_c \int \frac{d^4 p_E}{(2\pi)^4} \left( \frac{\Pi_1^L}{\Pi_0^L} - \frac{\Pi_1^R}{\Pi_0^R} \right), \quad \beta = \int \frac{d^4 p_E}{(2\pi)^4} \left( \frac{3(N-2)}{4} \frac{\Pi_1^A}{\Pi_0^A} - 2N_c \frac{M^2}{p_E^2 \Pi_0^L \Pi_0^R} \right). \quad (3.31)$$

This potential has a flat maximum for  $\alpha \simeq 2\beta$ ,  $\beta > 0$ . The gauge contribution can now give us a positive value for  $\beta$ . Thus, for a region of parameter space, this is a viable inflationary potential.

Including more fermions in our model will lead to a wider class of diagrams contributing to the Coleman-Weinberg potential. If we expand consistently to first order in  $\Pi_1/\Pi_0$  and  $(M/\Pi_0)^2$  however, the only terms that appear at leading order will be those coming from diagrams in which only a single fermion, or an alternating pair of fermions, propagates around the loop. Equation (3.30) will therefore be the generic leading order result, although the coefficients will be modified. In particular,  $\alpha$  will be given generally by

$$\alpha = -2N_c \int \frac{d^4 p_E}{(2\pi)^4} \left( \sum_i (-1)^{a_i} \frac{\Pi_1^i}{\Pi_0^i} \right), \quad (3.32)$$

where  $a_i = 0$  if  $\psi_i$  is embedded in the upper half of an  $SO(N)$  spinor, and  $a_i = 1$  if  $\psi_i$  is embedded in the lower half.

We should also consider whether including NLO terms in the log expansion changes any of the above conclusions. Assuming that the log expansion is valid, we expect the NLO terms to be suppressed. A small  $\sin^4(\phi/f)$  or  $\cos(\phi/f)\sin^2(\phi/f)$  addition to the potential will only have the effect of changing slightly the conditions on the coefficients. For example, the potential

$$V(\phi) = \alpha \cos(\phi/f) + \beta \sin^2(\phi/f) + \delta \cos(\phi/f) \sin^2(\phi/f), \quad (3.33)$$

has the flatness condition  $\alpha = 2(\beta + \delta)$ .

To satisfy the phenomenological constraint that the inflaton potential should be zero at its minimum  $V(\phi_{min}) = 0$ , we now insert a constant term  $C_\Lambda$  by hand:

$$V(\phi) = C_\Lambda + \alpha \cos(\phi/f) + \beta \sin^2(\phi/f). \quad (3.34)$$

In this case,  $C_\Lambda = \alpha$ . As conventional when writing inflaton potentials we may factor out a scale  $\Lambda^4$  to obtain (3.3), with a redefinition of the coefficients  $\alpha$  and  $\beta$ .

The result that fermions in *fundamental* representations cannot induce a satisfactory inflation potential holds generically for any group, for precisely the reasons outlined above. It is for this reason that we did not consider  $SU(N)$  symmetries, since the only single-index representations of  $SU(N)$  are fundamental (or anti-fundamental) representations. Embedding fermions in spinorial representations will generally lead, at first order, to a potential of the form (3.30). Since spinorial representations only exist in  $SO(N)$ , we conclude that an  $SO(N)$  symmetry of the strong sector is the simplest and most natural way to generate a realistic inflaton potential. Isomorphisms such as  $SO(6) \simeq SU(4)$  and  $SO(4) \simeq SU(2) \times SU(2)$  allows us to extend this result a little further. For example, embedding fermions in a vector of  $SO(4)$  should lead to the same result as fermions embedded in a  $(2, 2)$  of  $SU(2) \times SU(2)$ .

### 3.3 Constraints from Inflation

After our discussion of the general structure of the inflaton potential, let us discuss the restrictions coming from inflation. We list some potentials that can give rise to inflation in Table 3.1.

We parameterise the flatness of the potential as usual in the slow roll approximation (SRA). That is, we require  $\epsilon \ll 1$  and  $\eta \ll 1$ , where  $\epsilon$  and  $\eta$  are here given by

$$\epsilon = \frac{M_p^2}{2} \left( \frac{V'(\phi)}{V(\phi)} \right)^2 \quad \text{and} \quad \eta = M_p^2 \frac{V''(\phi)}{V(\phi)}. \quad (3.35)$$

To simplify our expressions, in this section we work in units of reduced Planck mass  $M_p$ ; that is, we will rescale our parameters  $\phi \rightarrow \frac{\phi}{M_p}$  and  $f \rightarrow \frac{f}{M_p}$ .

The number of e-foldings in the slow-roll approximation is then given by

$$N = \frac{1}{\sqrt{2}} \int_{\phi_E}^{\phi_I} \frac{1}{\sqrt{\epsilon}} \quad (3.36)$$

where  $\phi_E$  is fixed as the field value for which either  $\epsilon = 1$  or  $\eta = 1$ , in other words, the field value for which the SRA breaks down. In our models slow roll breaks down by the second condition. Here and in the following we conservatively choose  $N = 60$  for our predictions, and this allows us to find the initial condition for  $\phi$ .

We compare the predictions of our model and the CMB data for the spectral tilt and the tensor-to-scalar ratio, which can be expressed in the SRA as

$$n_s = 1 + 2\eta - 6\epsilon \quad (3.37)$$

$$r = 16\epsilon \quad (3.38)$$

respectively.

A generic potential for a pseudo-Goldstone boson would contain powers of periodic functions,  $c_\phi = \cos \phi/f$  and  $s_\phi = \sin \phi/f$ , which we parametrize as

$$V(\phi) = \Lambda^4 (C_\Lambda + \sum_n \alpha_n c_\phi^n + \beta_n s_\phi^n) \quad (3.39)$$

The derivatives of this potential are again proportional to the same periodic functions. Roughly speaking, the flatness of the potential can be achieved in two ways. One possibility is setting the argument,  $\phi/f$ , to be very small (modulo  $2\pi$ ) as in the Natural Inflation scenario. As the fluctuations of the inflaton can be large, this condition typically implies  $f \gtrsim M_p$ , hence spoiling the predictivity of the model.

Model	$ \tilde{\beta}  =  \beta/\alpha $	$\beta/ \beta $	$C_\Lambda$ (pheno)
$V = \Lambda^4 \left( C_\Lambda + \alpha \cos \frac{\phi}{f} + \beta \sin \frac{\phi}{f} \right)$	Like vanilla NI: no solution for $f \leq M_p$	$+/-$	$C_\Lambda = \sqrt{\alpha^2 + \beta^2}$
$V = \Lambda^4 \left( C_\Lambda + \alpha \cos \frac{\phi}{f} + \beta \sin^2 \frac{\phi}{f} \right)$ $= \Lambda^4 \left( \tilde{C}_\Lambda + \alpha \cos \frac{\phi}{f} - \beta \cos^2 \frac{\phi}{f} \right)$	$\lesssim 1/2$	$+$	$C_\Lambda = \alpha$ $\tilde{C}_\Lambda = \alpha + \beta$
$V = \Lambda^4 \left( C_\Lambda + \alpha \sin^2 \frac{\phi}{f} + \beta \sin^2 \frac{\phi}{f} \cos^2 \frac{\phi}{f} \right)$ $= \Lambda^4 \left( \bar{C}_\Lambda - \alpha \cos^2 \frac{\phi}{f} + \beta \sin^2 \frac{\phi}{f} \cos^2 \frac{\phi}{f} \right)$ $= \Lambda^4 \left( C_\Lambda + (\alpha + \beta) \sin^2 \frac{\phi}{f} - \beta \sin^4 \frac{\phi}{f} \right)$ $= \Lambda^4 \left( \bar{C}_\Lambda + (\beta - \alpha) \cos^2 \frac{\phi}{f} - \beta \cos^4 \frac{\phi}{f} \right)$	$\lesssim 1/2$	$+$	$C_\Lambda = \alpha$ $\bar{C}_\Lambda = 2\alpha$

Table 3.1: *Goldstone models for inflation:* Trigonometric inflationary potentials, grouped by equivalence upon a rotation in parameter space.

Another possibility, and that is what we pursue here, is to look for models with  $f < M_p$ , which in turn implies that two oscillating terms contribute to the flatness of the potential. This may seem like it would introduce fine-tuning in the model, but in the next section we quantify that tuning, finding it is milder than e.g. Supersymmetry with TeV scale superpartners.

Note that different models are equivalent from a cosmological perspective and can be transformed into each other by a rotation in parameter space. We list these redefinitions of the parameters and the cosmological constant in Table 3.1 as well.

In the limit that the ratio  $\tilde{\beta} = \beta/\alpha$  is  $\pm 1/2$ , the potential is exactly flat at the origin and the spectrum is scale-invariant, i.e.  $n_s = 1$  as shown in Fig. 3.2.

As the Planck data indicates a small deviation from scale invariance, we expect a small deviation of  $\tilde{\beta}$  with respect to  $1/2$ . We find that the smaller  $f$  compared to  $M_p$ , the closer  $\tilde{\beta}$  must be to the values in the table. The deviation  $\delta\tilde{\beta} = 1/2 - \beta$  is then

$$1 \times 10^{-2} \left( \frac{f}{M_p} \right)^2 < \delta\tilde{\beta} < 2 \times 10^{-2} \left( \frac{f}{M_p} \right)^2 \quad (3.40)$$

for all models in the table, but most importantly the model motivated in the previous section (3.34).

This is the range of  $\tilde{\beta}$  for which the model is compatible with the Planck data, as we plot in Fig. 3.3. for the well motivated example  $V = \Lambda^4 (C_\Lambda + \alpha \cos \phi/f + \beta \sin^2 \phi/f)$ . Our models predict negligible tensors, so the measurement of  $r$  imposes no constraint on

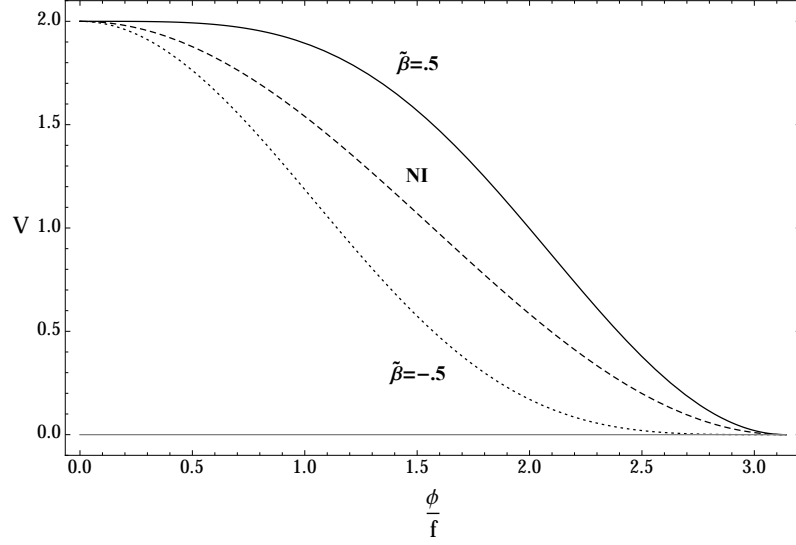


Figure 3.2: *Form of the potential*: Shape of the potential for  $\tilde{\beta} = \pm 1/2$  respectively. Different values will interpolate between these extreme cases. We show the shape of the vanilla NI (3.2) for comparison. The height of the potential is normalised to  $\Lambda$ .

$\tilde{\beta}$ . In fact, the tensor to scalar ratio will scale as

$$r \propto \left( \frac{f}{M_p} \right)^4 \quad (3.41)$$

such that the lower the symmetry breaking scale, the smaller the predicted tensor modes are.

The scale of inflation can be found from the amplitude of the scalar power spectrum, as measured by Planck [83],

$$A_s = \frac{\Lambda^4}{24\pi^2 M_p^4 \epsilon} = \frac{e^{3.089}}{10^{10}} \quad (3.42)$$

where  $\epsilon = r/16$  is the first slow roll parameter. For our case this implies

$$\Lambda_{inf} \approx 10^{15} \left( \frac{f}{M_p} \right) \text{ GeV}. \quad (3.43)$$

It is seen that  $\Lambda_{inf}$  is expected to be of order of the GUT scale, but can be lower if we allow for tuning. The symmetry breaking should occur before the onset of inflation, and therefore the scale  $f$  is expected to lie in the interval  $\Lambda_{inf} < f < M_p$ . Indeed, from the above relation, it is seen that  $\Lambda_{inf} \approx 10^{-3} f$ . Lowering the scale  $f$  as a result of more tuning thus directly results in lowering the scale inflation; for example, the model predicts  $f \approx M_{GUT} \rightarrow \Lambda_{inf} \approx 10^{12} \text{ GeV}$  for  $\delta\tilde{\beta} \approx 10^{-6}$ . We will quantify the tuning in the model more precisely in the next section.

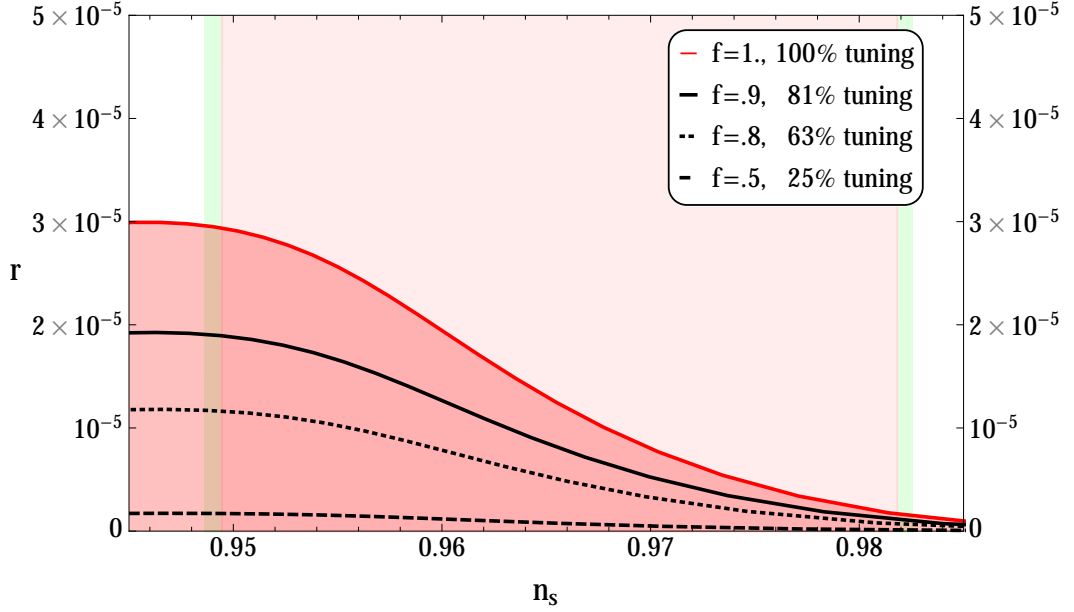


Figure 3.3: *Model predictions:* Parameters  $n_s$  and  $r$  plotted against the Planck 2015 data [83] for the model (3.34) for  $f = M_p$  (red upper bound). For lower values  $f < M_p$ ,  $r \rightarrow 0$  (shaded region).

### 3.3.1 Fine-tuning

One may note that the specific relationship between  $\alpha$  and  $\beta$  in the model described above requires one to fine-tune it. Here we quantify the amount of fine-tuning that one will typically expect.

Defining tuning as is customary in Particle Physics [105, 106], we have

$$\Delta = \left| \frac{\partial \log n_s}{\partial \log \tilde{\beta}} \right| = \left| \frac{\tilde{\beta}}{n_s} \frac{\partial n_s}{\partial \tilde{\beta}} \right| \approx [1.02 - 1.05] \left( \frac{f}{M_p} \right)^{-2} \quad (3.44)$$

This relation is not unexpected because for large  $f > M_p$  the potential will very flat over a large field range  $\Delta\phi$ , and this flatness is not sensitive to the specific value of  $\tilde{\beta}$ . For  $f < M_p$  one needs a (partial) cancelation in  $\alpha$  and  $\beta$ , at the cost of fine-tuning.

Then we can define the percentage of tuning as

$$\text{Percentage tuning} = \frac{100}{\Delta} \% \approx 95 \left( \frac{f}{M_p} \right)^2 \%$$

It is seen in particular that if we take the upper bound  $f = M_p$  seriously, the minimal tuning is at 95%. In Fig. 3.4 we plot the tuning  $\Delta$  as defined in (3.44) for the model at hand, (3.3). It is seen that for  $M_p/10 \lesssim f < M_p$  one expects no tuning below the percent level. One should note that  $f < 10^{-2}M_p \approx M_{GUT}$  is not expected, as the symmetry breaking pattern should occur before the onset of inflation.

One can compare this amount of tuning with the one required to avoid the destabilization of the electroweak scale in Supersymmetry. For example, stops at 1 TeV

require a much worse fine-tuning, at the level of 1% [107].

It is also noteworthy that the tuning necessary in the other models in Table 3.1 will be very similar to the tuning in  $V = \Lambda^4 (C_\Lambda + \alpha \cos \phi/f + \beta \sin^2 \phi/f)$ .

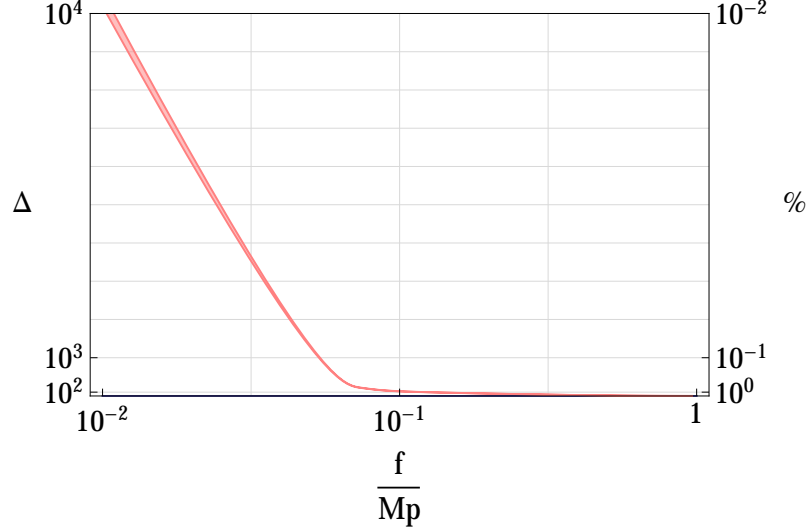


Figure 3.4: *Tuning*: The parameter  $\Delta$  as defined above for  $V = \Lambda^4 (C_\Lambda + \alpha \cos \phi/f + \beta \sin^2 \phi/f)$ . Outside of the pink zone the spectral index  $n_s$  predicted by the model is incompatible with the Planck data ( $n_s < .948$  above the region,  $n_s > .982$  below).

### 3.3.2 Non-Gaussianity and its relation to Goldstone scattering

Even before switching on the Coleman Weinberg potential, Goldstone bosons interact with themselves through higher-order derivative terms. Indeed, consistent with the shift symmetry, one can write terms containing a number of derivatives of the field,

$$\mathcal{L} = \sum_n \frac{c_n}{f^{2n-4}} X^n, \text{ with } X = \frac{1}{2} \partial_\mu \Sigma \partial^\mu \Sigma^\dagger \quad (3.45)$$

The first order term ( $n = 1$ ) is the usual kinetic term, whereas any other term ( $n \geq 2$ ) would involve interactions of  $2n$  pions. This expansion is called in the context of Chiral Perturbation Theory [108–110] as order  $\mathcal{O}(p^n)$  in reference to the number of derivatives involved. Goldstone self-interactions appear at order  $\mathcal{O}(p^4)$ .

Alongside the Coleman-Weinberg potential we derived in the previous section, the derivative self-interactions are relevant for inflation as well, as a nontrivial speed of sound arises from a non-canonical kinetic term. Specifically, the sound speed is a parameterisation of the difference of the coefficients of the spatial and temporal propagation terms for the Goldstone bosons  $\phi$ :

$$\mathcal{L} \ni (\partial_t \phi)^2 - c_s^2 (\partial_i \phi)^2 \quad (3.46)$$

This difference arises from higher dimensional kinetic terms  $X^n$  and the fact that inflation breaks Lorentz invariance. This can of course already be seen from the metric,

$$ds^2 = (dt)^2 - a(t)^2(dx_i)^2 \quad \rightarrow \quad g_{00} \neq g_{ii} \quad (3.47)$$

The speed of sound is then given by

$$c_s^2 = \left( 1 + 2 \frac{X \mathcal{L}_{XX}}{\mathcal{L}_X} \right)^{-1} \quad (3.48)$$

where  $\mathcal{L}_X$  and  $\mathcal{L}_{XX}$  denote the first and the second derivative of the Lagrangian with respect to  $X$  respectively, and where  $c_s$  is expressed in units of the speed of light. It is immediately seen that models with a canonical kinetic term predict  $c_s = 1$ . The background equations of motion can be used to relate coefficients to the Hubble expansion parameter,

$$X \mathcal{L}_X = \dot{H} M_p^2 \approx c_1 f^4 \quad (3.49)$$

To second order, the kinetic term will have the form<sup>7</sup>

$$\mathcal{L}_2 = \frac{M_p^2 \dot{H} + M_p^2 \dot{H} (c_s - 1)}{f^4} (\partial_t \phi)^2 = \frac{M_p^2 \dot{H} c_s}{f^4} (\partial_t \phi)^2 \quad (3.50)$$

Canonically normalising the kinetic term thus implies,

$$f^4 = 2 \dot{H} M_p^2 c_s \quad (3.51)$$

These higher order derivatives are also constrained by arguments of unitarity, analyticity and crossing symmetry of Goldstone scattering amplitudes such as shown in Fig. 3.5,

$$\phi(p_1) \phi(p_2) \rightarrow \phi(p_3) \phi(p_4) . \quad (3.52)$$

This scattering amplitude must be a function of the Mandelstam parameters  $s$ ,  $t$  and  $u$ , e.g.  $s = (p_1 + p_2)^2 = (p_3 + p_4)^2$ .<sup>8</sup> This amplitude  $A(s, t, u)$  must be analytical in the complex  $s$  plane, except for branch cuts (due to unitarity) and isolated points (due to the possible exchange of a resonance) [113–116]. Unitarity then implies the existence of a branch at some position  $s \geq s_0$ . Similarly, other branch crossings can be obtained by using crossing symmetry. Using these arguments, one can show that the amplitude would be non-analytical for  $s > 4m_\phi^2$ , where  $m_\phi$  is the mass of the pseudo-Goldstone. Moreover, analyticity restricts the dependence of the amplitude on  $s$ , namely

$$\frac{d^2}{ds^2} A(s, t, u) \geq 0 \quad (3.53)$$

<sup>7</sup>Here we use the expansions  $\mathcal{L} \in (X \mathcal{L}_X + 2X^2 \mathcal{L}_{XX}) (\partial_t \phi)^2 / f^4$  and  $c_s - 1 \approx \frac{X \mathcal{L}_{XX}}{\mathcal{L}_X}$ .

<sup>8</sup>In this simplified analysis we have neglected the curvature of space-time. Various issues related to the curvature, and the relevant assumptions one should make to obtain the positivity constraint were discussed in [111] and [112].



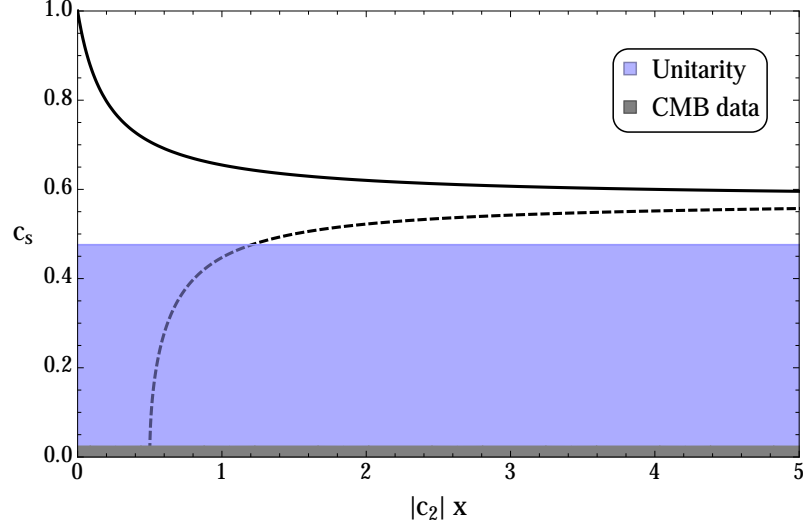


Figure 3.5: *Sound speed*: Predictions for  $c_2 x$ . In dark grey the Planck bound; the shaded region indicates the perturbativity bound. The continuous lines are the predictions for  $c_2 > 0$ , which is relevant for our model as discussed in the text. We also indicate the hypothetical situation  $c_2 < 0$  with dashed curves. It is seen that the prediction approaches the asymptote  $c_s = 1/\sqrt{3}$  for large  $c_2$ , as expected from (3.55). Note that we plot against the absolute value  $|c_2|x$ .

where  $s$ ,  $t$  and  $u$  are restricted to the physical region, e.g.  $s \leq 4m_\phi^2$ . This translates into bounds for the coefficients of the Lagrangian in (3.45). At leading order in the Goldstone interactions,

$$\mathcal{L}^{(p^4)} = c_2 f^{-4} (\partial_\mu \phi^\dagger \partial^\mu \phi)^2 \quad (3.54)$$

the aforementioned conditions lead to a bound for  $c_2$ . In particular,  $c_2$  must be positive and larger than some function of the Goldstone mass.<sup>9</sup>

The positivity of  $c_2$  constrains possible deviations from the speed of sound in the model with Goldstone inflatons. Indeed,

$$c_s = \left( 1 + 2 \frac{2c_2 X}{f^2 + 2c_2 X} \right)^{-1/2} = \left( 1 + 2 \frac{2c_2 x}{1 + 2c_2 x} \right)^{-1/2} \quad (3.55)$$

Where we have defined the dimensionless parameter  $x = X/f^2$ . As  $X \sim p^2$ , we expect the effective theory to be valid up to

$$X \leq (4\pi f)^2 \quad \text{or} \quad x \leq (4\pi)^2 \quad (3.56)$$

The current bound by Planck is  $c_s > .024$  [83]. In Fig. 3.5 one can see how for positive  $c_2$  the speed of sound is in agreement with Planck for any value of  $c_2 x$ .

<sup>9</sup>Note that  $c_2$  in the case of two- and three-flavour QCD have been computed, assuming that its dominant contribution comes from vector meson exchange [117, 118] or with the inclusion of scalar and pseudo-scalar resonances [76]

As mentioned above, the sound speed is also constrained by arguments of (perturbative) unitarity. The scale at which violation of perturbative unitarity occurs was computed by Ref. [119] (and corrected in [120]) from imposing partial wave unitarity in the quartic interaction, and reads,

$$\Lambda_u^4 = \frac{24\pi}{5} \left( \frac{2M_p^2 |\dot{H}| c_s^5}{1 - c_s^2} \right) \quad (3.57)$$

We are in particular concerned with how  $\Lambda_u$  relates to the symmetry breaking scale  $f$ . If  $\Lambda_u < f$ , the action needs a completion below the symmetry breaking scale, possibly in terms of strongly coupled dynamics or new low-energy physics. The effective theory is therefore no longer a good description. One may thus consider a critical sound speed  $(c_s)_*$ , defined by [120]

$$\Lambda_u^4 = \frac{24\pi}{5} \left( \frac{2M_p^2 |\dot{H}| (c_s)_*^5}{1 - (c_s)_*^2} \right) = f^4 \quad (3.58)$$

For  $c_s > (c_s)_*$  our model predicts  $\Lambda_u > f$ . Canonically normalising using (3.51), we have

$$\frac{24\pi}{5} \left( \frac{(c_s)_*^4}{1 - (c_s)_*^2} \right) > 1 \quad (3.59)$$

This theoretical lower bound is also shown in Fig. 3.5 for different values of  $x$  (subject to (3.56)). One can see how, once axiomatic conditions from Goldstone scattering are imposed, the inflaton evades both bounds.

The speed of sound is related to non-Gaussianity by

$$f_{NL}^{eq} \sim \frac{1}{c_s^2} \quad (3.60)$$

One does not expect significant contributions to non-Gaussianity from the non-derivative terms in the potential, as they will be slow-roll suppressed.

It is worth noting that a deviation from one in the speed of sound will modify the tensor to scalar ratio [120]

$$r = 16\epsilon c_s \quad (3.61)$$

The predictions for  $r$  will in this case be lowered, but as the Planck bound is consistent with  $r = 0$ , this is only to the merit of models with a pGB inflaton.

### 3.4 Link to UV models

We saw above that the model (3.3) gives inflation compatible with the CMB data for particular relations between the coefficients. Here we discuss what these relations indicate for the UV theory.

Firstly, we noticed that to have the right shape of the potential, we should require  $\beta$  to be positive, that is

$$\beta = \int \frac{d^4 p_E}{(2\pi\Lambda)^4} \left( \frac{3(N-2)}{4} \frac{\Pi_1^A}{\Pi_0^A} - 2N_c \frac{M^2}{p_E^2 \Pi_0^L \Pi_0^R} \right) > 0 \quad (3.62)$$

Then we saw in Table 3.1 that the requirement of a sufficiently flat potential gives the condition  $\alpha \approx 2\beta$ , which will give a relation between the form factors of the form

$$\begin{aligned} \alpha &= -2N_c \int \frac{d^4 p_E}{(2\pi\Lambda)^4} \left( \frac{\Pi_1^L}{\Pi_0^L} - \frac{\Pi_1^R}{\Pi_0^R} \right) \\ &= 2 \int \frac{d^4 p_E}{(2\pi\Lambda)^4} \left( \frac{3(N-2)}{4} \frac{\Pi_1^A}{\Pi_0^A} - 2N_c \frac{M^2}{p_E^2 \Pi_0^L \Pi_0^R} \right) = 2\beta \end{aligned} \quad (3.63)$$

Lastly we have that the phenomenological condition  $V(\phi_{min}) = 0$  gives a preferred value of the constant  $C_\Lambda$  in terms of the model parameters. In explicit models this will give a condition of the form<sup>10</sup>

$$\alpha = -2N_c \int \frac{d^4 p_E}{(2\pi\Lambda)^4} \left[ \frac{\Pi_1^L}{\Pi_0^L} - \frac{\Pi_1^R}{\Pi_0^R} \right] = C_\Lambda \quad (3.64)$$

where  $C_\Lambda$  is a cosmological constant during inflation.

To obtain explicit expressions for the form factors  $\Pi_X$  one would need a UV-complete theory. However, using the relations above we can make some general remarks about their large momentum behaviour. First, we can use an operator product expansion to find the scaling of  $\Pi_1$ . This implies that  $\Pi_1$  scales as  $\langle \mathcal{O} \rangle / p^{d-2}$ , where  $\mathcal{O}$  is the lowest operator responsible for the breaking  $G \rightarrow H$ , with mass dimension  $d$ . In our case, we expect  $\mathcal{O}$  to be a fermion condensate with  $d = 6$ . Secondly we can require finiteness of the fermion Lagrangian (3.27). The scaling of the other form factors can be found by consideration of the kinetic terms in the high momentum limit. We will discuss this in the next section. We summarise our conclusions in Table 3.2.

In the next section we will assume a light resonance connection to derive more specific conclusions in this approximation.

### 3.5 Light resonance connection

In this section we attempt to derive some of the properties of the UV theory, assuming that the integrated-out dynamics is dominated by the lightest resonances of the strong sector.

---

<sup>10</sup>Note that in some models  $C_\Lambda$  will be related to  $\alpha \pm \beta \approx 3/2 \alpha$ , as is seen in Table 3.1.

Form factor	Large momentum behaviour	Argument
$\Pi_1$	$\sim \langle \mathcal{O} \rangle / p^{d-2} = 1/p^4$	OPE coupling
$\Pi_0$	$\sim p^2$	Recovering the bosonic Lagrangian
$\Pi_1^r$	$\sim 1/p^6$	OPE coupling
$\Pi_0^r$	$\sim p^0$	Recovering the fermion Lagrangian
$M^r$	$\sim 1/p^2$	OPE coupling

Table 3.2: *Connection to the UV theory*: Scaling of the form factors derived from an operator product expansion and symmetry restoration at high energies.

To simplify what follows, we note that the form factor  $M$  in equation (3.29) is ‘naturally’ small in the ’t Hooft sense [11]. This is because in the limit  $M \rightarrow 0$  we have an enhanced  $U(1)_L \times U(1)_R$  global symmetry under which  $\psi_L$  and  $\psi_R$  transform with independent phase-rotations. Therefore in the following we will assume that the dominant contributions to  $\alpha$  and  $\beta$  come from the  $\Pi_{0,1}^i$  form factors. Note that this observation makes it very plausible that condition (3.62) is satisfied.

Note that to ensure a convergent behaviour of the form factors at high scales  $Q^2$ , one would have to introduce an amount of resonances to saturate the Weinberg sum rules. The minimum number of resonances depends on the behaviour of the form factor with  $Q$ . This behaviour is described in the previous section. The convergence of these form factors in the large- $Q$  regime is not a necessary condition for a generic model of strong interactions, but rather helps on describing the interpolation between the low-energy regime of the theory with an asymptotically free UV theory (provided this is the case).

Irrespective of these issues of interpolation with the UV behaviour, one can consider a spectral decomposition of the form factor. A common description, valid for a  $SU(N)$  gauge sector in the large- $N$  limit is form factors as infinite sums over narrow resonances of the strong dynamics [78, 79, 121]. In the following, we assume that the  $\Pi_1^i$  form factors can be well approximated by considering only the contribution from the lightest of these resonances.

We expect that  $\Pi_1^i$  has a pole at the mass of the lightest resonance  $m_i^2$ , and that the residue of this pole is equal to the square of the amplitude to create the resonance from the vacuum. This amplitude,  $f_i$ , is equivalent to the decay constant of the resonance. This leads us to the following approximation for the fermionic  $\Pi_1^i$ :

$$\Pi_1^i(p^2) = \frac{f_i^2}{p^2 + m_i^2}. \quad (3.65)$$

In the gauge case, this expression is modified to

$$\frac{1}{p^2}\Pi_1^A(p^2) = \frac{f^2}{p^2} + \frac{f_A^2}{p^2 + m_A^2}, \quad (3.66)$$

which now has a pole at  $p^2 = 0$ , since the broken  $SO(N)/SO(N-1)$  currents can excite the Goldstones from the vacuum [24].

We approximate the  $\Pi_0$  form factors with their tree level values. By inspecting (3.7) and (3.27), we see that to recover the tree level fermion and gauge Lagrangians we must have  $\Pi_0 = 1$  in the fermionic case, and  $\Pi_0 = p^2/g^2$  in the gauge case, where  $g$  is the gauge coupling.

Let us study the minimal model we can construct that leads to successful inflation. We will only need one external fermion – in this case we take the  $\psi_R$  of Sec. 3.2. Then  $\alpha$  and  $\beta$  will be given by

$$\alpha = 2N_c \int \frac{d^4p}{(2\pi\Lambda)^4} \left( \frac{\Pi_1^R}{\Pi_0^R} \right), \quad \beta = \frac{3(N-2)}{4} \int \frac{d^4p}{(2\pi\Lambda)^4} \left( \frac{\Pi_1^A}{\Pi_0^A} \right). \quad (3.67)$$

Now we assume that  $\Pi_1^R$  and  $\Pi_1^A$  are given respectively by (3.65) and (3.66). With a single resonance, we cannot guarantee convergence of the integrals in (3.67) – generally this can be done by introducing more resonances and demanding that the form factors satisfy Weinberg sum rules [122, 123]. However we can argue that, since our effective theory is only expected to be valid up to a scale  $\Lambda_{UV} = 4\pi f$ , we should cut off the momentum integrals at  $p^2 = \Lambda_{UV}^2$ .

Putting all this together, we find:

$$\alpha = \frac{a}{8\pi^2\Lambda^4} \int_0^{\Lambda_{UV}^2} dp^2 \frac{p^2 f_R^2}{p^2 + m_R^2} = \frac{a f_R^2}{8\pi^2\Lambda^4} \left[ \Lambda_{UV}^2 - m_R^2 \log \left( \frac{m_R^2 + \Lambda_{UV}^2}{m_R^2} \right) \right], \quad (3.68)$$

where  $a = 2N_c$ , and

$$\beta = \frac{b g^2}{8\pi^2\Lambda^4} \int_0^{\Lambda_{UV}^2} dp^2 f^2 = \frac{b g^2}{8\pi^2} \left[ \Lambda_{UV}^2 f^2 + \Lambda_{UV}^2 f_A^2 - f_A^2 m_A^2 \log \left( \frac{m_A^2 + \Lambda_{UV}^2}{m_A^2} \right) \right], \quad (3.69)$$

where  $b = 3(N-2)/4$ .

The approximate relation  $\alpha \simeq 2\beta$  then implies a relationship between the parameters of the UV theory. If we demand that the quadratic cutoff dependence cancels, we obtain the relation

$$a f_R^2 = 2b g^2 (f^2 + f_A^2), \quad (3.70)$$

and

$$a f_R^2 m_R^2 \log \left( \frac{m_R^2 + \Lambda_{UV}^2}{m_R^2} \right) = 2b g^2 f_A^2 m_A^2 \log \left( \frac{m_A^2 + \Lambda_{UV}^2}{m_A^2} \right). \quad (3.71)$$

Inserting (3.70) into (3.71) we obtain

$$\frac{2bg^2 f_A^2}{af_R^2} = \frac{f_A^2}{f^2 + f_A^2} = \frac{m_R^2 \log[(m_R^2 + \Lambda_{UV}^2)/m_R^2]}{m_A^2 \log[(m_A^2 + \Lambda_{UV}^2)/m_A^2]}, \quad (3.72)$$

which implies that  $m_R < m_A$ .

If  $f_A \gg f$ , one finds that  $m_R \simeq m_A$ , i.e. there would be a degeneracy between fermionic and bosonic resonances. Note that this condition will be satisfied no matter the scale factor between  $\alpha$  and  $\beta$  is, as long as they are proportional,  $\alpha \propto \beta$ . This kind of *mass-matching* situation [124–126] where resonances from different sectors acquire the same mass is reminiscent of what had been found in trying to build successful Technicolor models, namely Cured Higgsless [127, 128] and Holographic Technicolor [129, 130] models.

### 3.6 Discussion and conclusions

The framework of slow-roll inflation has been corroborated to a good precision by the Planck data. This framework, however, suffers from an *inflationary hierarchy problem*, namely the strain of providing sufficient inflation while still satisfying the amplitude of the CMB anisotropy measurements. This balancing act requires a specific type of potential, with a width much larger than its height.

This tuning is generically unstable unless some symmetry protects the form of the potential. In this paper we explored the idea that this potential could be related to the inflaton as a Goldstone boson, arising from the spontaneous breaking of a global symmetry.

Another issue for inflationary potentials, including Goldstone Inflation, is that they are only effective descriptions of the inflaton physics. With the inflationary scale relatively close to the scale of Quantum Gravity, one expects higher-dimensional corrections to the inflationary potential. These corrections would de-stabilise the inflationary potential unless the model is small-field [131, 132]. In other words, as the inflaton field value approaches  $M_p$  the Effective Theory approach breaks down.

We found out that in Goldstone Inflation a predictive effective theory is indeed possible, and it leads to specific predictions. For example, in single-field inflation, we computed the most general Coleman-Weinberg inflaton potential and learnt that 1.) Only the breaking of  $SO(N)$  groups provide successful inflation and 2.) fermionic and bosonic contributions to the potential must be present and 3.) for fermions in single-index representations, a successful inflaton potential is given uniquely by  $V = \Lambda^4(C_\Lambda + \alpha \cos(\phi/f) + \beta \sin^2(\phi/f))$ , with  $\alpha \approx 2\beta$ . When linking to UV completions of Goldstone Inflation, we have been able to show how relations among the fermionic and bosonic resonances are linked to the

flatness of the potential.

As we have developed a specific model for inflation, we were able to address the amount of tuning required to make it work, and found that it is not dramatic. Indeed, we found that the tuning is milder than that found in Supersymmetric models nowadays.

Another advantage of this framework is the ability to examine the higher-order derivative terms in the Goldstone Lagrangian from several different points of view: modifications of the CMB speed of sound, constraints from unitarity and also axiomatic principles from Goldstone scattering.

We have presented results in a rather generic fashion and for single-field inflation, and delegated to the appendices a discussion of a specific model of single-field inflation, and few examples of hybrid inflation which originate from this framework.

There are other aspects of Goldstone Inflation which deserve further study. For example, in these models, hybrid inflation and reheating are quite predictive as the inflaton and waterfall fields come from the same object and naturally the inflaton can decay to other, lighter pseudo-Goldstones. Moreover, there may be interesting features of the phase transition causing the spontaneous breaking of the global symmetry, which we plan to investigate.

## Acknowledgements

We would like to thank Juanjo Sanz-Cillero for discussion on the Goldstone boson scattering, and Ewan Tarrant for explaining aspects of reheating. This work is supported by the Science Technology and Facilities Council (STFC) under grant number ST/L000504/1.

## Appendix A: Successful patterns of breaking: an example of single field

The simplest instance of the general model outlined in Section 3.2 takes the global symmetry of the strong sector to be  $SO(3)$ , breaking to  $SO(2)$ .<sup>11</sup> This gives rise to two Goldstone bosons, one of which is eaten when we gauge the remaining  $SO(2)$  symmetry. We parameterise the Goldstones via:

$$\Sigma(x) = \exp(iT^{\hat{a}}\phi^{\hat{a}}/f)\Sigma_0, \quad (3.73)$$

---

<sup>11</sup>This coset was also studied in the context of inflation in [133].

with  $\hat{a} = 1, 2$ . We can take the generators of  $SO(3)$  to be

$$T^1 = \frac{i}{\sqrt{2}} \begin{pmatrix} 0 & 0 & 0 \\ 0 & 0 & -1 \\ 0 & 1 & 0 \end{pmatrix}, \quad T^2 = \frac{i}{\sqrt{2}} \begin{pmatrix} 0 & 0 & 1 \\ 0 & 0 & 0 \\ -1 & 0 & 0 \end{pmatrix}, \quad T^3 = \frac{i}{\sqrt{2}} \begin{pmatrix} 0 & -1 & 0 \\ 1 & 0 & 0 \\ 0 & 0 & 0 \end{pmatrix}. \quad (3.74)$$

The broken generators satisfy  $T^{\hat{a}}\Sigma_0 \neq 0$ . If, following Sec. 3.2, we take  $\Sigma_0$  to be

$$\Sigma_0 = \begin{pmatrix} 0 \\ 0 \\ 1 \end{pmatrix}, \quad (3.75)$$

then  $T^1$  and  $T^2$  are the broken generators.  $T^3$  remains unbroken, and will generate the  $SO(2)$  gauge symmetry. A suitable gauge transformation then allows us to set  $\phi^1 = \phi$ ,  $\phi^2 = 0$ , and we can write

$$\Sigma = \begin{pmatrix} \sin(\phi/f) \\ 0 \\ \cos(\phi/f) \end{pmatrix}. \quad (3.76)$$

Following (3.7) the effective Lagrangian for the  $SO(2)$  gauge boson is

$$\mathcal{L}_{eff} = \frac{1}{2}(P_T)^{\mu\nu} [\Pi_0^A(p^2)A_\mu^3 A_\nu^3 \text{Tr}\{T^3 T^3\} + \Pi_1^A(p^2)A_\mu^3 A_\nu^3 \Sigma^T T^3 T^3 \Sigma], \quad (3.77)$$

$$= \frac{1}{2}(P_T)^{\mu\nu} \left[ \Pi_0^A(p^2) + \frac{1}{2}\Pi_1^A(p^2) \sin^2(\phi/f) \right] A_\mu^3 A_\nu^3. \quad (3.78)$$

This leads to the Coleman-Weinberg potential

$$V = \frac{3}{2} \int \frac{d^4 p}{(2\pi)^4} \log \left[ 1 + \frac{1}{2} \frac{\Pi_1^A}{\Pi_0^A} \sin^2(\phi/f) \right]. \quad (3.79)$$

Now we embed a fermion in an  $SO(3)$  spinor:

$$\Psi_L = \begin{pmatrix} \psi_L \\ 0 \end{pmatrix}. \quad (3.80)$$

The gamma matrices of  $SO(3)$  can be taken to be the Pauli matrices  $\sigma^a$ . Thus the most general effective Lagrangian for the fermion is

$$\mathcal{L}_{eff} = \bar{\Psi}_L \not{p} [\Pi_0^L(p) + \Pi_1^L(p) \sigma^a \Sigma^a] \Psi_L. \quad (3.81)$$

We find that

$$\sigma^a \Sigma^a = \begin{pmatrix} \cos(\phi/f) & \sin(\phi/f) \\ \sin(\phi/f) & -\cos(\phi/f) \end{pmatrix}, \quad (3.82)$$



so

$$\mathcal{L}_{eff} = \bar{\Psi}_L \not{p} [\Pi_0^L(p) + \Pi_1^L(p) \cos(\phi/f)] \Psi_L, \quad (3.83)$$

from which we derive the Coleman-Weinberg potential:

$$V = -2N_c \int \frac{d^4 p}{(2\pi)^4} \log \left[ 1 + \frac{\Pi_1^L}{\Pi_0^L} \cos(\phi/f) \right]. \quad (3.84)$$

Combining both gauge and fermion contributions, and expanding the logs at first order, we obtain

$$V(\phi) = \alpha \cos(\phi/f) + \beta \sin^2(\phi/f), \quad (3.85)$$

where

$$\alpha = -2N_c \int \frac{d^4 p}{(2\pi)^4} \left( \frac{\Pi_1^L}{\Pi_0^L} \right), \quad \beta = \frac{3}{4} \int \frac{d^4 p}{(2\pi)^4} \left( \frac{\Pi_1^A}{\Pi_0^A} \right). \quad (3.86)$$

## Appendix B: Successful patterns of breaking: an example of hybrid inflation

We can also construct models in which more than one physical Goldstone degree of freedom is left in the spectrum. This can be done by only gauging a subgroup of the unbroken  $SO(N-1)$  symmetry. Let us look briefly at a simple example of such a model, in which we take the global symmetry breaking to be  $SO(5) \rightarrow SO(4)$ . In such a case we have four Goldstone bosons, and  $\Sigma$  is given by

$$\Sigma = \frac{\sin(\phi/f)}{\phi} \begin{pmatrix} \phi^1 \\ \phi^2 \\ \phi^3 \\ \phi^4 \\ \phi \cot(\phi/f) \end{pmatrix}, \quad (3.87)$$

where we have  $\phi = \sqrt{\phi^{\hat{a}} \phi^{\hat{a}}}$ , as before.

If we gauge only  $SO(2) \in SO(4)$ , taking for instance the gauged generator to be

$$T_g^1 = \frac{i}{\sqrt{2}} \begin{pmatrix} 0 & 0 & 0 & -1 & 0 \\ 0 & 0 & 0 & 0 & 0 \\ 0 & 0 & 0 & 0 & 0 \\ 1 & 0 & 0 & 0 & 0 \\ 0 & 0 & 0 & 0 & 0 \end{pmatrix}, \quad (3.88)$$

then the gauge freedom allows us to set  $\phi^4 = 0$ .

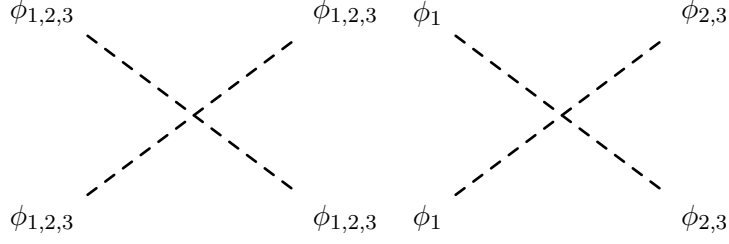


Figure 3.6: Goldstone quartic interactions

Following the same steps as before, the effective Lagrangian for the gauge field will be

$$\mathcal{L}_{eff} = \frac{1}{2}(P_T)^{\mu\nu} \left[ \Pi_0^A(p^2) + \frac{1}{2}\Pi_1^A(p^2) \left( \frac{\phi^1}{\phi} \right)^2 \sin^2(\phi/f) \right] A_\mu A_\nu. \quad (3.89)$$

If we, as in Appendix 3.6, consider the contribution from a single left-handed fermion, now embedded in an  $SO(5)$  spinor like so:

$$\Psi_L = \begin{pmatrix} \psi_L \\ 0 \\ 0 \\ 0 \end{pmatrix}, \quad (3.90)$$

then in fact the effective fermion Lagrangian will still be given by (3.83). Thus the Coleman-Weinberg potential will be given by

$$V(\phi) = \alpha \cos(\phi/f) + \beta \left( \frac{\phi_1}{\phi} \right)^2 \sin^2(\phi/f), \quad (3.91)$$

with  $\alpha$  and  $\beta$  given by

$$\alpha = -2N_c \int \frac{d^4 p}{(2\pi)^4} \left( \frac{\Pi_1^L}{\Pi_0^L} \right), \quad \beta = \frac{3}{4} \int \frac{d^4 p}{(2\pi)^4} \left( \frac{\Pi_1^A}{\Pi_0^A} \right). \quad (3.92)$$

If we expand the trigonometric functions for small field excursions, we obtain, up to constant terms:

$$\begin{aligned} V(\phi_1, \phi_2, \phi_3) = & \frac{1}{f^2} \left( \beta - \frac{\alpha}{2} \right) \phi_1^2 - \frac{\alpha}{2f^2} (\phi_2^2 + \phi_3^2) + \frac{1}{f^4} \left( \frac{\alpha}{24} - \frac{\beta}{3} \right) \phi_1^4 \\ & + \frac{\alpha}{24f^4} (\phi_2^4 + \phi_3^4) + \frac{1}{f^4} \left( \frac{\alpha}{12} - \frac{\beta}{3} \right) (\phi_1^2 \phi_2^2 + \phi_1^2 \phi_3^2) + \frac{\alpha}{12f^4} \phi_2^2 \phi_3^2 + \mathcal{O} \left( \frac{\phi^6}{f^6} \right). \end{aligned} \quad (3.93)$$

We see that the three Goldstones have masses

$$m_1^2 = \beta - \alpha/2, \quad m_2^2 = m_3^2 = -\alpha/2, \quad (3.94)$$

and we have, among others, the quartic interactions shown in Fig. 3.6.

We can remove another of the Goldstone fields by gauging a further generator of  $SO(2)$ . For instance, if we gauge

$$T_g^2 = \frac{i}{\sqrt{2}} \begin{pmatrix} 0 & 0 & -1 & 0 & 0 \\ 0 & 0 & 0 & 0 & 0 \\ 1 & 0 & 0 & 0 & 0 \\ 0 & 0 & 0 & 0 & 0 \\ 0 & 0 & 0 & 0 & 0 \end{pmatrix}, \quad (3.95)$$

then the potential will be exactly as in (3.93), with  $\phi_3$  set to zero. We must also replace  $\beta \rightarrow 2\beta$ , since the potential now receives contributions from two gauge bosons.

We note further that if instead we gauged the generator

$$T_g^2 = \frac{i}{\sqrt{2}} \begin{pmatrix} 0 & 0 & 0 & 0 & 0 \\ 0 & 0 & -1 & 0 & 0 \\ 0 & 1 & 0 & 0 & 0 \\ 0 & 0 & 0 & 0 & 0 \\ 0 & 0 & 0 & 0 & 0 \end{pmatrix}, \quad (3.96)$$

then we obtain

$$V(\phi) = \alpha \cos(\phi/f) + \beta \left( \frac{\phi_1^2 + \phi_2^2}{\phi^2} \right) \sin^2(\phi/f) = \alpha \cos(\phi/f) + \beta \sin^2(\phi/f), \quad (3.97)$$

which is symmetric in  $\phi_1$  and  $\phi_2$ .

## Chapter 4

# Composite Higgses with seesaw EWSB

### Abstract

We introduce a new class of Composite Higgs models in which electroweak symmetry is broken by a seesaw-like mechanism. If a global symmetry is broken sequentially at different scales, two sets of pseudo-Goldstone bosons will arise, one set being typically heavier than the other. If two Composite Higgs doublets mix, then the mass-squared of the lighter state can be driven negative, and induce EWSB. We illustrate with the example  $SO(6) \rightarrow SO(5) \rightarrow SO(4)$ , and derive an estimate of the light Higgs potential. We find that the introduction of an extra scale can ease many of the tensions present in conventional Composite Higgs models, especially those related to fine-tuning. In particular we find that we can significantly raise the upper bound on the mass of the elusive top partners.

## 4.1 Introduction

The Composite Higgs paradigm offers a beautiful solution to the hierarchy problem of Higgs physics. By suggesting that the Higgs is realised as a composite pseudo-Goldstone boson, Composite Higgs (CH) models provide a dynamical origin of the electroweak scale while protecting the Higgs mass from UV corrections. The existence of a new, strongly coupled sector with resonances not far above the electroweak scale offers tantalising prospects for new physics at the LHC and future colliders.

A central component of CH models is the idea of partial compositeness [23]. If Standard Model (SM) fermions couple linearly to strong sector operators, Yukawa terms can be generated via the mixing of composite and elementary states. Partial compositeness provides a compelling mechanism for the large hierarchy in the quark masses, while at the same time evading flavour constraints [134, 135].

There are however, important tensions within CH models; for instance the generic requirement for top partners [136] lighter than the spin-one counterparts. This feature is difficult to reconcile with arguments based on the large- $N_c$  expansion [78, 79, 137], where the expectation is indeed the opposite, namely  $m_{s=1/2}/m_{s=1} \sim \mathcal{O}(N_c)$ , as well as a naive understanding of these resonances as bound states of *techni-quarks*.

This tension partly arises from the necessity of generating a *negative* mass-squared for the Higgs, which is crucial for electroweak symmetry breaking (EWSB). This is usually induced via loops of fermions [24]; of these, the top quark is expected to give the largest contribution. Since the top quark is responsible for the mass of the Higgs, this results in a relationship between the Higgs mass and the mass of the lightest top partner. In general, a significant amount of tuning is required to lift the top partner mass much higher than a TeV [138] (for further developments in CH model-building see [30, 38, 46, 47, 103, 139–145]; for a discussion of CH phenomenology [146–157] and searches for top partners [44, 158–172]).

In this paper we present a model that provides an entirely different means for the Higgs to acquire a negative mass-squared. As was noted in [32], if a composite Higgs doublet were to mix with an elementary scalar doublet, diagonalisation of the mass matrix could lead to a negative mass-squared for one of the resulting physical eigenstates.<sup>1</sup> Of course, introducing a new elementary scalar will inevitably lead to a new hierarchy problem, of the kind we are trying to avoid. We propose a new class of models in which the extra doublet is also composite, and arises as a pseudo-Goldstone boson from another

---

<sup>1</sup>A similar mechanism for obtaining a negative Higgs mass-squared from the mixing of two doublets has also been explored in supersymmetric contexts, for instance [173].

spontaneous symmetry breaking. We propose that the dynamics of the strong sector are such that its global symmetry  $\mathcal{G}$  is broken successively:  $\mathcal{G} \rightarrow \mathcal{H}_1 \rightarrow \mathcal{H}_2$ . If the breakings occur at different scales, or if there are different sources of explicit symmetry breaking (see Section 4.3), the mass of one of the doublets can be significantly higher than the other. Assuming the strong sector dynamics generate a linear coupling between the two, then the heavy doublet can drive the mass of the lighter state negative, via a seesaw-like diagonalisation of the mass matrix.

We present one realisation of this class of models, in which the symmetry breaking has the appealing structure  $SO(6) \rightarrow SO(5) \rightarrow SO(4)$ . As is known from the minimal [19,174] and next-to-minimal [28] CH models, both breakings can give rise to a doublet of a gauged  $SU(2)_L \subset SO(4)$ . As we show, the mixing of these doublets can lead to a negative mass-squared for the lighter eigenstate, which in turn can break the same  $SU(2)_L$  electroweak symmetry.

We also find that, if one wants to retain partial compositeness as a means to generate quark masses, a setup can be constructed in which the mass of the light Higgs is no longer tied to the masses of the top partners. The top partners can comfortably be accommodated at or close to the scale of the first breaking, significantly raising the upper bound on their masses.

The paper is structured as follows. In Section 4.2, we specify the general outline for this class of models. In Section 4.3 we work through the  $SO(6 \rightarrow 5 \rightarrow 4)$  model in detail, deriving an estimate for the Higgs potential by integrating out the heavy doublet at tree level. In Section 4.4, we give the modifications to the gauge-Higgs couplings, and how they differ to the results obtained in conventional CH models. In Section 4.5, we discuss the generation of quark masses, and explain how this class of models can relax the bounds on top partner masses. In Section 4.6 we review our findings.

## 4.2 Seesaw symmetry breaking

At high scales we assume that the strong sector has a global symmetry  $\mathcal{G}$ . The global symmetry undergoes two successive spontaneous breakings at different scales:  $\mathcal{G}$  breaks to  $\mathcal{H}_1$  at scale  $F_1$ , and  $\mathcal{H}_1$  breaks to  $\mathcal{H}_2$  at scale  $F_2$ . The minimal requirement on these groups is that both the broken  $\mathcal{G}/\mathcal{H}_1$  and the  $\mathcal{H}_1/\mathcal{H}_2$  cosets each contain four Goldstone bosons that transform as bidoublets of a custodial  $SU(2)_L \times SU(2)_R \in \mathcal{H}_2$ . The  $SU(2)_L$  subgroup will eventually become the electroweak gauge group of the Standard Model. Extending this picture to accommodate hypercharge is straightforward as discussed elsewhere [24].

We denote the doublet coming from the first breaking  $H$ , and the second doublet  $h$ .

After the first breaking, the spectrum consists of the doublet  $H$ , which can acquire a Coleman-Weinberg potential via radiative corrections from SM gauge bosons and fermions [26]. We expect  $H$  to acquire a mass

$$m_1^2 \sim \frac{g_1^2 F_1^2}{(4\pi)^2} \equiv f_1^2 \quad (4.1)$$

where  $g_1$  represents a coupling which breaks explicitly the symmetry  $\mathcal{G}$  (a gauge coupling, for instance). Note that we define the reduced scale  $f_1$ , the typical mass scale of the pseudo-Goldstones. After the second breaking, the light doublet  $h$  appears in the spectrum, which acquires a CW potential and gets a mass  $m_2^2 \sim f_2^2$ , where  $f_2 = g_2 F_2 / (4\pi)$ , as before. Both potentials arise via the Coleman-Weinberg mechanism, at different scales. Note also that if the UV theory contains other sources of explicit breaking (for instance, a fermion mass term), then the Goldstones could get further contributions to their mass (in analogy to the pions in QCD).

If we assume that a bilinear coupling is generated between  $H$  and  $h$ :

$$V_{mix} = \frac{\mu^2}{2} H^\dagger h + h.c. \quad (4.2)$$

or some more generic function  $V_{mix} = V_{mix}(H, h)$ , then, for  $\mu^2 > 2m_1 m_2$ , diagonalisation of the mass matrix

$$\begin{pmatrix} m_1^2 & \mu^2/2 \\ \mu^2/2 & m_2^2 \end{pmatrix} \quad (4.3)$$

will lead to a negative mass-squared for the lighter eigenstate. Therefore  $V(h)$  becomes unstable at the origin, and electroweak symmetry will be spontaneously broken. In particular, in the limit where  $m_1^2 \gg m_2^2$ , the physical masses become

$$m_h^2 \approx -\frac{\mu^4}{4m_1^2} + m_2^2, \quad (4.4)$$

$$m_H^2 \approx m_1^2. \quad (4.5)$$

Using a slight abuse of notation, we will continue to refer to the physical eigenstates as  $H$  and  $h$ , which are ‘mostly’ the original states, provided  $m_2/m_1$  is small. To obtain the potential for the light Higgs, we need to integrate out the heavy state. We can do this consistently at tree-level by solving the equations of motion for  $H$  and setting derivative terms to zero (since the heavy particle is effectively non-propagating). This amounts to solving

$$\frac{\partial V_1(H)}{\partial H^\dagger} + \frac{\partial V_{mix}(H, h)}{\partial H^\dagger} = 0, \quad (4.6)$$

for  $H$ , and an analogous expression for  $H^\dagger$ . Substituting back into the Lagrangian will give a consistent approximation to the light Higgs potential. We illustrate with an example in the next section, where we will also discuss the origin and expected size of the mixing term.

### 4.3 $SO(6 \rightarrow 5 \rightarrow 4)$

In this section we study in detail a specific model, in which the symmetry breaking is

$$\mathcal{G} \rightarrow \mathcal{H}_1 \rightarrow \mathcal{H}_2 = SO(6) \rightarrow SO(5) \rightarrow SO(4). \quad (4.7)$$

The  $SO(6)/SO(5)$  coset consists of five Goldstone bosons, a doublet of  $SU(2)$  (the heavy Higgs  $H$ ) and a singlet, which we denote  $\eta$  [28]. The  $SO(5)/SO(4)$  coset contains just a single doublet (the SM-like Higgs  $h$ ).

We parameterise the Goldstone bosons using a non-linear Sigma model, following the CCWZ formalism [21]. We choose the vacua:

$$\langle \Sigma_1 \rangle = (0, 0, 0, 0, 0, F_1)^T, \quad \langle \Sigma_2 \rangle = (0, 0, 0, 0, F_2)^T, \quad (4.8)$$

so that the  $SO(6)/SO(5)$  Goldstones are parameterised by

$$\Sigma_1 = \exp(i(X^a H^a + X^5 \eta)/F_1) \langle \Sigma_1 \rangle, \quad (4.9)$$

which, for an appropriate choice of generators (see Appendix), can be written

$$= F_1 \frac{\sin(\tilde{H}/F_1)}{\tilde{H}} (H^1, H^2, H^3, H^4, \eta, \tilde{H} \cot(\tilde{H}/F_1))^T, \quad (4.10)$$

where  $\tilde{H} = \sqrt{H^\dagger H + \eta^2}$ . The  $SO(5)/SO(4)$  Goldstones are parameterised by

$$\Sigma_2 = \exp(i\tilde{X}^a h^a/F_2) \langle \Sigma_2 \rangle \quad (4.11)$$

$$= F_2 \frac{\sin(\tilde{h}/F_2)}{\tilde{h}} (h^1, h^2, h^3, h^4, \tilde{h} \cot(\tilde{h}/F_2))^T, \quad (4.12)$$

where  $\tilde{h} = \sqrt{h^\dagger h}$ . With this parameterisation  $\Sigma_1$  and  $\Sigma_2$  transform as a **6** of  $SO(6)$  and a **5** of  $SO(5)$  respectively. That is, they both transform in fundamental representations. The  $SU(2)_L$  doublets can be written

$$h = \begin{pmatrix} h^1 + ih^2 \\ h^3 + ih^4 \end{pmatrix}, \quad H = \begin{pmatrix} H^1 + iH^2 \\ H^3 + iH^4 \end{pmatrix}. \quad (4.13)$$

As the perceptive reader will note, the bilinear mixing term in equation (4.2) explicitly breaks the shift symmetry acting on the Goldstone bosons, i.e. transformations of the form



$h^a \rightarrow h^a + \chi^a$ . This can only be justified if the UV completion contains explicit breaking of both  $SO(6)/SO(5)$ , the shift symmetry acting on  $H$  and  $\eta$ , and  $SO(5)/SO(4)$ , the shift symmetry acting on  $h$ . However, breaking  $SO(5)/SO(4)$  explicitly spoils the role of  $h$  as a Goldstone boson, allowing it to get a (potentially large) mass.

We note that terms of the form

$$\Delta\mathcal{L} = A(\Sigma_2 \cdot \mathbf{H}) + B(\Sigma_2 \cdot \mathbf{H})^2 + \dots, \quad (4.14)$$

where  $\mathbf{H} = (H^1, H^2, H^3, H^4, \eta)$  is a vector of  $SO(5)$  containing the first set of Goldstone bosons, break only the  $SO(6)/SO(5)$  shift symmetry. We thus come to an important conclusion: *In order to generate bilinear couplings between the two sets of Goldstone bosons, the theory must contain explicit breaking of at least  $SO(6)/SO(5)$ .*

Breaking  $SO(6)/SO(5)$  allows us to write down explicit mass terms  $m_H^2 H^\dagger H$  and  $m_\eta^2 \eta^2$ , but this is not problematic since a mass hierarchy between  $H$  and  $h$  is desirable.<sup>2</sup> In the  $SO(5)$  invariant limit we expect  $m_H = m_\eta$ , but gauging  $SU(2)_L \in SO(6)$  (as is usual practice in composite Higgs models) means that  $H$  will get corrections to its mass from loops of gauge bosons, while  $\eta$  will not [28].

This gauging of  $SU(2)_L$  explicitly breaks the symmetry down to the custodial  $SO(4)$  subgroup. Since  $H$  and  $\eta$  transform differently under  $SU(2)_L$ , we should allow for the possibility that their couplings to the light doublet  $h$  are modified. To this end we embed  $H$  and  $\eta$  in *different* multiplets of  $SO(5)$ , so that  $\mathbf{H}_4 = (H^1, H^2, H^3, H^4, 0)$  and  $\mathbf{H}_1 = (0, 0, 0, 0, \eta)$ . We then split up (4.14) into terms invariant under the unbroken  $SO(4)$ :

$$\Delta\mathcal{L} = A_1(\Sigma_2 \cdot \mathbf{H}_4) + A_2(\Sigma_2 \cdot \mathbf{H}_1) + B_1(\Sigma_2 \cdot \mathbf{H}_4)^2 + B_2(\Sigma_2 \cdot \mathbf{H}_1)^2 + 2B_3(\Sigma_2 \cdot \mathbf{H}_4)(\Sigma_2 \cdot \mathbf{H}_1), \quad (4.15)$$

$$= A_1 F_2 \frac{(H \cdot h)}{\tilde{h}} s_h + A_2 F_2 \eta c_h + B_1 F_2^2 \frac{(H \cdot h)^2}{\tilde{h}^2} s_h^2 + B_2 F_2^2 \eta^2 c_h^2 + 2B_3 F_2^2 \frac{(H \cdot h)}{\tilde{h}} \eta s_h c_h, \quad (4.16)$$

where  $s_h = \sin(h/F_2)$  and  $c_h = \cos(h/F_2)$ . We recover  $SO(5)$  invariance in the limit where  $A_1 = A_2$ ,  $B_1 = B_2 = B_3$ , and  $m_H = m_\eta$ . In this limit we expect that  $h$  should not be able to acquire a potential from  $H$  and  $\eta$ , due to the  $SO(5)/SO(4)$  shift symmetry. We have discarded any higher order terms since their contributions to the final Higgs potential will be of order  $\mathcal{O}(h^6/F_2^6)$ .

---

<sup>2</sup>Note that this raises the possibility that the two symmetry breakings occur at the same scale, (i.e.  $F_1 = F_2$ ), since the explicit mass terms give us a different way of generating a mass hierarchy between  $m_H$  and  $m_h$ .

Without loss of generality, we can rotate  $h$  along the direction in which it is to get a VEV, so that

$$h = \begin{pmatrix} 0 \\ \tilde{h} \end{pmatrix}. \quad (4.17)$$

Then the only part of  $H$  that couples to the light doublet will be  $H^3$ , so from now on we will simply redefine  $H^3 \equiv H$  and  $\tilde{h} \equiv h$ . Then  $\Delta\mathcal{L}$  can be written

$$\Delta\mathcal{L} \equiv V_{mix} = A_1 F_2 H s_h + A_2 F_2 \eta c_h + B_1 F_2^2 H^2 s_h^2 + B_2 F_2^2 \eta^2 c_h^2 + 2B_3 F_2^2 H \eta s_h c_h. \quad (4.18)$$

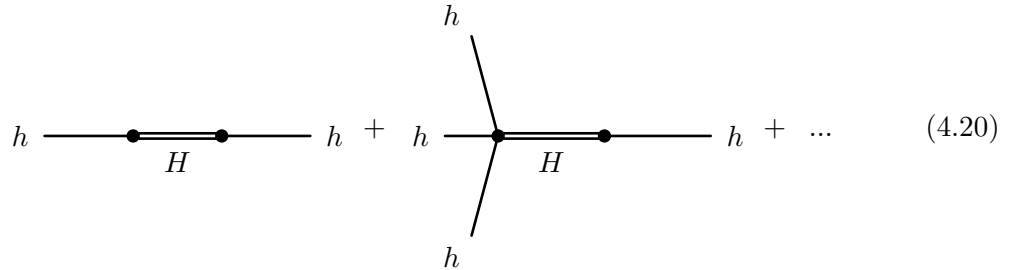
Comparing with the notation of the previous section, we see that the coefficient of the linear coupling is  $\mu^2 = A_1$ .

It is worth commenting on the expected sizes of the  $A$  and  $B$  terms. Their mass dimensions are  $[A] = 2$  and  $[B] = 0$ . From a naive EFT perspective, we expect  $\mathcal{O}(1)$  values for the dimensionless  $B$  parameters. How about the  $A$  terms? All the terms in (4.15) explicitly break the  $SO(6)$  symmetry, so, assuming this explicit breaking has the same source as the heavy doublet mass term, we might naively expect the dimensionful  $A$  terms to be comparable in size to  $m_H^2$ .

As we show in the appendix, the gauging of  $SU(2)_L$  gives a  $\sin^2$  potential to the light  $h$ :

$$V_{CW}(h) = m_{CW}^2 F_2^2 \sin^2(h/F_2). \quad (4.19)$$

Furthermore  $h$  gets corrections to its potential via tree level exchange of the heavy Higgs and the singlet, for example:



$$h \text{ --- } \bullet \text{ --- } \text{H} \text{ --- } \bullet \text{ --- } h + h \text{ --- } \bullet \text{ --- } \text{H} \text{ --- } \bullet \text{ --- } h + \dots \quad (4.20)$$

To integrate out  $H$ , we follow the procedure outlined in the previous section: we solve the equations of motion for  $H$ , setting derivative terms to zero, and substitute back into the original potential.

Thus the equations of motion for  $H$  are approximately given by

$$\frac{\partial V}{\partial H} = H (2m_H^2 + 2B_1 F_2^2 s_h^2) + A_1 F_2 s_h + 2B_3 F_2^2 \eta s_h c_h = 0, \quad (4.21)$$

which gives us our formal solution<sup>3</sup> for  $H$ :

$$H = -\frac{A_1 F_2 s_h + 2B_3 F_2^2 \eta s_h c_h}{2(m_H^2 + B_1 F_2^2 s_h^2)}. \quad (4.22)$$

Substituting back into  $V$ :

$$V(\eta, h) = m_\eta^2 \eta^2 + A_2 F_2 \eta c_h + B_2 F_2^2 \eta^2 c_h^2 - \frac{(A_1 F_2 s_h + 2B_3 F_2^2 \eta s_h c_h)^2}{4(m_H^2 + B_1 F_2^2 s_h^2)} + V_{CW}(h). \quad (4.23)$$

We can repeat the process to rewrite  $\eta$  in terms of  $h$ . We obtain the final Higgs potential:

$$V(h) = -\frac{\left(\frac{A_1 B_3 F_2^3 s_h^2 c_h}{m_H^2 + B_1 F_2^2 s_h^2} - A_2 F_2 c_h\right)^2}{4\left(m_\eta^2 + B_2 F_2^2 c_h^2 - \frac{B_3^2 F_2^4 s_h^2 c_h^2}{m_H^2 + B_1 F_2^2 s_h^2}\right)} - \frac{A_1^2 F_2^2 s_h^2}{4(m_H^2 + B_1 F_2^2 s_h^2)} + V_{CW}(h). \quad (4.24)$$

A nice feature of this potential, is that in the  $SO(5)$  invariant limit where  $A_1 = A_2$ ,  $B_1 = B_2 = B_3$  and  $m_H = m_\eta$ , the first two terms become constant, independent of  $h$ . This is what we expect, since  $h$  can only get a potential through  $SO(5)$  violating effects.

To get a feel for the contributions to the Higgs mass, let us look at the simplified case in which  $B_1 = B_2 = B_3 = 0$ . In this case, the potential reduces to

$$V(h) = \left(\frac{A_2^2}{4m_\eta^2} - \frac{A_1^2}{4m_H^2} + m_\eta^2\right) F_2^2 \sin^2(h/F_2), \quad (4.25)$$

plus constant terms independent of  $h$ . The contribution to the Higgs mass is

$$m_h^2 = \frac{A_2^2}{4m_\eta^2} - \frac{A_1^2}{4m_H^2} + m_{CW}^2. \quad (4.26)$$

This is to be compared to equation (4.4). In this model specific equation, we see that the presence of the singlet leads to positive contributions to the Higgs mass.

If we let  $\delta A = A_1 - A_2$  and  $\delta m^2 = m_H^2 - m_\eta^2$ , then to first order in  $\delta A$  and  $\delta m^2$ :

$$m_h^2 = -\frac{A_2}{2m_\eta^2} \delta A + \frac{A_2^2}{4m_\eta^4} \delta m^2 + m_{CW}^2. \quad (4.27)$$

The purpose of this equation is to show the relative sizes of the contributions. As was mentioned earlier, we naively expect the  $A$  terms and the masses of the heavy Goldstones to come from a common source of  $SO(6)/SO(5)$  breaking. Thus our naive expectation is that

$$\frac{A_2}{m_\eta^2} \sim \mathcal{O}(1). \quad (4.28)$$

The *differences*  $\delta A$  and  $\delta m^2$  come from the gauging of  $SU(2)_L$ , and are therefore expected to be of order

$$\delta A \sim \delta m^2 \sim g^2 F_1^2 / (4\pi)^2. \quad (4.29)$$

---

<sup>3</sup>We should note at this point that integrating out  $H$  leads to a kinetic term for  $h$  that is not canonically normalised. After  $h$  gets a VEV we must make a field redefinition, as discussed in Section 4.4.

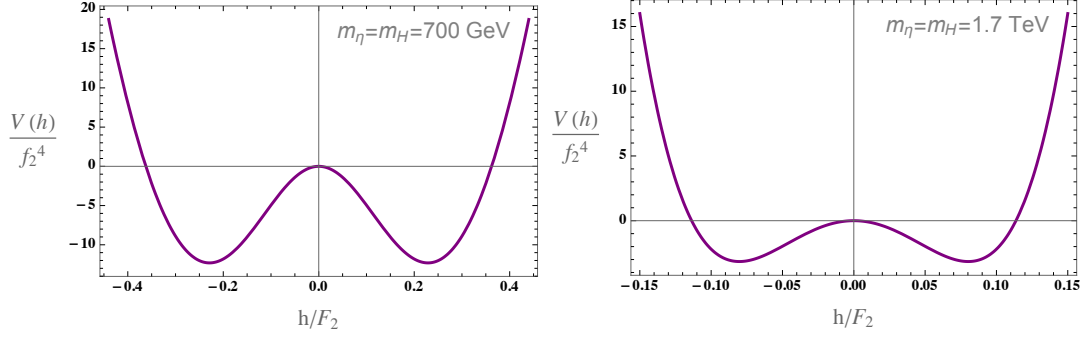


Figure 4.1: Plots of the light Higgs potential for different combinations of model parameters. Left: In this case the heavy Goldstone mass comes out at 700 GeV. We choose  $A_1 = 2m_H$  and  $\delta A \sim (4m_{CW})^2$ . Right: In this case the heavy Goldstone mass is 1.7 TeV. Again we choose  $A_1 = 2m_H$  and  $\delta A \sim (2m_{CW})^2$ . In both cases we have taken  $B_1 = 2$ ,  $B_2 = B_3 = 1$ .

If  $F_1$  is not too far above  $F_2$  (or indeed if the two scales are equal), then the terms in equation (4.27) are expected to be of comparable size. Thus no particular fine tuning is required to obtain a negative Higgs mass which is small compared to  $F_2$ .

Of course a pure  $\sin^2$  potential, such as in equation (4.25), leads to a Higgs VEV at  $v = (\pi/2)F_2$ , which is not phenomenologically viable. Fortunately switching on the  $B$  terms can increase the quartic coupling, and help to lower the VEV.

The scale of  $SO(6)/SO(5)$  explicit breaking, which determines the sizes of  $A_{1,2}$  and  $m_{H,\eta}^2$ , could in fact be large ( $> \text{TeV}$ ). As we show in Fig. 4.1, a light Higgs with a realistic VEV can still be obtained for  $m_{H,\eta} \sim 2.5 \text{ TeV}$ , so long as the loop-induced  $\delta m^2, \delta A$  corrections are of order  $m_{CW}^2$ . It is worth noting that the shape of the potential (including the small value of the Higgs VEV) is reasonably robust, and it not hard to find values of the parameters (obeying the expected scaling) that lead to a satisfactory potential.

## 4.4 Gauge couplings

As shown in the appendix, the effective Lagrangian for the gauge fields is

$$\mathcal{L}_{gauge} = \frac{1}{2}(P_T)^{\mu\nu} \left[ \Pi_0(p^2) + \frac{1}{4}F_1^2\Pi_1^1(p^2)\frac{H^\dagger H}{\tilde{H}^2} \sin^2(\tilde{H}/F_1) + \frac{1}{4}F_2^2\Pi_1^2(p^2) \sin^2(\tilde{h}/F_2) \right] W_\mu^a W_\nu^a. \quad (4.30)$$

At low energies we expect  $\Pi_0(0) = 0$  and  $\Pi_1^{1,2}(0) = 1$  [24]. To leading order in  $1/F_2$ , we can get an approximate expression for  $H$  by expanding our formal solution up to first

order in  $h$ :<sup>4</sup>

$$H = \left( -\frac{A_1}{2m_H^2} + \frac{A_2 B_3 F_2^2}{2(m_\eta^2 + B_2 F_2^2)m_H^2} \right) h \equiv -\varepsilon h. \quad (4.31)$$

Substituting this back in the gauge Lagrangian, we can estimate the effect that integrating out  $H$  has on the couplings of the light Higgs to the  $SU(2)$  gauge bosons. Expanding around the Higgs VEV:

$$\begin{aligned} \mathcal{L}_{gauge} = & \frac{1}{2}(P_T)^{\mu\nu} \left[ \frac{1}{4} \left( F_2^2 \sin^2 \frac{\langle h \rangle}{F_2} + F_1^2 \sin^2 \frac{\varepsilon \langle h \rangle}{F_1} \right) \right. \\ & + \frac{1}{4} \left( 2F_2 \cos \frac{\langle h \rangle}{F_2} \sin \frac{\langle h \rangle}{F_2} + 2\varepsilon F_1 \cos \frac{\varepsilon \langle h \rangle}{F_1} \sin \frac{\varepsilon \langle h \rangle}{F_1} \right) h \\ & \left. + \frac{1}{4} \left( \left( 1 - 2 \sin^2 \frac{\langle h \rangle}{F_2} \right) + \varepsilon^2 \left( 1 - 2 \sin^2 \frac{\varepsilon \langle h \rangle}{F_1} \right) \right) h^2 + \dots \right] W_\mu^a W_\nu^a. \end{aligned} \quad (4.32)$$

Of course, making the replacement (4.31) leads to a correction  $\varepsilon^2(\partial_\mu h^\dagger)(\partial^\mu h)$  to the kinetic term. Thus we must redefine  $h \rightarrow h/\sqrt{1+\varepsilon^2}$  in order that the physical Higgs field is canonically normalised.

In the ‘Composite Higgs’ limit  $\varepsilon \rightarrow 0$ , we recover the well-known modifications of the gauge-Higgs couplings:

$$g_{WW h} = g_{WW h}^{SM} \sqrt{1-\xi} \approx g_{WW h}^{SM} \left( 1 - \frac{\xi}{2} \right), \quad g_{WW hh} = g_{WW hh}^{SM} (1 - 2\xi), \quad (4.33)$$

where now  $\xi = \sin^2(h/F_2)$ , since this is the value of the VEV that we infer from measurement of the  $W$  and  $Z$  mass, which is slightly different to the true value of the Higgs VEV  $\langle h \rangle$ . The correction terms from integrating out  $H$  change these relations. For small values of  $\xi$  and  $\varepsilon$  the relations are

$$g_{WW h} = g_{WW h}^{SM} \left( 1 - \frac{\xi}{2} (1 - \varepsilon^2) \right), \quad g_{WW hh} = g_{WW hh}^{SM} (1 - 2\xi (1 - \varepsilon^2)). \quad (4.34)$$

Thus we see that the corrections to the SM gauge couplings are generally smaller than in ordinary Composite Higgs models, depending on the value of  $\varepsilon$ . This can be seen in Figure 4.2 where we plot the value of  $\kappa_V \equiv g_{WW h}/g_{WW h}^{SM}$  against  $\xi$  for different values of  $\varepsilon$ .

## 4.5 Quark masses and top partners

An important question to ask is whether this mechanism can tell us anything about the generation of quark masses. Assuming that quark masses are generated in the usual way,

---

<sup>4</sup>We use the equations of motion for  $H$  to first write  $H = H(\eta, h)$ , then the equations of motion for  $\eta$  to write  $H = H(\eta(h), h)$ .

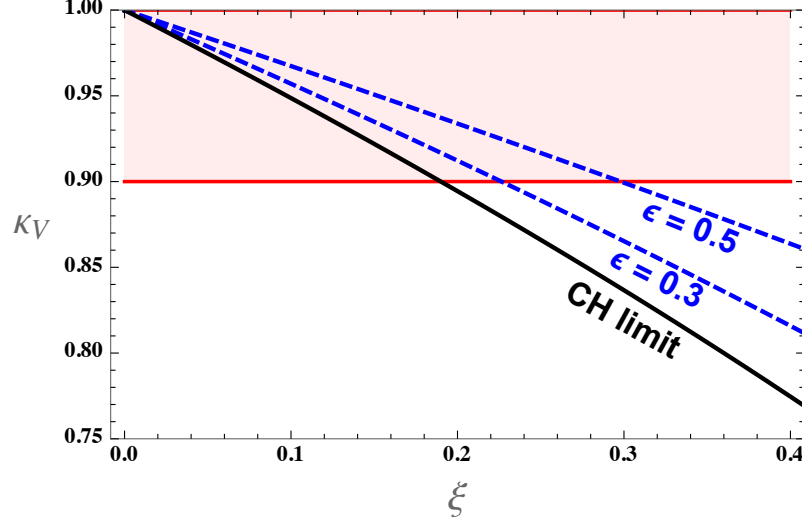


Figure 4.2:  $\kappa_V$  plotted against  $\xi$  for different values of  $\varepsilon$ . The red band corresponds to a measurement with 10% accuracy.

via linear couplings to composite fermionic operators (partial compositeness), can our model modify the bounds on top partner masses?

An attractive consequence of our model is that we manage to induce electroweak symmetry breaking without considering any fermionic contributions to the Higgs potential. Usually fermionic contributions are required to generate a negative mass-squared for the Higgs, but we achieve this via diagonalisation of a mass-mixing matrix. However it is important to address the issue of quark masses within this context.

Let us first review how Yukawa couplings are generated in conventional CH models. One can introduce the fermionic operators,  $T, \tilde{T}$ , and allow them to have linear couplings to the elementary top quarks, and well as their own mass terms [136]:

$$\Delta\mathcal{L} = -(y_L F \bar{t}_L T_R + y_R F \bar{t}_R \tilde{T}_L) - m_T^* \bar{T} T - m_{\tilde{T}}^* \bar{\tilde{T}} \tilde{T}. \quad (4.35)$$

One then assumes that the strong dynamics generates a Yukawa-like coupling between the composite operators

$$\mathcal{L}_{yukawa} = Y h \bar{T} \tilde{T} + h.c. \quad (4.36)$$

The top Yukawa is then interpolated via the following diagram:

$$\sim Y y_L y_R \frac{F^2}{m_T m_{\tilde{T}}}, \quad (4.37)$$

where  $m_T, m_{\tilde{T}}$  are the physical masses of the top partners. It can be shown that the composite Yukawa  $Y$  is not in fact independent and is related to other dimensionful parameters [136]:

$$Y \sim m_{T,\tilde{T}}^*/F. \quad (4.38)$$

Thus the heavier the top partners, the larger must be  $y_{L,R}$  in order to keep the top Yukawa  $\mathcal{O}(1)$ .

However the couplings  $y_L, y_R$  are also related to the mass of the Higgs. In conventional CH models the greatest contribution to the Higgs potential is the CW contribution from the top quark, so we can relate the Higgs mass directly to  $y_{L,R}$ :

$$m_H^2 \simeq \frac{N_c y^4}{2\pi^2} v^2. \quad (4.39)$$

where  $N_c$  is the number of QCD colours, and where  $y$  stands for either  $y_L$  or  $y_R$ . The reason the mass is proportional to  $y^4$  and not  $y^2$  is that in order to achieve a realistic VEV with  $\xi < 1$  one is required to tune the contribution from the top quark such that the leading order term ( $\sim y_{L,R}^2 F^2$ ) is of the same order as the next-to-leading order term ( $\sim y_{L,R}^4 F^2$ ).

Combining (4.37), (4.38) and (4.39), one arrives at a relation between the Higgs mass and the mass of the lightest top partner:

$$m_H \sim \frac{\sqrt{N_c}}{\pi} \frac{m_t m_T}{F}, \quad (4.40)$$

where  $m_t$  is the mass of the top quark.

Insisting that the top partners are heavy is therefore in conflict with the requirement that the Higgs is light compared to  $F$ . Models in which the top partners are much heavier than a TeV tend therefore to be highly tuned.

This tension can be eased in our model. Let us assume that the top partners are associated with the scale of the first symmetry breaking,  $F_1$ . Equation (4.35) now reads

$$\Delta\mathcal{L} = -(y_L F_1 \bar{t}_L T_R + y_R F_1 \bar{t}_R \tilde{T}_L) - m_T^* \bar{T} T - m_{\tilde{T}}^* \bar{\tilde{T}} \tilde{T}. \quad (4.41)$$

We assume that there is a Yukawa-like coupling between the heavy Higgs and the top partners:

$$\mathcal{L}_{\text{yukawa}} = Y_H H \bar{T} \tilde{T}, \quad (4.42)$$

but that the corresponding Yukawa coupling between the light Higgs and the top partners is suppressed. Now the top Yukawa is interpolated by the following diagrams:

$$y_t \sim \left( \frac{A_1}{2m_H^2} - \frac{A_2 B_3 F_2^2}{2(m_\eta^2 + B_2 F_2^2)m_H^2} \right) Y_H Y_L Y_R \frac{F_1^2}{m_T m_{\tilde{T}}} = \varepsilon Y_H Y_L Y_R \frac{F_1^2}{m_T m_{\tilde{T}}}, \quad (4.44)$$

We do not expect the heavy doublet to get a VEV, and we no longer need to fine tune the leading order and next-to-leading order CW contributions against each other. The CW contribution to the heavy Higgs mass is therefore given by

$$\delta m_H^2 \sim \frac{N_c}{16\pi^2} y^2 F_1^2. \quad (4.45)$$

$$\frac{N_c}{16\pi^2}y^2 < 1, \quad (4.46)$$
$$\delta m_H^2 \sim \frac{1}{\varepsilon} \frac{N_c}{16\pi^2} m_T F_1. \quad (4.47)$$
$$m_T \leq \varepsilon \frac{16\pi^2}{N_c} F_1. \quad (4.48)$$

<sup>5</sup>Note that the  $\varepsilon \rightarrow 0$  limit is not physically relevant, since in this limit the heavy doublet decouples and the top Yukawa cannot be generated via diagrams of the form (4.43).



As we have already mentioned, a hierarchy between the two doublet masses is not problematic. Our model permits the existence of heavier top partners than the usual CH scenarios, since (as shown in Sec. 4.3 and Fig. 4.1) a light Higgs with a realistic VEV can still be realised with  $H$  and  $\eta$  at the TeV scale. However a more thorough investigation of the parameter space is perhaps warranted.

Another pleasing feature of our setup is that we manage to avoid the particularly unnatural tuning mentioned earlier in this section – the need in CH models to tune the second order term of the fermionic CW potential to be comparable in size to the leading order term. In our model we can get a realistic Higgs mass together with a small value of  $\xi$  simply by tuning the  $A$  and  $B$  parameters against one another. As shown in Section 4.3, the tuning required is reasonably mild.

## 4.6 Discussion and conclusions

The two challenges facing Composite Higgs models are 1) generating a naturally light Higgs, and 2) breaking electroweak symmetry in a phenomenologically viable way. Conventional CH models attempt to address both of these issues by introducing a new scale  $f$ , the scale of some spontaneous symmetry breaking that gives rise to a pseudo-Goldstone Higgs boson. In order that the Higgs can fulfil its purpose and break electroweak symmetry, it needs to acquire a negative mass-squared. This is done by allowing loops of fermions to generate a potential for the Higgs radiatively.

As is now well known, this procedure inevitably leads to the presence of light top partners. Top partner searches at the LHC are now putting some of the strongest bounds on CH models. Evading the constraints these null-results are putting on CH models requires increasingly fine tuning, and thus 2) becomes in tension with 1) – we begin to lose some of the naturalness of the light Higgs.

We address these tensions by introducing a new scale. The new scale provides us with an entirely new mechanism by which the Higgs can acquire a negative mass-squared, and significantly more freedom with which to address 2). In particular, the masses of the top partners need no longer be tied to the mass of the Higgs.

In this paper, we have presented a detailed model, with the symmetry breaking structure  $SO(6 \rightarrow 5 \rightarrow 4)$ . We have found that with minimal tuning this setup can lead to a satisfactory Higgs potential with small values of  $\xi$ . We have also found that the corrections to the Standard Model gauge couplings are generally milder than in conventional CH models. Interestingly, this can help relax the bounds that the model faces from

precise measurement of the gauge-Higgs couplings. For the same values of  $\xi$ , our model can account for gauge couplings much closer to the SM values than the corresponding conventional CH prediction.

In addition to this, the model has a rich phenomenology, with an extended Higgs sector containing another doublet and a singlet, see e.g. [57, 175, 176] for the type of phenomenological analyses one can perform. Finally, the flavour structure of the model in particular deserves more detailed study, since it is clear that it can be quite distinct from the conventional CH scenarios [177–181].

## Appendix: The gauge Lagrangian

### Generators of $SO(6)$

The basis for the  $SO(6)$  generators that we use in this paper are as follows:

- $SU(2)_L$

$$T_{ij}^{a_L} = -\frac{i}{2} \left[ \frac{1}{2} \epsilon^{abc} (\delta_i^b \delta_j^c - \delta_j^b \delta_i^c) + (\delta_i^a \delta_j^4 - \delta_j^a \delta_i^4) \right], \quad a_L = 1, 2, 3, \quad (4.49)$$

- $SU(2)_R$

$$T_{ij}^{a_R} = -\frac{i}{2} \left[ \frac{1}{2} \epsilon^{abc} (\delta_i^b \delta_j^c - \delta_j^b \delta_i^c) - (\delta_i^a \delta_j^4 - \delta_j^a \delta_i^4) \right], \quad a_R = 1, 2, 3, \quad (4.50)$$

- $SO(5)/SO(4)$

$$\tilde{X}^a = -\frac{i}{\sqrt{2}} (\delta_i^a \delta_j^5 - \delta_j^a \delta_i^5), \quad a = 1, \dots, 4, \quad (4.51)$$

- $SO(6)/SO(5)$

$$X^a = -\frac{i}{\sqrt{2}} (\delta_i^a \delta_j^6 - \delta_j^a \delta_i^6), \quad a = 1, \dots, 5. \quad (4.52)$$

Together these 15 generators comprise a complete basis.

### Gauge effective Lagrangian

There are two effective Lagrangians of interest: those characterising the interactions of both the  $\mathcal{G}/\mathcal{H}_1$  and the  $\mathcal{H}_1/\mathcal{H}_2$  Goldstones with the  $SU(2)_L$  gauge bosons. In the first case, we want to write down a Lagrangian consistent with the  $SO(6)$  symmetry, in the second case, the  $SO(5)$  symmetry. One can do this by first assuming that the entire global symmetry is gauged. Then, for instance, the term in the effective Lagrangian for  $H$  is

$$\frac{1}{2} (P_T)^{\mu\nu} \Pi_1^1(p^2) \Sigma_1 A_\mu A_\nu \Sigma_1, \quad (4.53)$$

where  $A_\mu = A_\mu^a T^a$ , for all 15 generators  $T^a$  of  $SO(6)$ , and  $\Pi_1^1(p^2)$  is a scale-dependent form factor. This term is  $SO(6)$  invariant. The explicit breaking comes from the fact that we only gauge the  $SU(2)_L$  subgroup, so we set all gauge fields other than those associated with the  $SU(2)_L$  generators to zero. It is not hard to show that the above expression then becomes

$$\frac{1}{2}(P_T)^{\mu\nu} \frac{1}{4} F_1^2 \Pi_1^1(p^2) \frac{H^\dagger H}{\tilde{H}^2} \sin^2(\tilde{H}/F_1) W_\mu^a W_\nu^a, \quad (4.54)$$

with  $\tilde{H} = \sqrt{H^\dagger H + \eta^2}$ . Working through the same procedure for the  $\mathcal{H}_1/\mathcal{H}_2$  Goldstones gives the effective Lagrangian

$$\frac{1}{2}(P_T)^{\mu\nu} \frac{1}{4} F_2^2 \Pi_1^2(p^2) \sin^2(\tilde{h}/F_2) W_\mu^a W_\nu^a, \quad (4.55)$$

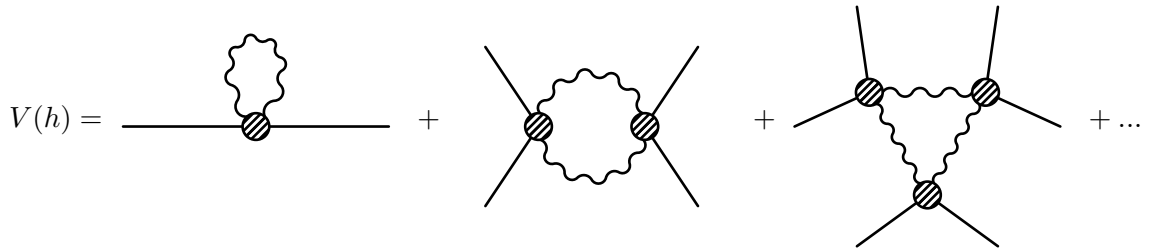
with  $\tilde{h} = \sqrt{h^\dagger h}$ . In both cases we can write down another term including only the gauge fields:

$$\frac{1}{2}(P_T)^{\mu\nu} \Pi_0(p^2) \text{Tr}(A_\mu A_\nu) = \frac{1}{2}(P_T)^{\mu\nu} \Pi_0(p^2) W_\mu^a W_\nu^a \quad (4.56)$$

We could write down terms with higher powers of the fields, but it is only these terms which are relevant for the calculation of the 1-loop Coleman-Weinberg potential.

### Coleman-Weinberg potential

The Coleman-Weinberg potential arises via the resummation of all 1-loop diagrams in which a gauge boson propagates around the loop. For instance, for the light doublet:



$$V(h) = \text{[tadpole diagram]} + \text{[bubble diagram]} + \text{[triangle diagram]} + \dots \quad (4.57)$$

This series of diagrams leads to the potential

$$V(h) = \frac{9}{2} \int \frac{d^4 p_E}{(2\pi)^4} \log \left[ 1 + \frac{1}{4} \frac{\Pi_1^2(p_E^2)}{\Pi_0(p_E^2)} F_2^2 \sin^2(\tilde{h}/F_2) \right], \quad (4.58)$$

where  $p_E^2 = -p^2$  is the Euclidean momentum. We expect  $\Pi_1^2(p_E^2)$  to go to zero at high energies. We make the usual assumption that it does so fast enough that the integral converges, and that to a good approximation the log can be expanded at first order:

$$V(h) = m_2^2 F_2^2 \sin^2(\tilde{h}/F_2), \quad (4.59)$$

where

$$m_2^2 = \frac{9}{8} \int \frac{d^4 p_E}{(2\pi)^4} \frac{\Pi_1^2(p_E^2)}{\Pi_0(p_E^2)}. \quad (4.60)$$

We have written the coefficient in such a way that  $m_2^2$  is the mass that the light doublet acquires from the gauge CW potential.

By an entirely analogous procedure, the CW potential for the  $\mathcal{G}/\mathcal{H}_1$  Goldstones is given by

$$V(H, \eta) = \frac{9}{2} \int \frac{d^4 p_E}{(2\pi)^4} \log \left[ 1 + \frac{1}{4} \frac{\Pi_1^1(p_E^2)}{\Pi_0(p_E^2)} \frac{H^\dagger H}{\tilde{H}^2} F_1^2 \sin^2(\tilde{H}/F_2) \right], \quad (4.61)$$

$$\approx m_1^2 F_1^2 \frac{H^\dagger H}{\tilde{H}^2} \sin^2(\tilde{H}/F_1). \quad (4.62)$$

## Chapter 5

# Tracking down quirks at the Large Hadron Collider

### Abstract

Non-helical tracks are the smoking gun signature of charged and/or colored quirks, which are pairs of particles bound by a new, long-range confining force. We propose a method to efficiently search for these non-helical tracks at the LHC, without the need to fit their trajectories. We show that the hits corresponding to quirky trajectories can be selected efficiently by searching for co-planar hits in the inner layers of the ATLAS and CMS trackers, even in the presence of on average 50 pile-up vertices. We further argue that backgrounds from photon conversions and unassociated pile-up hits can be removed almost entirely, while maintaining a signal reconstruction efficiency as high as  $\sim 70\%$ . With the  $300\text{ fb}^{-1}$  dataset, this implies a discovery potential for string tension between 100 eV and 30 keV, and colored (electroweak charged) quirks as heavy as 1600 (650) GeV may be discovered.

## 5.1 Introduction

With run II of the Large Hadron Collider (LHC) well underway, signatures of beyond the Standard Model physics have yet to reveal themselves. As the LHC transitions to its luminosity driven-phase, its focus will shift toward precision measurements and low rate signals. It is hereby imperative to consider new physics signatures that may not yet be covered; a task which has become increasingly difficult as the collaborations have greatly expanded and refined their search strategies in recent years. Nevertheless, there is considerable room for further progress, in particular in the context of long-lived exotica. The reason is that triggering and tracking often raise unique challenges, such that the sensitivity of more traditional searches is very poor or non-existent, and specialized strategies are needed. Nonetheless, once these challenges are addressed, these dedicated exotica searches (e.g. Long-lived particles, R-hadrons, disappearing tracks, hidden valleys [182–186]), have resulted in some of the most stringent experimental limits to date [187–192], precisely because of their qualitative departure from known standard model phenomena.

In this paper, we consider the quirks scenario [193], for which traditional tracking algorithms break down. A quirk/anti-quirk pair is a pair of new heavy stable charged particles (HSCP’s), that is connected by a flux tube of dark gluons. Such quirks can be present in models of dark matter [194] or neutral naturalness, like the quirky little Higgs [195], folded supersymmetry [196,197] and certain twin Higgs models [198,199]. The regime we consider here is defined by a large hierarchy between the quirk mass ( $m_Q$ ) and the dark confining scale  $\Lambda$ , *i.e.*  $m_Q \gg \Lambda$ . In this limit, the breaking of the dark flux tube, by pulling a quirk/anti-quirk pair from the vacuum, is suppressed by  $\sim \exp(-m_Q^2/\Lambda^2)$ . This is to be contrasted with standard model QCD, for which  $m_Q \ll \Lambda$ . In QCD, an excited flux tube can therefore easily break into multiple bound states, which is the process known as hadronization. For quirks, the flux tube does not break and instead induces a spectacular, macroscopic oscillatory motion before the quirks eventually annihilate. In the center of mass (CM) frame of the quirk/anti-quirk pair, the characteristic amplitude of this oscillation is

$$d_{\text{cm}} \sim 2 \text{ cm } (\gamma - 1) \left( \frac{m_Q}{100 \text{ GeV}} \right) \left( \frac{\text{keV}}{\Lambda} \right)^2, \quad (5.1)$$

where  $\gamma = 1/\sqrt{1-v^2}$  is the Lorentz boost factor of quirks at the moment of their production.

For large  $\Lambda \gtrsim 30 \text{ keV}$ , the oscillation length will typically be smaller than the detector resolution (roughly  $\sim 100 \mu\text{m}$ ), and the combined motion of the quirks is resolved as a

single, nearly straight track. In the track reconstruction, this would be seen as a very high  $p_T$  track with high  $dE/dx$ . A dedicated search of this type was carried out by the D0 collaboration at the Tevatron [200]. This search has not yet been repeated at the LHC, but it is conceivable that the existing HSCP searches have nevertheless sensitivity to this scenario. We leave this possibility for future work. In the opposite regime, where  $\Lambda \lesssim 100$  eV, the length of the string is of the order of the detector size or larger. For this regime it has recently been shown that the existing HSCP searches already set rather strong limits [201].

In the intermediate regime where  $100 \text{ eV} \lesssim \Lambda \lesssim 10 \text{ keV}$ , most events will have an oscillation amplitude of roughly  $d \sim 0.1$  to  $10$  cm. In this case, no tracks are reconstructed with existing algorithms, and the only current constraint comes from the jets +  $\cancel{E}_T$  search [201]. Although cm-size oscillating tracks would be a truly spectacular signature, it is thought to be very difficult to design a reconstruction algorithm for such tracks, especially with current high pile-up conditions and given that the  $m_Q$  and  $\Lambda$  are not a priori known. Even for fixed  $\Lambda$  and  $m_Q$ , the trajectories depend strongly on the initial velocities of the quirks and can differ greatly on an event-by-event basis.

Rather than attempting to reconstruct the tracks directly, we will therefore take advantage of some of the universal features of the motion of two particles subject to a central force. This allows us to develop a strategy that is largely independent of  $\Lambda$ ,  $m_Q$  and the kinematic configuration of the event. In particular, we will argue that the angular momentum of the quirk/anti-quirk system is approximately conserved as it traverses the ATLAS/CMS tracker. Since the quirk and anti-quirk interact via a central force and the external torque on the system is negligible, *the trajectories lie on a plane* to a good approximation. The idea is therefore to search for pairs of hits in each layer which all lie on a single plane (See Fig. 5.1).

The remainder of this paper is organized as follows: In Sec. 5.2, we review quirk dynamics and how to model their motions. We present details on our search strategy in Sec. 5.3 and the main results and sensitivity estimates in Sec. 5.4. We reserve some additional results on  $dE/dx$  for App. 5.4.

## 5.2 Quirk Dynamics

At the LHC, quirks can be pair-produced through either electroweak (Drell-Yan) and/or QCD interactions. Below we study the dynamics of quirks after they are pair-produced. As our benchmark scenarios, we will consider vector-like quirks in the  $(1, 1)_1$  and  $(3, 1)_{\frac{2}{3}}$

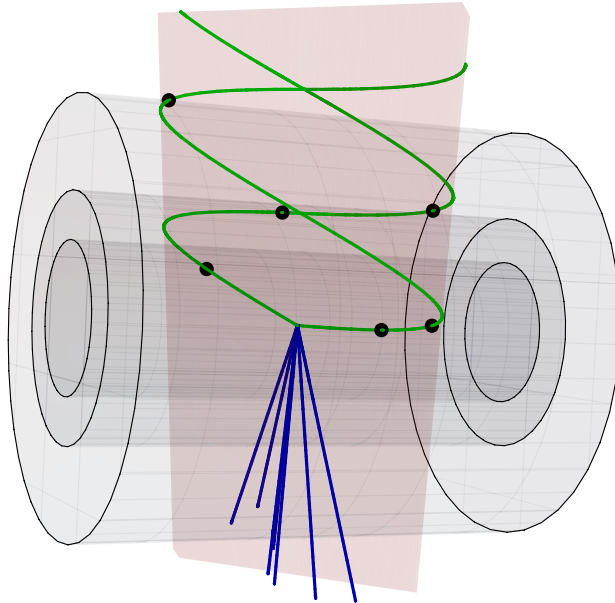


Figure 5.1: Schematic event display of a pair of quirks (green) with an ISR jet (blue). The cylinders represent the three innermost layers of the ATLAS/CMS tracker. The hits (black dots) all lie on a single plane (shaded red).

representations. In the latter case, the quirks will quickly hadronize into quirk-hadrons, and the probability for those final states to have  $\pm 1$  charges is roughly 30% as estimated using `Pythia8` [202]. Our analysis is largely independent on the charges of the quirk-hadrons, as long as both quirk-hadrons carry non-zero electric charge, such that they leave a signal in the inner trackers of ATLAS and CMS. In what follows we will loosely refer to the quirk-hadrons as quirks.

The quirks are approximately free right after they are produced. As their separation length becomes larger than  $\Lambda^{-1}$ , confinement will lead to an unbreakable flux-tube connecting the two quirks. This system can be described by the Nambu-Goto action with massive endpoints, which has been shown to correctly capture the properties of the heavy quark potential in QCD [203]. More general actions are possible, but should not affect our results significantly, as long as the string tension is much larger than the Lorentz force exerted by the magnetic field. The action for the quirks and the flux-tube (effectively a string) is then,

$$S = -m_Q \sum_{i=1,2} \int d\tau_i - \Lambda^2 \int dA + S_{\text{ext}}, \quad (5.2)$$

where  $A$  is the area of the string worldsheet,  $\tau_i$  the proper time of the two quirks, and  $S_{\text{ext}}$  describes external forces on the system. The boundaries of the string worldsheet are fixed to be the worldlines of the quirks. Note that we have taken  $\Lambda^2$  to be the string tension,



which will also serve as a precise definition for  $\Lambda$ . Eq. 5.2 leads to the following sets of equations for the quirks [193]

$$\frac{\partial}{\partial t}(m\gamma\mathbf{v}) = -\Lambda^2 \left( \frac{\sqrt{1-v_\perp^2}}{v_\parallel} \mathbf{v}_\parallel + \frac{v_\parallel}{\sqrt{1-v_\perp^2}} \mathbf{v}_\perp \right) + \mathbf{F}_{\text{ext}}, \quad (5.3)$$

where  $\mathbf{v}$  is the quirk velocity,  $\mathbf{v}_\parallel$  and  $\mathbf{v}_\perp$  are the components of the velocity parallel and perpendicular to the string ( $\mathbf{v}_\parallel + \mathbf{v}_\perp = \mathbf{v}$ ). There is one equation for each quirk, and the dynamics of the string in general leads to another, very complicated partial differential equation that couples to Eq. 5.3. Fortunately, in the region where  $\Lambda \gg 100$  eV, the force from the string is large compared to other interactions, and the string can be approximated as straight. In this limit, and in the center of mass frame,  $\mathbf{v}_\parallel$  will lie along the displacement vector between the quirks, and Eq. 5.3 alone suffices to describe the motion of the quirks. Ignoring  $\mathbf{F}_{\text{ext}}$ , and for a pair of quirks produced back-to-back with initial velocity  $v$ , the motion for one period  $0 \leq t \leq 2v\gamma m_Q/\Lambda^2$  is given by

$$d_{\text{cm}}(t) = \frac{m_Q}{\Lambda^2} \left[ \gamma - \sqrt{1 + \left( \frac{\Lambda^2 t}{m_Q} - v\gamma \right)^2} \right], \quad (5.4)$$

where  $\gamma = 1/\sqrt{1-v^2}$ . This gives the amplitude in Eq. 5.1.

In ATLAS and CMS, the trajectory in Eq. 5.4 will be modified by the inclusion of  $\mathbf{F}_{\text{ext}}$ , which is the Lorentz force exerted by the magnetic field as well as forces exerted during the passage through the detector material. Then, to justify our proposed search strategy, we must verify two crucial features of the quirk trajectories taking  $\mathbf{F}_{\text{ext}}$  into account:

1. The probability that the quirks annihilate before reaching the outer part of the inner tracker is very small.
2. The quirk/anti-quirk system does not pick up a large amount of angular momentum as it traverses the detector material and the magnetic field.

It is straightforward to see that a typical quirk/anti-quirk system does not annihilate in the presence of a magnetic field, as the  $B$ -field will induce a macroscopic amount of internal angular momentum in the system, which will prevent it from annihilating. To estimate the effect of the  $B$ -field, it is useful to move to the center of mass frame. In this frame, the magnetic field is seen as a combination of an  $E$ -field and a  $B$ -field. If we neglect the effect of the  $B$ -field in this frame, we can estimate the torque due to the  $E$ -field:

$$\boldsymbol{\tau} \sim 2\mathbf{d} \times (e\mathbf{E}_{\text{cm}}) = 2e\gamma_{\text{cm}} \mathbf{d} \times (\mathbf{v}_{\text{cm}} \times \mathbf{B}), \quad (5.5)$$

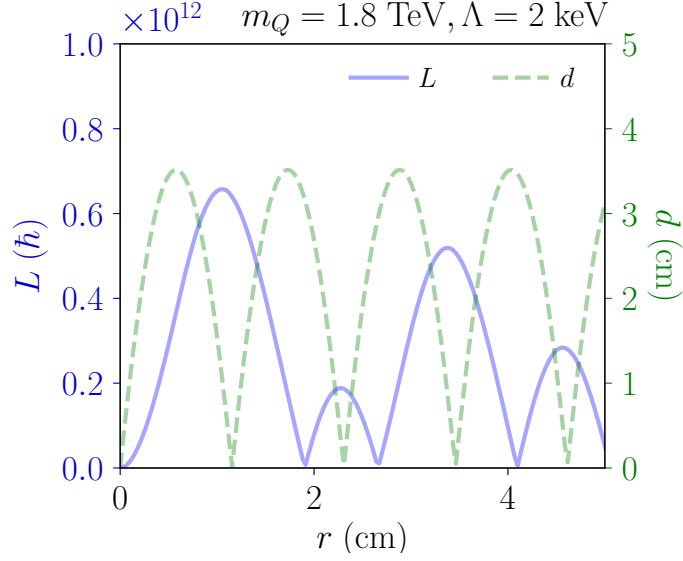


Figure 5.2: Angular momentum  $L$  and the relative distance between the quirks  $d$ , as a function of the radial distance of the center of mass to the interaction point for a representative event, with  $B = 2$  T. The displacement  $d$  varies several orders of magnitude over the quirk trajectories, but despite the appearance on this figure, it does not vanish except at the origin ( $r=0$ ).

where  $\gamma_{\text{cm}} = 1/\sqrt{1 - v_{\text{cm}}^2}$  and  $\mathbf{v}_{\text{cm}}$  is the center-of-mass velocity.  $2\mathbf{d}$  is the typical displacement of the quirks in the center of mass frame, and  $\mathbf{B}$  the magnetic field in the lab frame. The angular momentum that is picked up in a single oscillation with period  $\Delta t$  is roughly

$$L \sim |\boldsymbol{\tau}| \Delta t \sim e v_{\text{cm}} \gamma_{\text{cm}} v \gamma (\gamma - 1) \frac{m_Q^2 B}{\Lambda^4} \quad (5.6)$$

$$\sim 10^{12} \hbar \left( \frac{v_{\text{cm}} v^3}{0.1} \right) \left( \frac{2 \text{ keV}}{\Lambda} \right)^4 \left( \frac{m_Q}{1.8 \text{ TeV}} \right)^2 \left( \frac{B}{2 \text{ T}} \right), \quad (5.7)$$

where we used  $|\mathbf{d}| \sim (\gamma - 1) \frac{m_Q}{\Lambda^2}$ ,  $\Delta t \sim 2v\gamma \frac{m_Q}{\Lambda^2}$  and taken the non-relativistic limit. For such large values of the angular momentum, the annihilation probability is negligible. Equivalently, it is possible to show that the distance of closest approach is much larger than  $1/m_Q$ . The angular momentum does however oscillate along the trajectory of the quirks. Although whenever  $|L| = 0$ , the separation between the quirks is large, and annihilation is suppressed by a small wave-function overlap. This is illustrated in Fig. 5.2 for a sample event.

While the internal angular momentum of the system is typically very large in units of  $\hbar$ , it is still small compared to the resolution of the trackers, and the trajectories remain co-planar as far as the experiments are concerned. We can see this by estimating the

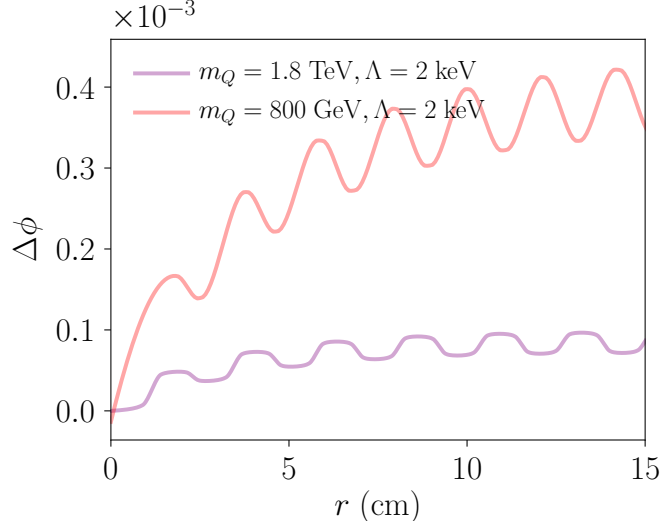


Figure 5.3:  $\Delta\phi$  as a function of the radial distance of the center of mass to the origin for two representative benchmark events, with  $B = 2$  T.

angular rotation of the plane spanned by the quirks' velocity vectors:

$$\Delta\phi \sim |\boldsymbol{\tau}|\Delta t^2/I \sim ev_{\text{cm}}\gamma_{\text{cm}} \frac{\gamma^2 v^2}{(\gamma-1)^2} \frac{B}{\Lambda^2} \quad (5.8)$$

$$\sim 10^{-5} \frac{v_{\text{cm}}}{v^2} \left( \frac{B}{2\text{ T}} \right) \left( \frac{2\text{ keV}}{\Lambda} \right)^2. \quad (5.9)$$

The key point here is that the effect of the torque on the angular acceleration is suppressed by the large moment of inertia of the system  $I \sim 2d^2 m_Q$ . There could be an enhancement for close to threshold quirks, where  $v \ll 1$ ; but this is relevant only for a very small part of phase space, and  $\Delta\phi$  is typically not larger than  $10^{-3}$ . We show  $\Delta\phi$  in Fig. 5.3 for two example events, as found in the full numerical solution of Eq. 5.3 with  $\mathbf{F}_{\text{ext}}$  the Lorentz force. In the numerical result,  $\Delta\phi$  oscillates and slowly accumulates as the quirks travel through the detector until it stabilizes around a fixed value. We see that the typical  $\Delta\phi$  is somewhat larger than  $10^{-5}$ , but is still small compared to the resolution of the tracker. The effect of the magnetic field is accounted for in all our simulations, and any potential efficiency loss due to shifting of the quirks' plane is included in our results.

Similarly, one can show that the rotation induced by the torque exerted by interactions with the detector material is small: the forces exerted by the ionization process when the quirks traverse a silicon layer are of the order  $\sim (100\text{ eV})^2$ , which induce an angular acceleration of up to  $\alpha \sim 10\text{ ns}^{-2}$ . The time it takes to traverse a  $\sim \text{cm}$  thick layer of detector material is  $\sim 10^{-2}\text{ ns}$ , such that the shift in angle is  $\Delta\phi \sim 10^{-3}$  for each layer the quirks traverse. We therefore neglect this effect in our simulations. It is worth noting that while we focused on the quirk action in Eq. 5.2, all arguments presented above hold for

an arbitrary central force, as long as the external forces are small compared to the central force between the particles.

Finally, a priori dark glueball radiation may also induce a change in angular momentum and therefore, a deviation from co-planarity. While there is no reliable calculation of the nonperturbative dark glueball radiation rate, naive dimensional analysis suggests that it is irrelevantly small [193]. Concretely, at large distance, the quirks' glueball radiation rate is proportional to the acceleration,  $a \sim \Lambda^2/m_Q$ , which is very small compared to the glueball mass  $\sim \Lambda$  [204]. This small acceleration strongly suppresses glueball radiation at large distances. On the other hand, when the quirks approach each other within a distance of  $\Lambda^{-1}$  or less,  $\sim \Lambda$  worth of energy may be radiated in a few glueballs. Such a radiation pattern changes the angular momenta of the quirk/anti-quirk system by a few quanta of  $\hbar$ , but does not modify the macroscopic trajectory of the quirks.

## 5.3 Search strategy

### 5.3.1 Signal simulation

We generate signal samples of vector-like fermions with up to 1 jet using `MadGraph5_aMC@NLO` [205, 206], which is subsequently matched using `Pythia8` [202, 207]. For electroweak production the quirks are taken to have unit charge and are produced in Drell-Yan, while for colored production only QCD contributions are included. The resulting four-momenta of the quirks are then evolved by numerically solving the equation of motion in (5.3) assuming a uniform 2T magnetic field along the  $z$ -direction. The intersections of the trajectories with a simplified model of the ATLAS inner detector are calculated, and the center of each pixel hit is used as the input for our analysis. We hereby use the parameters of the various detector elements as specified in [208]. Specifically, for the pixel detector we use the pixel size rather than the resolution and for the silicon microstrip tracker (SCT) we conservatively assume a resolution of twice the intrinsic accuracy quoted in [208]. Hits in neighboring pixels, according to the above definitions, are merged to a single hit, in an attempt to model the ATLAS hit merging procedure. We further apply a uniform, gaussian smearing with width 45 mm to the  $z$ -coordinates of all the hits, to account for the finite longitudinal size of the beamspot. For simplicity, we only included the barrel of the pixel and SCT detectors in our simulations, which effectively restricts the fiducial range to  $|\eta| \lesssim 1.8$ . Including additional detector components such as the endcaps, calorimeters and/or the transition radiation tracker would further enhance the sensitivity, although it

would require a more careful consideration as our co-planar approximation may be invalid for denser materials, and the timing constraint ( $t < 25$  ns) may become important for components farther away from the interaction point.

### 5.3.2 Trigger

Similar to conventional Heavy Stable Charged Particles (HSCPs), we do not expect quirks with a moderate boost to stop in the material of the calorimeters. This implies that the quirks will typically leave a handful of hits in the ATLAS muon detectors, which may be a triggering opportunity. In particular, the L1 trigger selection requires a coincidence of hits in two or three layers of the muon system, depending on the  $p_T$  threshold associated with the trigger path [209, 210]. The High Level Trigger (HLT) subsequently attempts to reconstruct a track, which is matched to a track in the inner detector. This step is likely to fail for the quirk signature, since a fit to a helix-shaped track is likely very poor for the string tensions we consider here [201]. It is however plausible that many of these events could be recovered with a dedicated quirk trigger at the HLT, for example by requiring pairs of nearby hits in multiple layers of the muon system. An important caveat here is that the quirks must reach the muon chamber in less than 25 ns, which may not be the case for a sizable fraction of the events.

If the event contains a sizable amount of transverse energy in the form of initial state radiation (ISR), the HLT will interpret the lack of a reconstructed track as missing transverse energy ( $\cancel{E}_T$ ). With start-up trigger thresholds for run-2 in mind [210], we therefore impose a  $p_T > 200$  GeV cut on the center mass momentum of the quirk/anti-quirk system. This requirement implies that the quirk/anti-quirk pair is essentially always central and sufficiently boosted, such that each quirk will most likely intersect each layer only once. The  $\cancel{E}_T$  cut also reduces the initial opening angle of the quirk pair, and therefore biases the sample towards smaller oscillation amplitudes. While we will make use of the latter feature, the precise value of the  $\cancel{E}_T$  cut does not significantly impact the reconstruction efficiency of our proposed algorithm.

Although the  $\cancel{E}_T$  trigger path is conceptually simple, it has a number of important downsides. Firstly, quirks with lower boost can traverse each layer multiple times, which can potentially lead to spectacular events with  $\mathcal{O}(10)$  hits in each tracker layer. The requirement of a hard ISR jet removes essentially all of these events.<sup>1</sup> Secondly, a tight ISR requirement substantially reduces the unusable signal cross sector, which can be problem-

---

<sup>1</sup>It would be interesting to investigate whether some of these events could be recovered with the future CMS and/or ATLAS hardware track triggers [211, 212], perhaps along the lines of [213].

atic especially for Drell-Yan production. Finally, the thresholds for the  $\cancel{E}_T$  triggers are expected to increase further as the instantaneous luminosity increases, which will further reduce the signal efficiency. Given that a substantial fraction of the quirk events would likely pass the L1 muon trigger, it would therefore be very interesting to design a suitable trigger path at the HLT which makes use of the muon chambers. Since the focus of this letter is on the off-line reconstruction strategy, we do not consider a potential muon trigger here.

### 5.3.3 Plane finding Algorithm

As argued above, the quirk trajectories largely lie on a single plane, which will be the essential ingredient for our proposed algorithm. We will assume that the primary vertex is identified correctly, and is located at the origin. A single hit is then defined by its position three-vector, and a candidate plane is fully specified by its normal unit vector. Our tracking algorithm is thus reduced to solving the following problem: Given a list of hits, what is the optimal plane that is close to as many hits as possible? To find a solution, one must first define a metric that specifies what ‘closeness’ means. One also needs to define when a hit is considered to be part of a plane, given the finite resolution of the tracker. Finally, the notion of an ‘optimal plane’ is ambiguous, given that one must weigh the goodness of the fit against the number of hits included. We will address these issues step by step in the remainder of this section.

A natural choice for the distance measure between a set of hits  $\{\mathbf{x}_a\}_{a \leq N}$  and a plane with normal vector  $\mathbf{n}$  is the root-mean-squared distance of the hits to the plane

$$d(\mathbf{n}, \mathbf{x}_a) \equiv \sqrt{\frac{1}{N-1} \sum_{a=1}^N (\mathbf{n} \cdot \mathbf{x}_a)^2}. \quad (5.10)$$

The distance can be rewritten as  $d = \sqrt{\mathbf{T}_{ij} \mathbf{n}_i \mathbf{n}_j}$ , where the two-tensor  $\mathbf{T}_{ij}$  is defined by

$$\mathbf{T}(\mathbf{x}_a)_{ij} \equiv \frac{1}{N-1} \sum_{a=1}^N x_i^a x_j^a. \quad (5.11)$$

Minimization of  $d$  with respect to  $\mathbf{n}$  simply reduces to solving an eigenvalue problem for  $\mathbf{T}$ . The smallest eigenvalue,  $\Delta s^2$ , then gives the minimum value of  $d^2$ , with an associated eigenvector  $\mathbf{n}_1$  equal to the normal vector of the optimal plane.  $\Delta s$  therefore gives a measure of the thickness of the plane.

There is additional useful information in the other eigenvalues and eigenvectors of  $\mathbf{T}$  that describe the geometry of the hits: Since  $\mathbf{T}$  is symmetric, the eigenvectors are orthogonal. The eigenvectors  $\mathbf{n}_2$  and  $\mathbf{n}_3$ , ordered by increasing eigenvalues, therefore lie

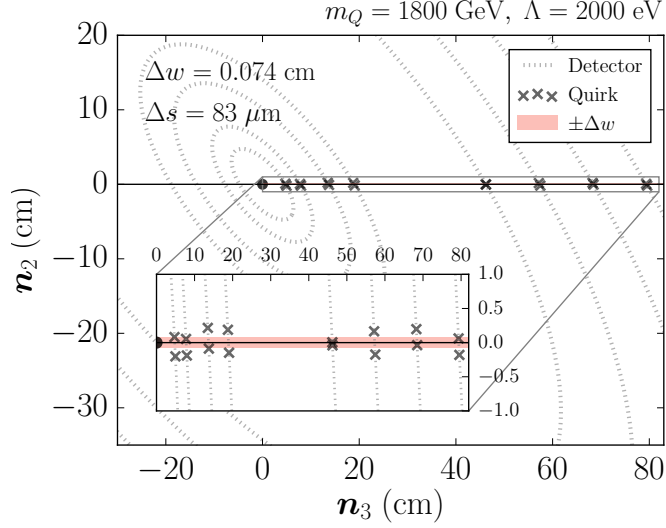


Figure 5.4: Hits for a sample signal event, projected onto the reconstructed plane spanned by  $(\mathbf{n}_3, \mathbf{n}_2)$ . The dotted line shows the cylindrical detector layers projected onto the signal plane as ellipses. The inner figure shows a zoomed-in view of the hit patterns, which lie roughly on a strip with width  $\Delta w \sim 0.074$  cm.

on the plane defined by  $\mathbf{n}_1$ . Geometrically,  $\mathbf{n}_2$  describes a second plane, orthogonal to the first, that has minimal root-mean-squared distance to all the hits. For a pair of quirks on a plane specified by  $\mathbf{n}_1$ , the  $\mathbf{n}_2$  plane roughly splits the pair of the hits. The second eigenvalue, denoted by  $\Delta w$ , then provides a measure of the width of the quirks' oscillations. As for the third eigenvector  $\mathbf{n}_3$ , it is orthogonal to  $\mathbf{n}_{1,2}$  and therefore provides a good estimate of the direction of the quirks' motion. In the limit that  $\Delta w$  is small compared to the detector size, all the quirks' hits will then be confined along a narrow planar strip. Specifically, the quirks signal we are after will lie in a positive direction  $(\mathbf{x}_a \cdot \mathbf{n}_3) > 0$ , with a small thickness  $\Delta s$  for the fitted plane and an oscillation width  $\Delta w$ .

Fig. 5.4 shows an example signal hit pattern, projected on the reconstructed plane spanned by  $(\mathbf{n}_3, \mathbf{n}_2)$ . The dotted ellipses show the tracking layers projected on the  $(\mathbf{n}_3, \mathbf{n}_2)$  plane. We see that all the hits lay in the positive  $\mathbf{n}_3$  direction, and that the hits mainly lay a few factors within  $\Delta w$ . As expected,  $\mathbf{n}_3$  reconstructs the quirks' direction to a good approximation.

With the key geometric variables defined, we now describe an algorithm that will iteratively reconstruct an 'optimal plane'. Given that for each list of hits, a best fitted plane can be computed as described above, the goal would then be to pick out an 'optimal list' of hits  $\{\mathbf{x}_a\}$  among thousands of unassociated hits in an event. The definition of what is optimal will involve a combination of  $\Delta s$  and  $\Delta w$  cuts, in addition to a few other selection cuts in the algorithm. For simplicity, we assume a detector geometry of 8 layers

of detector, following the ATLAS pixel layers and SCT; although our description may be generalized to other detector elements. The algorithm is split into two main stages, the seeding and iterative fitting stage:

1. Seeding: Define initial hits for iterative fitting
  - (a) Start from the 8<sup>th</sup> layer, collect all pairs of hits with  $\Delta\phi < 0.1$  and  $\Delta z < 2\text{cm}$ . Repeat the same for the 7<sup>th</sup> layer.
  - (b) Construct four-hits combinations by choosing one pair from each initial layer. Compute the tensor  $\mathbf{T}$  and apply the follow cuts:  $\mathbf{x}_a \cdot \mathbf{n}_3 > 0$  for all hits,  $\Delta s < 0.05\text{ cm}$  and  $\Delta w < 1\text{ cm}$ .
2. Iterative fitting: for each seed, loop over the remaining 6 layers outside-in, and collect more hits consistent with the initial fit
  - (a) Start from the 6<sup>th</sup> layer, collect all hits that satisfy  $(\mathbf{x} \cdot \mathbf{n}_3) > 0$ ,  $|\mathbf{x} \cdot \mathbf{n}_1| < 0.05\text{ cm}$  and  $|\mathbf{x} \cdot \mathbf{n}_2| < 1\text{ cm}$ .
  - (b) Loop over selected hits, starting with the one with the smallest  $|\mathbf{x} \cdot \mathbf{n}_1|$ . Together with the list  $\{\mathbf{x}_a\}$ , recompute  $\mathbf{T}$  and associated variables. If  $\Delta s$  and  $\Delta w$  do not increase by a factor of 3, add the hit to the list.
  - (c) Iterate the previous steps all the way to the first layer, then construct the final list  $\{\mathbf{x}_a\}$  and compute associated variables.
3. Event Selection: Gather all the reconstructed lists, apply the final cut  $\Delta w < 1\text{ cm}$ . If there are more than one plane identified, keep the one with the smallest  $\Delta s$ .

In summary, after the plane-finding algorithm has identified a set of candidate plains, the main discriminating variables of our analysis are

- First eigenvalue of (5.11), or the “thickness”,  $(\Delta s)^2$
- Second eigenvalue of (5.11), or the “width”,  $(\Delta w)^2$
- Number of hits found

It is important to note that the selection cuts on these variables can be easily modified to accommodate better signal acceptance and/or background rejection. A tighter selection will generally boost computational efficiency at a cost of reduced signal efficiency, which is what has been chosen in this work. Looser selection can easily be implemented at a cost of increased computational time, and may require additional adjustments on the final cuts to maintain the same level of background rejection.



An amortized  $\mathcal{O}(N)$  time complexity can be achieved for the tracking algorithm, assuming that the  $(\Delta\phi, \Delta z)$  cut is adjusted so that roughly a constant number of hits are within such a window.<sup>2</sup> An algorithm of this sort may be sufficiently fast for implementation at the high level trigger (HLT), which would partially remedy the problem of the stringent  $\cancel{E}_T$  trigger.

There are additional variables that can potentially enhance background rejection and/or the efficiency of the seeding step. For instance,  $\mathbf{n}_3$  is expected to be aligned with  $\vec{\cancel{E}}_T$  in the transverse plane, which can limit the region of interest in the detector for reconstruction. Additionally, we did not include  $dE/dx$  information, which can be leveraged for heavier masses; although we found that the algorithm described above already provided sufficient discriminating power (see Sec. 5.4). Since  $dE/dx$  information could nevertheless be of interest for a realistic experimental implementation, we include a brief summary of our relevant results in App. 5.4.

### 5.3.4 Backgrounds

The biggest background for our search are unassociated hits, which predominantly come from pile-up tracks for which the track reconstruction failed. For this purpose we use the public available tracking efficiency plots [214], where we neglect the  $\eta$ -dependence of the efficiency, as long as the track is within the  $\eta$ -range of the barrel. For our study we assume an average of  $\langle\mu\rangle = 50$  pile-up interactions with a longitudinal beam spot spread of 45 mm, where the former is conservative compared to current conditions by roughly a factor of 2. We model pile-up by randomly selecting minimum bias events from a sample of  $125 \times 10^3$  events generated by `Pythia8`, processed by the simplified detector described in [215]. We approximately account for all elements of the inner detector, including the beam pipe, service layers and endcaps and include the effects of bremsstrahlung and energy loss from ionization. For more details we refer to appendix A of [215]. We did not attempt to model secondaries from hadronic interactions with the inner detector material, which will increase the hit counts in the outer layers of the pixel and SCT detectors. We however verified that this deficiency is roughly offset by our conservative choice for  $\langle\mu\rangle$ .

A second potential background arises from isolated photon conversions in the beam pipe. These conversions give rise to a fairly collimated  $e^+e^-$  pair, which results in a nearby pair of hits in each layer of the tracker. For some conversion events, these hits could all approximately lie on a plane, and thus fake a quirk signal. We model this background by

---

<sup>2</sup>Assuming that the hits are stored in such a way that access through  $(\phi, z)$  coordinates takes constant time.

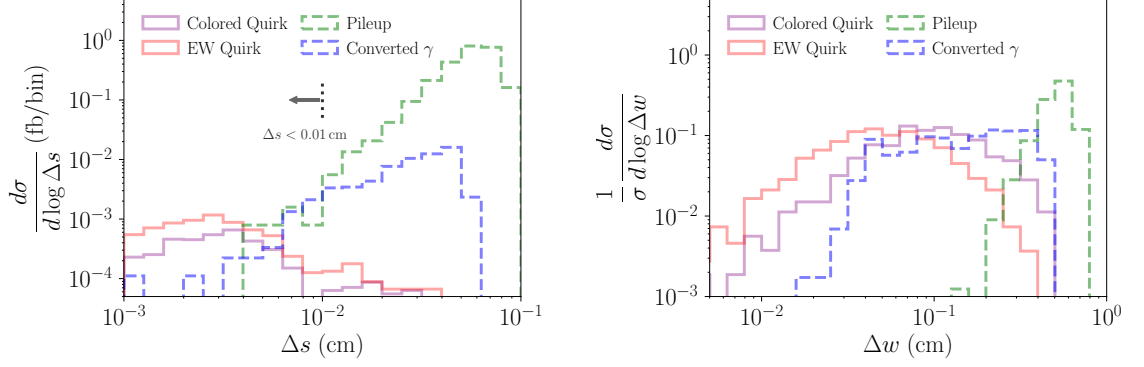


Figure 5.5: Signal and background distributions for thickness and width of the strip, parametrized by  $\Delta s$  (left) and  $\Delta w$  (right) respectively. The signal benchmarks for colored (EW) quirks are given by  $m_Q = 1.8$  TeV and  $\Lambda = 2000$  eV ( $m_Q = 800$  GeV and  $\Lambda = 4000$  eV). A signal selection cut  $\Delta s < 0.01$  cm is indicated on the left figure.

generating a  $Z + \gamma + j$  sample with `MadGraph5_aMC@NLO`, where we decay the  $Z$  to neutrinos and require at least 200 GeV of  $\cancel{E}_T$ , to satisfy our trigger requirement. We further require the  $p_T$  of the photon be larger than 0.5 GeV. The fiducial cross section for this process is  $\sim 1$  pb, which drops to  $\sim 10$  fb if we require that the photon converts in the beampipe using the conversion probability from figures 33.16 and 33.17 of [216]. Then we assume equal energy sharing between both electrons, which is conservative, as softer electrons would bend more strongly and lead to poor fit to a plane. The  $e^+e^-$  pair is then passed through the same detector simulation as described for the pile-up background. We subsequently overlay pile-up hits and pass the resulting set of hits through our reconstruction algorithm.

## 5.4 Results

Given the  $\mathcal{O}(1000)$  unassociated pile-up hits per layer in the tracker, a subset of these hits do accidentally land on a plane. Through our reconstruction algorithm, only  $\sim 10^{-3}$  of all background events contain a plane with at least one hit in 4 out of 8 layers. The number rapidly drops to  $6 \times 10^{-5}$ , for events with a plane that contains at least one hit in each layer. Still the majority of these planes have only one hit in most of the layers. Our signal region is then defined by the following cuts:

1. At least one plane reconstructed under the tracking algorithm
2. All but one layer must contain 2 hits, the remaining layer must contain at least 1 hit
3.  $\Delta w < 1.0$  cm and  $\Delta s < 0.01$  cm

For a quirk signal, as long as the length scale of oscillation  $m_Q/\Lambda^2$  is smaller than  $\sim 1$  cm, and if the quirks pass through all 8-layers, the reconstruction efficiency for these cuts can be as high as  $\sim 73\%$ .

Fig 5.5 shows the  $\Delta s$  and  $\Delta w$  distribution for background and our benchmark signal before the final cut on those variables are imposed. We see that the signal and background have distinctive distributions. In order to compensate for the lack of simulation statistics, the pileup backgrounds are derived by taking the distribution from events that are allowed to have 1-hit per layer, weighted by the overall efficiency of passing the more stringent requirement in point 2 above. For the pile-up background, the number of hits is anti-correlated with the thickness and the width of the plane, and as such this yields a conservative estimate for the pile-up background in the signal region. We deliberately do not impose a tight cut on  $\Delta w$ , as the efficiency for such a cut is strongly signal dependent. The rather loose cut of  $\Delta w < 1.0$  cm is intended to retain decent efficiencies for quirks with larger oscillation amplitude (low  $\Lambda$ ). Even though Fig 5.5 suggests a few background events after the final selection cut of  $\Delta s < 0.01$  cm, we suspect that they can easily be removed through either a  $\Delta\phi$  requirement between  $\vec{\not{E}}_T$  and  $\mathbf{n}_3$ , and/or by examining  $dE/dx$  pattern for the reconstructed hits. We have also not used any direct information on the quirk trajectory, other than the semi-strip geometry. Should our background estimates prove to be overly optimistic in a real experimental setup, it should be possible to further increase signal discrimination by fitting a quirk trajectory to the hits identified by our method. If any quirk candidates are observed, this would also be an obvious way to try to measure the mass and string tension.

We factorize the total signal efficiency into the trigger efficiency ( $\epsilon_{\text{trig}}$ ), the fiducial efficiency ( $\epsilon_{\text{fid}}$ ) and the reconstruction efficiency ( $\epsilon_{\text{reco}}$ ) such that the total efficiency  $\epsilon$  is given by

$$\epsilon = \epsilon_{\text{trig}} \times \epsilon_{\text{fid}} \times \epsilon_{\text{reco}} . \quad (5.12)$$

The trigger efficiency tends to be low, especially for Drell-Yan production, but it may be possible to improve on this with dedicated trigger strategies, as outlined in Sec. 5.3.2. The fiducial efficiency parametrizes the likelihood that each quirk intersect with each layer at least once, in events passing the trigger. We also include a 25 ns timing cut, which causes a slight drop in  $\epsilon_{\text{fid}}$  for heavier quirks, which tend to be slower. Inclusion of the endcaps should increase  $\epsilon_{\text{fid}}$  without significantly impacting the tracking algorithm. The reconstruction efficiency is defined as the efficiency of our algorithm in finding quirks which satisfy both the trigger and fiducial requirements. The various efficiencies are shown in

$m_Q$ (GeV)	$\Lambda$ (keV)	$\epsilon_{\text{trig}}$	$\epsilon_{\text{fid}}$	$\epsilon_{\text{reco}}$
800 (DY)	1	0.10	0.28	0.11
	2			0.41
	3			0.65
	4			0.72
	5			0.74
1800 (QCD)	1	0.24	0.28	0.083
	2			0.35
	3			0.59
	5			0.74
	10			0.58

Table 5.1: Breakdown of the signal efficiencies for two benchmarks, one for Drell-Yan (DY) production, and one for colored production (QCD).  $\epsilon_{\text{trig}}$  and  $\epsilon_{\text{fid}}$  are independent of  $\Lambda$ , the latter with the exception of small edge effects. For  $\Lambda \gtrsim 5$  keV,  $\epsilon_{\text{reco}}$  deteriorates as pairs of hits start merging into a single pixel.

Tab. 5.1 for two benchmark points. We see that the peak  $\epsilon_{\text{reco}}$  can be as high as  $\sim 70\%$ , while  $\epsilon_{\text{reco}}$  drops at lower  $\Lambda$ , where the iterative algorithm may fail to capture enough hits largely due to a stringent  $\Delta w$  requirements. At high  $\Lambda$ ,  $\epsilon_{\text{reco}}$  drops as well since the separation is small enough for the hits to start merging, at which point a plane cannot be found.

In Fig. 5.6, we show the expected 95% exclusion for an integrated luminosity of  $300 \text{ fb}^{-1}$ , assuming negligible irreducible backgrounds. We also show a tentative ‘discovery’ curve, corresponding to an expected signal of 5 events. (Discovery with only a few events may be possible when multiple events show hit patterns consistent with a common  $(m_Q, \Lambda)$ .) Our results are highly complimentary with recent (projected) constraints from HSCP searches [201], which are very stringent in the low string tension regime.

In summary, we show that searching for planar hits in the inner tracker is a powerful way to search for quirks with intermediate string tensions. It is moreover possible to design a generic search, which has good acceptance to all string tensions and quirk masses in the qualitative regime of interest ( $\mu\text{m-cm}$  size oscillations). Additionally, we show that an efficient algorithm can be straightforwardly implemented, while providing strong background rejection. While our theory study is no substitute for a full analysis, including understanding more subtle detector effects and backgrounds, we are optimistic that this

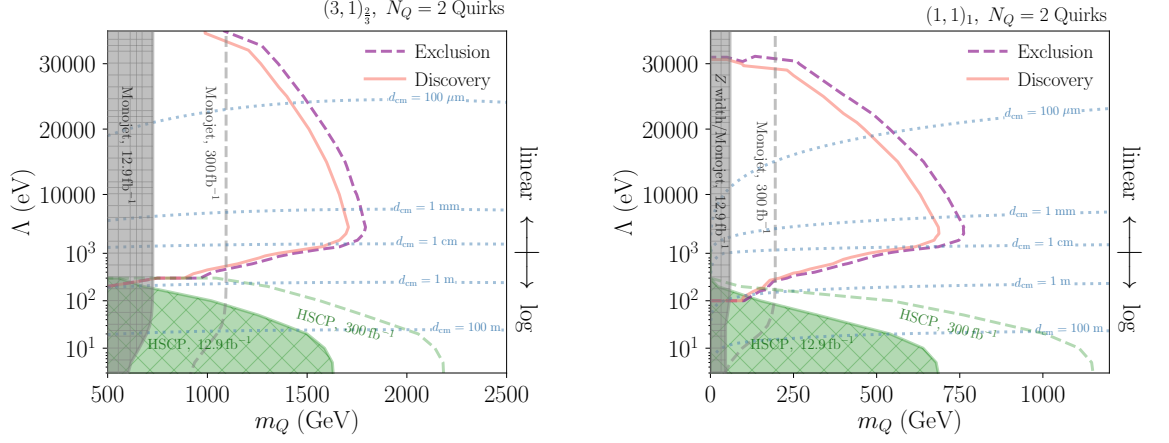


Figure 5.6: Contours of having 3 (5) events in the  $m_Q$  vs  $\Lambda$  plane for an integrated luminosity of  $\int L dt = 300 \text{ fb}^{-1}$ , overlaid with (projected) HSCP and monojet limits [217], where we extrapolated the latter to high  $\Lambda$ . In reality, the monojet limits may deteriorate in high  $\Lambda$  part of the plot, where the quirk system may be reconstructed as a single, high  $p_T$  track. The 3 events bound corresponds to  $2\text{-}\sigma$  exclusion given no background. Discovery is defined by 5 events, which may be achieved by close examination of each individual event and by showing that they are compatible with a fixed mass and tension. The dashed blue contour shows the average separation of the quirks in the CM frame,  $d_{\text{cm}}$ , as defined in Eq. 5.1.

type of search could be (nearly) free of irreducible backgrounds, especially if a quirk track is fitted to the hits identified by a plane-finding algorithm.

**Acknowledgements** We are grateful to Jared Evans, Marco Farina, Maurice Garcia-Sciveres, Laura Jeanty, Matthew Low, Markus Luty, Benjamin Nachman, Simone Pagan Griso and Jesse Thaler for useful discussions. We thank Marco Farina and Matthew Low for supplying us with the HSCP and monojet limits in Fig. 5.6, and thank Jared Evans and Matthew Low for comments on the manuscript. We further thank Wei-Ming Yao for bringing the conversion background to our attention. SK, HL and MP are supported in part by the LDRD program of LBNL under contract DE-AC02-05CH11231, and by the National Science Foundation (NSF) under grants No. PHY-1002399 and PHY-1316783. JS was supported by the Science and Technology Facilities Council (UK). JS is grateful to the Berkeley Center For Theoretical Physics and Lawrence Berkeley National Lab for their hospitality when part of this work was completed. This research used resources of the National Energy Research Scientific Computing Center, which is supported by the Office of Science of the DoE under Contract No. DE-AC02-05CH11231.

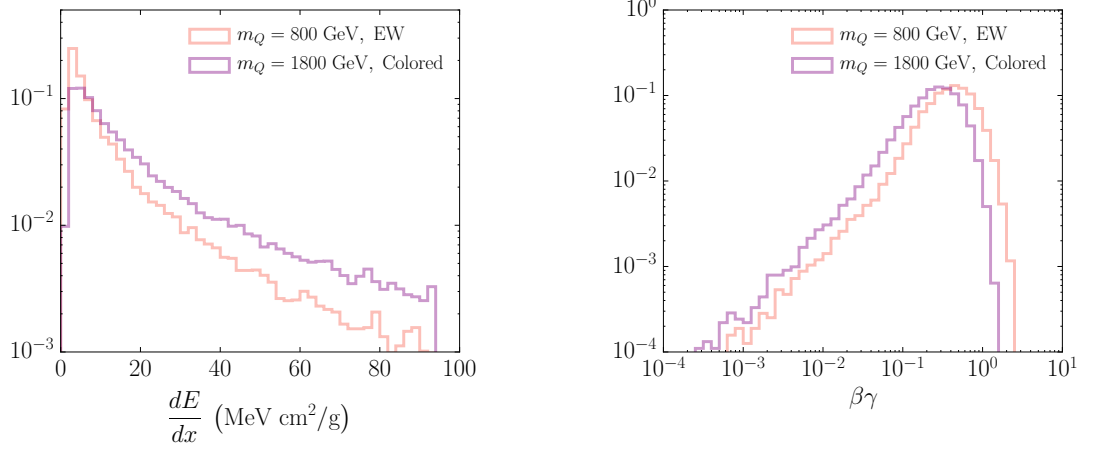


Figure 5.7: Differential distribution of  $dE/dx$  (left) and  $\beta\gamma$  (right) for two signal benchmark points with  $\Lambda = 2 \text{ keV}$  in our simulation of the ATLAS pixel detector.

## Appendix: $dE/dx$ information

Although we did not make use of variables relying on  $dE/dx$  measurements in our analysis, we here include a brief discussion for completeness. In Fig. 5.7 we show the include the  $dE/dx$  and  $\beta\gamma$  distributions for the hits in the ATLAS pixel detector for a few signal benchmarks. For the  $dE/dx$  we use the most probable value as a function of  $\beta\gamma$  [216]. Since this simplified treatment of the  $dE/dx$  distribution is not accurate for very slow particles, we omitted hits with  $\beta\gamma < 0.1$  in the left-hand panel of Fig. 5.7. While  $dE/dx$  is a powerful variable in conventional HSCP searches, its utility for quirks is more subtle because the quirks accelerate and decelerate along their trajectory through the detector. This implies that a substantial fraction of hits has rather low  $dE/dx$ , and as such a tight cut is most probably not advisable if a high signal efficiency is desired. On the other hand, should an excess of events be observed, we expect that  $dE/dx$  will be important to measure the mass and string tension.

## Chapter 6

# Composite Higgs models in disguise

### Abstract

We present a mechanism for *disguising* one composite Higgs model as another. Allowing the global symmetry of the strong sector to be broken by large mixings with elementary fields, we show that we can disguise one coset  $\mathcal{G}/\mathcal{H}$  such that at low energies the phenomenology of the model is better described with a different coset  $\mathcal{G}'/\mathcal{H}'$ . Extra scalar fields acquire masses comparable to the rest of the strong sector resonances and therefore are no longer considered pNGBs. Following this procedure we demonstrate that two models with promising UV-completions can be disguised as the more minimal  $SO(5)/SO(4)$  coset.

## 6.1 Introduction

The hierarchy problem is one of the most puzzling aspects of the Standard Model, and still it lacks a satisfactory solution. Composite Higgs models [19, 32, 33, 44] offer a fascinating explanation of the origin of the electroweak scale – the Higgs is a composite pseudo-Nambu Goldstone boson (pNGB), which arises when a new sector becomes strongly interacting and confines. This new sector is endowed with a global symmetry, and it is the breaking of this global symmetry by non-perturbative vacuum condensates which leads to the appearance of the Higgs as a pNGB.

The low-energy behaviour of Composite Higgs (CH) models can be studied in an Effective Field Theory (EFT) framework, in which the heavy resonances of the strong sector are integrated out. This picture is useful, since we do not need to know the details of the UV-completion in order to understand the spectrum of the theory at energies below the confinement scale. The only features of the strong sector that we need to specify are its global symmetry  $\mathcal{G}$  and the manner in which this symmetry breaks:  $\mathcal{G} \rightarrow \mathcal{H}$ . The pNGBs will come in a non-linear representation of the broken symmetry coset  $\mathcal{G}/\mathcal{H}$ , and the top partners – the light, fermionic resonances that are present in all realistic realisations – will come in full representations of  $\mathcal{G}$ . A sigma-model approach then allows for a derivation of the pNGB potential (albeit in terms of unknown form-factors). In this way the main phenomenological differences between different CH models can be readily inferred from the symmetry structure of the theory.

Of course, merely plucking a symmetry out of the air is not equivalent to claiming it is *realisable* in a QFT framework. Some work has been done towards constructing UV-completions of Composite Higgs models [29–31, 35, 218]. Not all symmetry cosets, it turns out, were created equal. The cosets  $SU(4)/Sp(4)$ ,  $SU(5)/SO(5)$ , and  $SU(4) \times SU(4)/SU(4)$  have been identified as the minimal cosets that have a UV-completion in the form of a fermion-gauge theory. The Minimal Composite Higgs Model (MCHM)  $SO(5)/SO(4)$  is notably not so easy to complete. From one perspective, it might be argued that one should restrict one’s attention to Composite Higgs models based on UV-completable cosets, and to take seriously the phenomenology they predict.

However in this work we describe a mechanism whereby a Composite Higgs model with the coset  $\mathcal{G}/\mathcal{H}$  might, at energies currently accessible to us, be *disguised* as a model with a different symmetry coset  $\mathcal{G}'/\mathcal{H}'$ , with  $\mathcal{G}' \subset \mathcal{G}$  and  $\mathcal{H}' \subset \mathcal{H}$ . This can happen in such a way that at or below the confinement scale  $f$ , only the resonances predicted by the  $\mathcal{G}'/\mathcal{H}'$  model are seen, while the remaining resonances acquire masses  $\gg f$  and could remain



hidden – thus the model is disguised.

This paper is organised as follows. In Section 6.2, we present a general description of the mechanism, assuming that the field responsible for deforming the strong sector is a new fermion  $\psi$  which is a singlet under the SM gauge group. In Section 6.3, we walk through two examples in which the original symmetry coset is  $SU(4)/Sp(4)$  and  $SU(5)/SO(5)$ , in both cases showing that they can be disguised as the MCHM coset  $SO(5)/SO(4)$ . Then in Section 6.4 we argue that the field responsible for the deformation could in fact be the right-handed top quark, if we take  $t_R$  to be ‘mostly’ composite. Finally in Section 6.5 we conclude our discussion.

## 6.2 Mechanism

In Composite Higgs models we assume that the new, strongly interacting sector is endowed with a global symmetry  $\mathcal{G}$ . The Higgs will be part of a set of pseudo-Nambu Goldstone bosons (pNGBs) that arise when  $\mathcal{G}$  is spontaneously broken to a subgroup  $\mathcal{H}$ . The  $n$  pNGBs live in the coset  $\mathcal{G}/\mathcal{H}$ , and there will be one for each broken generator, i.e.  $n = \dim \mathcal{G} - \dim \mathcal{H}$ . The Higgs and other pNGBs can only acquire a potential if the global symmetry  $\mathcal{G}$  is explicitly broken by couplings to an external sector. This is normally accomplished by allowing the SM to couple to the strong sector – these couplings then explicitly break  $\mathcal{G}$  and induce a loop-level potential for the pNGBs.

We are going to consider a modified scenario, in which some new fields couple to the strong sector and provide an extra source of explicit breaking. We are particularly interested in the case where these new couplings are *strong*. We will say that the new couplings deform, or rather, *disguise* the strong sector’s symmetry properties – due to the explicit breaking, its apparent global symmetry is now a subgroup of the original symmetry, and the pattern of spontaneous breaking has been modified.

Depending on the nature of these new fields, there are different ways they could couple to the strong sector. We are going to focus on the case where the new fields are fermionic, and couple to the strong sector via the partial compositeness mechanism [22, 23]. This mechanism is normally employed to allow the SM quarks (or at the very least, the top), to interact with the composite sector. Ordinarily we consider terms such as

$$\mathcal{L} \supset y_L f \bar{q}_L \mathcal{O}_L + y_R f \bar{t}_R \mathcal{O}_R + h.c., \quad (6.1)$$

where  $q_L = (t_L, b_L)$ . The  $\mathcal{O}_{L,R}$  are composite fermionic operators with the same SM quantum numbers as  $q_L, t_R$ . Thus the elementary top quark mixes with the ‘top partners’,

allowing the physical, partially composite eigenstate to couple to the Higgs.

Now, the couplings in (6.1) will explicitly break the global symmetry  $\mathcal{G}$ . If we were to write the couplings in full we would have, for instance:

$$\mathcal{L} \supset y_L f(\bar{q}_L)_\alpha (\Delta_L)_i^\alpha \mathcal{O}_L^i + y_R f(\bar{t}_R)_\alpha (\Delta_R)_i^\alpha \mathcal{O}_R^i, \quad (6.2)$$

where  $i$  is an index belonging to  $\mathcal{G}$  and  $\alpha$  belongs to the SM gauge group. The tensor  $\Delta$  carries indices under both the SM gauge group and  $\mathcal{G}$ , parametrising precisely how the symmetry  $\mathcal{G}$  is broken [136]. One can think of  $(\bar{t}_L)_\alpha \Delta_i^\alpha$  as an embedding of the SM top into a ‘spurionic’ representation of  $\mathcal{G}$ . The representation into which the top is embedded should match the representation in which  $\mathcal{O}_L$  transforms, and this ensures that the explicit breaking is treated in a way formally consistent with the symmetries of the strong sector.

As an example, let us consider the MHCM, which has the pNGB coset  $SO(5)/SO(4)$ . The  $SO(4)$  in this model becomes the custodial  $SO(4) \simeq SU(2)_L \times SU(2)_R$ . We can take  $\mathcal{O}_L$  and  $\mathcal{O}_R$  to both be in the  $\mathbf{5}$  of  $SO(5)$ , which decomposes under the custodial group as  $(\mathbf{2}, \mathbf{2}) \oplus (\mathbf{1}, \mathbf{1})$ . The  $q_L$  then couples to the bidoublet, while the  $t_R$  couples to the singlet. This translates into the following expressions [174] for  $\Delta_{L,R}$  in (6.2):

$$\begin{aligned} \Delta_L &= \frac{1}{\sqrt{2}} \begin{pmatrix} 0 & 0 & 1 & -i & 0 \\ 1 & i & 0 & 0 & 0 \end{pmatrix} \\ \Delta_R &= -i \begin{pmatrix} 0 & 0 & 0 & 0 & 1 \end{pmatrix}. \end{aligned} \quad (6.3)$$

Proceeding along similar lines, let us introduce a new fermion  $\psi$ , which mixes with a composite operator  $\mathcal{O}_\psi$ . For simplicity, let us take  $\psi$  to be a singlet under the SM gauge group. The mixing terms look like:

$$\mathcal{L}_\mathcal{G} = y_\psi f \bar{\psi} \Delta_i \mathcal{O}_\psi^i + h.c. \quad (6.4)$$

Note that the  $\alpha$  index has been omitted, since  $\psi$  is a singlet under the Standard Model. Now we are going to assume that the mixing parameter  $y_\psi$  is large – so that  $\mathcal{G}$  is no longer a good symmetry. Let us define  $\mathcal{G}' \subset \mathcal{G}$  such that  $\mathcal{G}'$  is the residual symmetry after the interactions with  $\psi$  are included. Suppose that the global symmetry of the original theory *spontaneously* breaks to  $\mathcal{H}$ , and define  $\mathcal{H}' = \mathcal{H} \cap \mathcal{G}'$ . Then, with the inclusion of  $\mathcal{L}_\mathcal{G}$ , the new theory appears to have the *new* symmetry breaking pattern  $\mathcal{G}'/\mathcal{H}'$ . One composite Higgs model has been disguised as another.

What do we mean when we say that  $y_\psi$  is large? In the language of [219, 220], we can broadly parametrise the strong sector via its typical mass scale  $m_\rho$  and coupling  $g_\rho$ , which scales in large- $N$  theories [79] as

$$g_\rho = \frac{4\pi}{\sqrt{N}}. \quad (6.5)$$

They are related to the symmetry-breaking scale via  $m_\rho = g_\rho f$ . The limit  $g_\rho = 4\pi$  represents the limit of validity of the effective theory; for stronger couplings a loop expansion in  $(g_\rho/4\pi)^2$  is no longer valid.

For  $y_\psi \approx g_\rho$ , the mixing angle between the elementary  $\psi$  and  $\mathcal{O}_\psi$  is large, and the physical eigenstates will have a large degree of compositeness. Operators induced by the coupling of  $\psi$  to the strong sector (which violate  $\mathcal{G}$ ) will be proportional to some power of  $(y_\psi/g_\rho)$ , and in the limit where  $y_\psi \approx g_\rho$ , these operators are no longer suppressed. We are justified in saying that the apparent global symmetry of the strong sector has been disguised, since operators which break the symmetry appear at the same order as operators which respect it.

In order to have a large value of  $y_\psi$ , we require the scaling dimension of  $\mathcal{O}_\psi$  to be close to  $5/2$ . This can happen if the dynamics above the compositeness scale are approximately conformal, and the operator  $\mathcal{O}_\psi$  has a large anomalous dimension [19]. A similar requirement holds for the mixings of the top quark to the top partners – in order to generate a sizeable  $\mathcal{O}(1)$  top Yukawa, the  $\mathcal{O}_{L,R}$  must have large anomalous dimensions so that the mixing terms become effectively relevant operators.

### 6.3 Two examples

It is often remarked that the Minimal Composite Higgs model (MCHM) [19] has no UV-completion in the form of a renormalisable gauge-fermion theory. As discussed in [29, 30], a theory whose UV-completion consists of  $n_i$  fermions in each representation  $R_i$  of the new strongly interacting gauge group (assuming it is simple) has the following global symmetry:

$$\mathcal{G} = SU(n_1) \times \cdots \times SU(n_p) \times U(1)^{p-1}, \quad (6.6)$$

where  $p$  is the number of different irreducible representations in the model. From this we see that there is no simple gauge-fermion theory that gives rise to an  $SO(5)/SO(4)$  pNGB coset.

In this section we will take two models which *do* have gauge-fermion UV-completions, and show that using the above procedure they can be disguised at low energy as the  $SO(5)/SO(4)$  model.

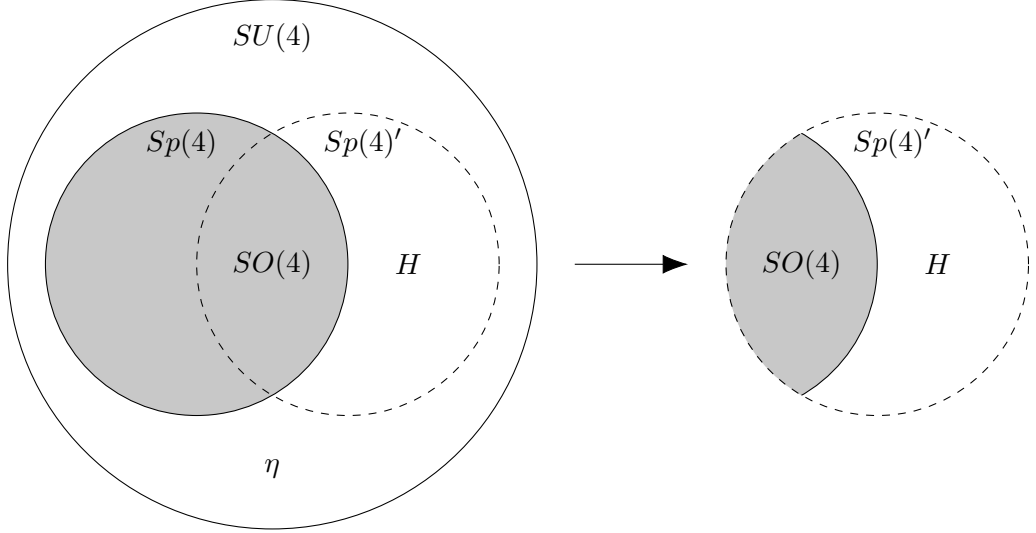


Figure 6.1: Symmetry breaking patterns in the disguised  $SU(4)/Sp(4)$  model. The solid circles represent the spontaneous breaking in the original model. The dashed circle represents the  $Sp(4)'$  subgroup preserved by the explicit breaking, so that the ‘disguised’ model becomes  $Sp(4)'/SO(4)$ .

### 6.3.1 $SU(4)/Sp(4)$

In this section we will look at the next to minimal Composite Higgs model [28, 221], in which the pNGB coset is  $SU(4)/Sp(4)$ .<sup>1</sup> This coset features one extra singlet pNGB, which we denote by  $\eta$ . The spontaneous breaking is achieved by a VEV in the antisymmetric **6** of  $SU(4)$ , which we will take to be proportional to

$$\langle \mathbf{6} \rangle \propto \begin{pmatrix} i\sigma^2 & 0 \\ 0 & i\sigma^2 \end{pmatrix}. \quad (6.7)$$

Then the pNGBs are parametrised as fluctuations around the vacuum:

$$\Sigma(\phi^i) = U \langle \mathbf{6} \rangle U^T, \quad U = \exp(i\phi^i X^i / f), \quad (6.8)$$

where  $\phi = \{H, \eta\}$  and  $X^i$  are the broken generators.<sup>2</sup>

As outlined in the previous section, we will introduce a new fermionic field  $\psi$ , singlet under the SM. In order to disguise this model as  $SO(5)/SO(4)$ , we must look for a  $\mathcal{L}_{\mathcal{G}}$  that explicitly breaks  $\mathcal{G}$  to  $\mathcal{G}' = SO(5)$ . This can be done, for instance, with  $\mathcal{O}_{\psi}$  in the **6** of  $SU(4)$ . In this case (6.4) looks like

$$\mathcal{L}_{\mathcal{G}} = y_{\psi} f \bar{\psi} \text{Tr}[\Delta \mathcal{O}_{\psi}] + h.c. \quad (6.9)$$

<sup>1</sup>A UV-completion of this coset was studied on the lattice with an  $SU(2)$  confining gauge force [222] – the results point to a large value of  $g_{\rho} \sim \mathcal{O}(10)$ , in line with the large- $N$  expectation.

<sup>2</sup>The calculations in this and the next section use a specific basis for the generators of  $SU(4)$  and  $SU(5)$ . We use the bases given in [28, 30], to which the interested reader can refer.

The  $\mathbf{6}$  decomposes under  $SU(2)_L \times SU(2)_R$  as:

$$\mathbf{6} = (\mathbf{2}, \mathbf{2}) \oplus (\mathbf{1}, \mathbf{1}) \oplus (\mathbf{1}, \mathbf{1}). \quad (6.10)$$

The new field  $\psi$  must couple to a linear combination of the two singlets in this decomposition. The two singlets correspond to

$$\Delta_{\pm} = \begin{pmatrix} \pm i\sigma_2 & 0 \\ 0 & i\sigma_2 \end{pmatrix}, \quad (6.11)$$

and one can verify that if we take

$$\Delta = \cos \theta \Delta_- + \sin \theta \Delta_+, \quad (6.12)$$

the unbroken symmetry is indeed an  $Sp(4)' \simeq SO(5)$  subgroup of the original  $SU(4)$ .

Notice that, using this notation,  $\langle \mathbf{6} \rangle \propto \Delta_+$ . So long as  $\theta \neq \pi/2$ , the explicit and spontaneous breakings preserve *different*  $Sp(4)$  subgroups. That is, in our earlier notation:

$$\begin{aligned} \mathcal{G}' &= Sp(4)' \\ \mathcal{H} &= Sp(4) \\ \mathcal{H}' &= \mathcal{H} \cap \mathcal{G}' = Sp(4) \cap Sp(4)'. \end{aligned} \quad (6.13)$$

If the spontaneous and explicit breakings preserved the *same*  $Sp(4)$  subgroup, then in the disguised model there would be no spontaneous symmetry breaking at all, since the spontaneously broken symmetry would never have been a good symmetry in the first place. In Fig. 6.1, this would correspond to the  $Sp(4)$  and  $Sp(4)'$  circles coinciding. In such a model there would be no Goldstone bosons – the explicit breaking leads  $H$  and  $\eta$  to acquire masses comparable to the other resonances of the strong sector.

Since we are trying to disguise  $SU(4)/Sp(4)$  as  $SO(5)/SO(4)$ , we want the Higgs (but not  $\eta$ ) to remain an exact Goldstone boson. One can verify that in the limit where  $\theta \rightarrow 0$ , the generators corresponding to the four degrees of freedom of the Higgs are preserved by the explicit breaking. This is the case shown in Fig. 6.1: the Higgs lives in the part of  $Sp(4)'$  which is spontaneously broken, while the  $\eta$  lives in the part of  $SU(4)$  which is broken by the explicit breaking, and thus acquires a large mass and is hidden. Thus we have disguised the  $SU(4)/Sp(4)$  coset as  $SO(5)/SO(4)$ .

Note that the angle  $\theta$  is parametrising some of our ignorance about the UV physics. Without having a specific UV model in mind we cannot predict the misalignment between the explicit breaking and the spontaneous breaking. With an explicit model one might be able to use lattice calculations, and/or an NJL-type analysis (see, for instance, [35]),

in order to obtain a better understanding of the true vacuum of the theory. For now, however, we are working at a more general level, and will treat  $\theta$  as a free parameter.

Another way of seeing this mechanism at work is to look at the Coleman-Weinberg potential for the pNGBs. Including only the corrections from loops of the new fermion field  $\psi$ , the potential must be constructed out of invariants of  $\Sigma$  and  $\Delta$ , i.e. it should be a function of  $\text{Tr}[\Delta^T \Sigma]$ . Taking  $\Delta$  as defined in (6.12), the lowest order contribution to the CW potential is

$$V \propto -\text{Tr}[\Delta^T \Sigma] \text{Tr}[\Delta \Sigma^\dagger] \quad (6.14)$$

$$= \cos^2 \theta \eta^2 + \sin^2 \theta (1 - h^2 - \eta^2). \quad (6.15)$$

We can see that in the limit  $\theta \rightarrow 0$ ,  $h$  remains an exact Goldstone boson, living in the coset  $SO(5)/SO(4)$ .

One should note that, in arriving at the above expression, we performed the following field redefinitions of the pNGB fields (following [28]):

$$\begin{aligned} \frac{h}{\sqrt{h^2 + \eta^2}} \sin \left( \frac{\sqrt{h^2 + \eta^2}}{f} \right) &\rightarrow h, \\ \frac{\eta}{\sqrt{h^2 + \eta^2}} \sin \left( \frac{\sqrt{h^2 + \eta^2}}{f} \right) &\rightarrow \eta. \end{aligned} \quad (6.16)$$

Field redefinitions of the form  $\phi \rightarrow \phi f(\phi)$ , (with  $f(0) = 1$ ), are valid in the context of the sigma-model [21]; the above redefinition is especially useful since it makes clear the fact that  $h$  is an *exact* pNGB in the  $\theta \rightarrow 0$  limit.<sup>3</sup>

In order for the disguising mechanism to work, we need a small value of  $\sin \theta$  – only then will there be a hierarchy between the masses of  $\eta$  and  $H$ . Having large values of both  $\sin \theta$  and  $y_\psi$  will spoil the role of the Higgs as a Goldstone boson, giving it a mass closer to that of the other strong sector resonances.

### 6.3.2 $SU(5)/SO(5)$

Another coset with a realistic UV-completion is  $SU(5)/SO(5)$  [30, 223, 224]. In this section we show that, in complete analogy with the previous section, this model can also be disguised as the MCHM via a suitable choice of  $\mathcal{L}_\mathcal{G}$ .<sup>4</sup>

<sup>3</sup>Furthermore, in this basis it is precisely the VEV of  $h$  which sets the scale of EWSB, i.e.  $m_W \propto \langle h \rangle$ .

<sup>4</sup>See [103] for a microscopic realisation

The spontaneous breaking  $SU(5) \rightarrow SO(5)$  can be achieved with a VEV in the symmetric **15** of  $SU(5)$ , which we take to be proportional to

$$\langle \mathbf{15} \rangle \propto \begin{pmatrix} \mathbb{1}_4 & 0 \\ 0 & 1 \end{pmatrix}. \quad (6.17)$$

This coset features 14 pNGBs, the Higgs, a charged  $SU(2)_L$  triplet  $\Phi_{\pm}$ , a neutral triplet  $\Phi_0$ , and a singlet  $\eta$ . These are parametrised by

$$\Sigma = U \langle \mathbf{15} \rangle U^T, \quad U = \exp(i\phi^a X^a/f), \quad (6.18)$$

but since in this case  $\langle \mathbf{15} \rangle$  is proportional to the identity, we can just write  $\Sigma = UU^T$ .

Let us assume that the new source of explicit breaking comes from a SM singlet fermion  $\psi$ . Then, just as before,  $\mathcal{L}_{\mathcal{G}}$  is given by:

$$\mathcal{L}_{\mathcal{G}} = y_{\psi} f \bar{\psi} \text{Tr}[\Delta \mathcal{O}_{\psi}] + h.c. \quad (6.19)$$

where now we take  $\mathcal{O}_{\psi}$  to be in the **15** of  $SU(5)$ . Notice that in both this and the previous example,  $\mathcal{O}_{\psi}$  was taken to be in the same representation as the operator whose VEV breaks the symmetry spontaneously.

Now the **15** of  $SU(5)$  decomposes under  $SU(2)_L \times SU(2)_R$  as:

$$\mathbf{15} = (\mathbf{3}, \mathbf{3}) \oplus (\mathbf{2}, \mathbf{2}) \oplus (\mathbf{1}, \mathbf{1}) \oplus (\mathbf{1}, \mathbf{1}). \quad (6.20)$$

If we take the new source of breaking to be a SM singlet, then, just as in the  $SU(4)/Sp(4)$  case, we have two singlets in the decomposition of the **15** to which  $\psi$  may couple. These two singlets correspond to:

$$\Delta_{\pm} = \begin{pmatrix} \mathbb{1}_4 & 0 \\ 0 & \pm 1 \end{pmatrix}. \quad (6.21)$$

For a linear combination of the two singlets,  $\Delta = \cos \theta \Delta_- + \sin \theta \Delta_+$ ,  $SU(5)$  is explicitly broken to  $SO(5)'$ . Precisely as before, only in the limit  $\theta \rightarrow 0$  is the Higgs untouched by the explicit breaking. Furthermore, the explicit breaking gives masses to  $\Phi_{\pm}$ ,  $\Phi_0$  and  $\eta$ . In the case where  $y_{\psi}$  is large, the pNGB coset is disguised as  $SO(5)/SO(4)$ .

## 6.4 Deforming with $t_R$

It has been noted [219, 225, 226] that it is phenomenologically possible, and perhaps desirable, for the  $t_R$  quark to be ‘mostly’ composite, in the sense that  $y_R$  in (6.1) is of order  $g_{\rho}$ . If this were the case, then the couplings of  $t_R$  to the strong sector can indeed be thought of

as changing the symmetry properties of the strong sector, and disguising the coset space as another.

Let us go back to the  $SU(4)/Sp(4)$  example. Of course, unlike our hypothetical field  $\psi$ ,  $t_R$  is not a Standard Model singlet – it is charged under  $U(1)_Y$  and  $SU(3)_c$ . This does not change the discussion of Section 6.3.1, however; we just replace  $\mathcal{O}_\psi$  with  $\mathcal{O}_R$ , which has the same SM quantum numbers as  $t_R$ . In the original paper studying this coset [28], the authors conclude that, in order to preserve the custodial symmetry that protects the  $Zb\bar{b}$  coupling, the left and right handed quarks ought to be embedded into the **6** of  $SU(4)$  – precisely as we did for  $\psi$  in Sec. 6.3.1.

It is clear that, if we want  $t_R$  to couple to the Higgs and to participate in Yukawa interactions, then we must have  $\theta \neq 0$ . As stated earlier, we can always take  $\theta$  to be small, such that a large hierarchy is generated between  $\eta$  and  $h$ . First however, we should check that small values of  $\theta$  are still consistent with a large enough top Yukawa coupling. We must embed  $q_L$  into the  $(\mathbf{2}, \mathbf{2})$  of the **6**, which fixes

$$\Delta_L = \begin{pmatrix} 0 & Q \\ -Q^T & 0 \end{pmatrix}, \quad (6.22)$$

with  $Q = (0, q_L)$ . Let us assume that the couplings of  $t_R$  are proportional to  $\Delta_R$  in analogy to (6.12):

$$\Delta_R = \cos \theta \Delta_- + \sin \theta \Delta_+. \quad (6.23)$$

Then the Yukawa coupling of the top is obtained from the effective operator:

$$M_t \bar{t}_L t_R \text{Tr}[\Delta_L^T \Sigma] \text{Tr}[\Delta_R \Sigma^\dagger], \quad (6.24)$$

where  $M_t$  is a momentum-dependent form factor which encodes the integrated-out dynamics of the strong sector. Expanding this operator informs us that the coupling  $\bar{t}_L t_R h$  will be proportional to  $\sin \theta$ .

We expect the Yukawa coupling also to be proportional to  $y_L y_R$ , and dimensional reasoning (discussed in detail in [136]) suggests it should also be proportional to  $f/m_T$ , where  $m_T$  is the mass of the lightest top partner. Thus we conclude that the top Yukawa scales, up to some numeric prefactor, as

$$y_t \approx y_L y_R \sin \theta \frac{f}{m_T}. \quad (6.25)$$

Furthermore, all contributions to the CW potential of the Higgs involving the right-handed top must be proportional to powers of  $\text{Tr}[\Delta_R \Sigma^\dagger]$  – therefore the contributions to the potential must always depend on powers of  $y_R \sin \theta$ . In fact, the usual analyses of the



size of the top Yukawa, the mass of the Higgs and the top partners, and the required tuning for successful EWSB, proceed along all the usual lines, with the replacement  $y_R \rightarrow y_R \sin \theta$ .

The disguising mechanism relies on small values of  $\sin \theta$ , but of course we can make  $\sin \theta$  small as long as  $y_R$  is sufficiently large. The mass of  $\eta$  will be proportional to  $\cos 2\theta$  (from equation (6.15)), and for small  $\theta$  the hierarchy between the ‘true’ pNGB  $h$  and the disguised pNGB  $\eta$  is assured. Thus the couplings of the top quark alone can fulfil the requirements of the disguising mechanism.

What is the phenomenology of such a scenario? We have a set of pNGBs which couple very strongly to the top – in this example just the  $\eta$ , but in the  $SU(5)/SO(5)$  case we would have  $\Phi_{\pm}, \Phi_0$  and  $\eta$ . In ordinary composite Higgs models we expect these extra scalars to be heavier than the Higgs by roughly a factor  $\xi = v^2/f^2$ . In models with around 10% tuning, this corresponds to a mass of around 400-500 GeV. In our scenario, they would be significantly heavier (how much heavier is of course dependent on the value of  $\theta$ , or how *disguised* the model is), but their Yukawa couplings to the top would be increased by the same factor.

At sufficiently high center of mass energies, these resonances would eventually appear, along with other fermionic and vector resonances. Evidence for the disguising mechanism would be the presence of *split* multiplets. For instance, in the  $SU(4)/Sp(4)$  model we have top partners in the **6** of  $SU(4)$ . In the disguised model, this would be split into  $\mathbf{5} \oplus \mathbf{1}$  of the unbroken  $SO(5)$ , with the singlet coupling most strongly to  $t_R$ . We would expect the large breaking of the  $SU(4)$  symmetry to lead to a mass splitting between the five-plet and the singlet.

## 6.5 Conclusion

We have presented a mechanism whereby the symmetry breaking pattern of the strong sector can be disguised, via couplings of an elementary field to a strong sector operator. This field could be a BSM field, or, as we argued in Section 6.4, it could be the right-handed top quark, avoiding the need for any new fields.

This is a useful observation, especially if one has reason to believe that some pNGB cosets might be more plausible than others – perhaps because one is concerned about UV-completions of the model. We have shown that two UV-completable cosets,  $SU(4)/Sp(4)$  and  $SU(5)/SO(5)$ , can be deformed in such a way that at low energies the pNGB spectrum is as we would expect in an  $SO(5)/SO(4)$  model.

This is certainly not equivalent to claiming that a UV-completion for the  $SO(5)/SO(4)$

coset has been found. After all, the mixing  $\bar{\psi}\mathcal{O}_\psi + h.c.$  will arise from a non-renormalisable operator, presumably a four-fermion operator involving  $\psi$  and three techni-fermions. Nonetheless, attempts at finding a ‘UV-completion’ of composite Higgs models so far do not speculate on the origin of these four-fermion interactions<sup>5</sup> (their scale can be significantly higher than the compositeness scale). Therefore it is fair to say that we have found a UV-completion of the  $SO(5)/SO(4)$  coset which is *just as complete* as any other composite Higgs UV-completion.

In the case where the  $t_R$  is responsible for the disguise, we have a model with a set of heavy scalar resonances with very strong couplings to the top – very strong in this case meaning close to the non-perturbative limit. We leave a detailed phenomenological analysis for future work. It would be interesting to study whether the large couplings of the scalars to the top can lead to sizable contributions to effective operators, and whether these can have any impact on Higgs or gauge boson production cross-sections.

---

<sup>5</sup>This discussion might call into question the usage of the term ‘UV-completion’ – there are always problems whose solutions can be delayed to a higher scale.

## Chapter 7

# Conclusions

### 7.1 Summary

In this thesis, I have discussed a number of strongly-coupled extensions to the Standard Model – in particular Composite Higgs models as a solution to the hierarchy problem.

In Chapter 2 we reviewed the status of different types of Composite Higgs models and put bounds on the value of the compositeness scale  $f$ . We considered different scenarios in which the Higgs might mix with other scalar pNGBs and discussed how this might affect the bounds.

In Chapter 3 we presented a novel approach to the study of inflation, borrowing the formalism from the Composite Higgs literature and applying it to a scenario in which the inflaton is a pseudo-Nambu Goldstone boson. We find that by considering general bosonic and fermionic contributions to the inflaton’s Coleman-Weinberg potential we can achieve successful inflation with sub-Planckian values of the inflaton decay constant.

In Chapter 4 we introduced a class of Composite Higgs models in which the Higgs mixes with an extra pNGB doublet. This mixing induces a negative mass-squared for one of the physical eigenstates, and therefore contributes to the destabilisation of the Higgs potential. We discussed the modifications of the couplings of the Higgs in such a model, focusing in particular on the successive breaking pattern  $SO(6) \rightarrow SO(5) \rightarrow SO(4)$ , and analysed the tuning required for a successful realisation.

In Chapter 5 we perform a phenomenological analysis of the quirks scenario, and proposed a method to efficiently search for these particles at the LHC. The method relies on the trajectory of the quirks being constrained to lie in a plane. Our simulations indicate that the search strategy has a high efficiency across a broad region of the quirk parameter space.

Finally, in Chapter 6 I presented a mechanism whereby one Composite Higgs model, based on a coset  $\mathcal{G}/\mathcal{H}$ , can be deformed so that it resembles a model with a different coset. Two examples were worked through and discussed, as was the possibility that the particle responsible for the deforming might be the right-handed top quark.

## 7.2 Directions for further study

A broad range of topics have been discussed in this thesis, opening up a variety of directions for future study.

More detailed study of UV-completable Composite Higgs models – i.e. those models based on the cosets identified in [29–31] – is merited. In particular, the  $SU(5)/SO(5)$  coset promises 10 extra scalar degrees of freedom besides the Higgs, which could lead to an incredibly rich phenomenology, especially considering the ways that these degrees of freedom might mix with each other. This could go hand in hand with a practical application of the mechanism developed in Chapter 6.

The complicated scalar structure of the theory, and the comparatively small number of free parameters that determine the scalar potential, could make such a model interesting to study in the context of other open problems in the Standard Model, for instance electroweak baryogenesis.

It would also be interesting to investigate whether the model studied in Chapter 4 can be UV-completed with a fermion-gauge theory. In particular, the mechanism discussed in Chapter 6 could be employed in order to generate the required mass hierarchy between the two scalar doublets in the model. The challenge would be finding an appropriate source of explicit breaking that is able to generate the required mixing between the two doublets. With a tentative UV completion we might be able to make more concrete statements about the tuning required to make such a model viable.

Further study of models featuring quirks is also warranted. Despite their unusual collider signatures, quirks are a fairly generic extension of the Standard Model, and can arise in well-motivated BSM models such as Twin Higgs models [198, 199]. It would be interesting to study whether there are any cosmological bounds that can be put on these models, especially in regions of their parameter space for which detection of quirks at colliders is unfeasible.

# Bibliography

- [1] V. Sanz and J. Setford, “Composite Higgs models after Run 2,” *Adv. High Energy Phys.* **2018** (2018) 7168480, [arXiv:1703.10190 \[hep-ph\]](#). ii, 14
- [2] D. Croon, V. Sanz, and J. Setford, “Goldstone Inflation,” *JHEP* **10** (2015) 020, [arXiv:1503.08097 \[hep-ph\]](#). ii, 15, 21, 23
- [3] V. Sanz and J. Setford, “Composite Higgses with seesaw EWSB,” *JHEP* **12** (2015) 154, [arXiv:1508.06133 \[hep-ph\]](#). ii, 15, 18, 24, 27
- [4] S. Knapen, H. K. Lou, M. Papucci, and J. Setford, “Tracking down Quirks at the Large Hadron Collider,” *Phys. Rev.* **D96** (2017) no. 11, 115015, [arXiv:1708.02243 \[hep-ph\]](#). ii, 15
- [5] J. Setford, “Composite Higgs models in disguise,” *JHEP* **01** (2018) 092, [arXiv:1710.11206 \[hep-ph\]](#). ii, 15
- [6] F. Englert and R. Brout, “Broken Symmetry and the Mass of Gauge Vector Mesons,” *Phys. Rev. Lett.* **13** (1964) 321–323. 3
- [7] P. W. Higgs, “Broken Symmetries and the Masses of Gauge Bosons,” *Phys. Rev. Lett.* **13** (1964) 508–509. 3
- [8] G. S. Guralnik, C. R. Hagen, and T. W. B. Kibble, “Global Conservation Laws and Massless Particles,” *Phys. Rev. Lett.* **13** (1964) 585–587. 3
- [9] **ATLAS** Collaboration, G. Aad *et al.*, “Observation of a new particle in the search for the Standard Model Higgs boson with the ATLAS detector at the LHC,” *Phys. Lett.* **B716** (2012) 1–29, [arXiv:1207.7214 \[hep-ex\]](#). 3
- [10] **CMS** Collaboration, S. Chatrchyan *et al.*, “Observation of a new boson at a mass of 125 GeV with the CMS experiment at the LHC,” *Phys. Lett.* **B716** (2012) 30–61, [arXiv:1207.7235 \[hep-ex\]](#). 3

- [11] G. 't Hooft, “Naturalness, chiral symmetry, and spontaneous chiral symmetry breaking,” *NATO Sci. Ser. B* **59** (1980) 135–157. 3, 49
- [12] S. P. Martin, “A Supersymmetry primer,” [arXiv:hep-ph/9709356](#) [hep-ph]. [Adv. Ser. Direct. High Energy Phys.18,1(1998)]. 3, 4
- [13] S. Weinberg, “Implications of Dynamical Symmetry Breaking,” *Phys. Rev.* **D13** (1976) 974–996. [Addendum: *Phys. Rev.*D19,1277(1979)]. 6
- [14] L. Susskind, “Dynamics of Spontaneous Symmetry Breaking in the Weinberg-Salam Theory,” *Phys. Rev.* **D20** (1979) 2619–2625. 6
- [15] S. Dimopoulos and L. Susskind, “Mass Without Scalars,” *Nucl. Phys.* **B155** (1979) 237–252. [2,930(1979)]. 6
- [16] M. E. Peskin and T. Takeuchi, “A New constraint on a strongly interacting Higgs sector,” *Phys. Rev. Lett.* **65** (1990) 964–967. 6
- [17] M. Golden and L. Randall, “Radiative Corrections to Electroweak Parameters in Technicolor Theories,” *Nucl. Phys.* **B361** (1991) 3–23. 6
- [18] M. E. Peskin and T. Takeuchi, “Estimation of oblique electroweak corrections,” *Phys. Rev.* **D46** (1992) 381–409. 7
- [19] K. Agashe, R. Contino, and A. Pomarol, “The Minimal composite Higgs model,” *Nucl. Phys.* **B719** (2005) 165–187, [arXiv:hep-ph/0412089](#) [hep-ph]. 7, 17, 18, 21, 33, 59, 93, 96
- [20] S. R. Coleman, J. Wess, and B. Zumino, “Structure of phenomenological Lagrangians. 1.,” *Phys. Rev.* **177** (1969) 2239–2247. 7
- [21] C. G. Callan, Jr., S. R. Coleman, J. Wess, and B. Zumino, “Structure of phenomenological Lagrangians. 2.,” *Phys. Rev.* **177** (1969) 2247–2250. 7, 18, 32, 61, 99
- [22] D. B. Kaplan, “Flavor at ssc energies: A new mechanism for dynamically generated fermion masses,” *Nuclear Physics B* **365** (1991) no. 2, 259 – 278. <http://www.sciencedirect.com/science/article/pii/S0550321305800215>. 9, 20, 94

- [23] R. Contino, T. Kramer, M. Son, and R. Sundrum, “Warped/composite phenomenology simplified,” *JHEP* **05** (2007) 074, [arXiv:hep-ph/0612180](#) [[hep-ph](#)]. 9, 20, 58, 94
- [24] R. Contino, “The Higgs as a Composite Nambu-Goldstone Boson,” in *Physics of the large and the small, TASI 09, proceedings of the Theoretical Advanced Study Institute in Elementary Particle Physics, Boulder, Colorado, USA, 1-26 June 2009*, pp. 235–306. 2011. [arXiv:1005.4269](#) [[hep-ph](#)].  
<https://inspirehep.net/record/856065/files/arXiv:1005.4269.pdf>. 9, 12, 18, 20, 33, 35, 50, 58, 59, 65
- [25] K. Agashe, R. Contino, L. Da Rold, and A. Pomarol, “A Custodial symmetry for  $Zb\bar{b}$ ,” *Phys. Lett.* **B641** (2006) 62–66, [arXiv:hep-ph/0605341](#) [[hep-ph](#)]. 10, 20
- [26] S. R. Coleman and E. J. Weinberg, “Radiative Corrections as the Origin of Spontaneous Symmetry Breaking,” *Phys. Rev.* **D7** (1973) 1888–1910. 11, 35, 60
- [27] **ATLAS** Collaboration, T. A. collaboration, “Search for pair production of vector-like top quarks in events with one lepton and an invisibly decaying Z boson in  $\sqrt{s} = 13$  TeV pp collisions at the ATLAS detector,”. 12, 26
- [28] B. Gripaios, A. Pomarol, F. Riva, and J. Serra, “Beyond the Minimal Composite Higgs Model,” *JHEP* **04** (2009) 070, [arXiv:0902.1483](#) [[hep-ph](#)]. 13, 18, 21, 33, 59, 61, 62, 97, 99, 101
- [29] G. Ferretti and D. Karateev, “Fermionic UV completions of Composite Higgs models,” *JHEP* **03** (2014) 077, [arXiv:1312.5330](#) [[hep-ph](#)]. 13, 14, 18, 20, 93, 96, 105
- [30] G. Ferretti, “UV Completions of Partial Compositeness: The Case for a  $SU(4)$  Gauge Group,” *JHEP* **06** (2014) 142, [arXiv:1404.7137](#) [[hep-ph](#)]. 13, 14, 18, 20, 21, 58, 93, 96, 97, 99, 105
- [31] G. Ferretti, “Gauge theories of Partial Compositeness: Scenarios for Run-II of the LHC,” *JHEP* **06** (2016) 107, [arXiv:1604.06467](#) [[hep-ph](#)]. 13, 14, 93, 105
- [32] D. B. Kaplan and H. Georgi, “ $SU(2) \times U(1)$  Breaking by Vacuum Misalignment,” *Phys. Lett.* **136B** (1984) 183–186. 17, 58, 93
- [33] D. B. Kaplan, H. Georgi, and S. Dimopoulos, “Composite Higgs Scalars,” *Phys. Lett.* **B136** (1984) 187–190. 17, 93

- [34] **ATLAS, CMS** Collaboration, G. Aad *et al.*, “Measurements of the Higgs boson production and decay rates and constraints on its couplings from a combined ATLAS and CMS analysis of the LHC pp collision data at  $\sqrt{s} = 7$  and 8 TeV,” *JHEP* **08** (2016) 045, [arXiv:1606.02266 \[hep-ex\]](#). 17, 18, 25
- [35] J. Barnard, T. Gherghetta, and T. S. Ray, “UV descriptions of composite Higgs models without elementary scalars,” *JHEP* **02** (2014) 002, [arXiv:1311.6562 \[hep-ph\]](#). 18, 20, 93, 98
- [36] R. Contino and A. Pomarol, “The holographic composite Higgs,” *Comptes Rendus Physique* **8** (2007) 1058–1067. 18
- [37] M. Carena, L. Da Rold, and E. Pontón, “Minimal Composite Higgs Models at the LHC,” *JHEP* **06** (2014) 159, [arXiv:1402.2987 \[hep-ph\]](#). 18, 21, 22
- [38] A. Carmona and F. Goertz, “A naturally light Higgs without light Top Partners,” *JHEP* **05** (2015) 002, [arXiv:1410.8555 \[hep-ph\]](#). 18, 21, 22, 58
- [39] R. Contino, “A Holographic composite Higgs model,” in *Proceedings, 18th Conference on High Energy Physics (IFAE 2006): Pavia, Italy, April 19-21, 2006*, pp. 215–218. 2007. [arXiv:hep-ph/0609148 \[hep-ph\]](#). 18, 21
- [40] S. De Curtis, S. Moretti, K. Yagyu, and E. Yildirim, “LHC Phenomenology of Composite 2-Higgs Doublet Models,” [arXiv:1610.02687 \[hep-ph\]](#). 18, 21, 24
- [41] S. De Curtis, S. Moretti, K. Yagyu, and E. Yildirim, “Perturbative unitarity bounds in composite two-Higgs doublet models,” *Phys. Rev.* **D94** (2016) no. 5, 055017, [arXiv:1602.06437 \[hep-ph\]](#). 18, 21, 24
- [42] J. Mrazek, A. Pomarol, R. Rattazzi, M. Redi, J. Serra, and A. Wulzer, “The Other Natural Two Higgs Doublet Model,” *Nucl. Phys.* **B853** (2011) 1–48, [arXiv:1105.5403 \[hep-ph\]](#). 18, 21
- [43] E. Bertuzzo, T. S. Ray, H. de Sandes, and C. A. Savoy, “On Composite Two Higgs Doublet Models,” *JHEP* **05** (2013) 153, [arXiv:1206.2623 \[hep-ph\]](#). 18, 21
- [44] A. Azatov and J. Galloway, “Light Custodians and Higgs Physics in Composite Models,” *Phys. Rev.* **D85** (2012) 055013, [arXiv:1110.5646 \[hep-ph\]](#). 18, 22, 58, 93



- [45] C. Csaki, T. Ma, and J. Shu, “The Maximally Symmetric Composite Higgs,” [arXiv:1702.00405 \[hep-ph\]](#). 18, 21
- [46] M. Low, A. Tesi, and L.-T. Wang, “Twin Higgs mechanism and a composite Higgs boson,” *Phys. Rev.* **D91** (2015) 095012, [arXiv:1501.07890 \[hep-ph\]](#). 18, 21, 27, 58
- [47] R. Barbieri, D. Greco, R. Rattazzi, and A. Wulzer, “The Composite Twin Higgs scenario,” *JHEP* **08** (2015) 161, [arXiv:1501.07803 \[hep-ph\]](#). 18, 21, 27, 58
- [48] R. Alonso, M. B. Gavela, L. Merlo, S. Rigolin, and J. Yepes, “The Effective Chiral Lagrangian for a Light Dynamical ”Higgs Particle”,,” *Phys. Lett.* **B722** (2013) 330–335, [arXiv:1212.3305 \[hep-ph\]](#). [Erratum: *Phys. Lett.*B726,926(2013)]. 18
- [49] G. Buchalla, O. Catà, and C. Krause, “Complete Electroweak Chiral Lagrangian with a Light Higgs at NLO,” *Nucl. Phys.* **B880** (2014) 552–573, [arXiv:1307.5017 \[hep-ph\]](#). [Erratum: *Nucl. Phys.*B913,475(2016)]. 18
- [50] I. Brivio, T. Corbett, O. J. P. Éboli, M. B. Gavela, J. Gonzalez-Fraile, M. C. Gonzalez-Garcia, L. Merlo, and S. Rigolin, “Disentangling a dynamical Higgs,” *JHEP* **03** (2014) 024, [arXiv:1311.1823 \[hep-ph\]](#). 18
- [51] I. Brivio, J. Gonzalez-Fraile, M. C. Gonzalez-Garcia, and L. Merlo, “The complete HEFT Lagrangian after the LHC Run I,” *Eur. Phys. J.* **C76** (2016) no. 7, 416, [arXiv:1604.06801 \[hep-ph\]](#). 18
- [52] G. Buchalla, O. Cata, and C. Krause, “A Systematic Approach to the SILH Lagrangian,” *Nucl. Phys.* **B894** (2015) 602–620, [arXiv:1412.6356 \[hep-ph\]](#). 18
- [53] C. G. Krause, *Higgs Effective Field Theories - Systematics and Applications*. PhD thesis, Munich U., 2016. [arXiv:1610.08537 \[hep-ph\]](#).  
<https://inspirehep.net/record/1494821/files/arXiv:1610.08537.pdf>. 18
- [54] P. Sikivie, L. Susskind, M. B. Voloshin, and V. I. Zakharov, “Isospin Breaking in Technicolor Models,” *Nucl. Phys.* **B173** (1980) 189–207. 19
- [55] B. Bellazzini, C. Csáki, and J. Serra, “Composite Higgses,” *Eur. Phys. J.* **C74** (2014) no. 5, 2766, [arXiv:1401.2457 \[hep-ph\]](#). 21, 33, 35
- [56] M. Montull, F. Riva, E. Salvioni, and R. Torre, “Higgs Couplings in Composite Models,” *Phys. Rev.* **D88** (2013) 095006, [arXiv:1308.0559 \[hep-ph\]](#). 22

- [57] M. Gorbahn, J. M. No, and V. Sanz, “Benchmarks for Higgs Effective Theory: Extended Higgs Sectors,” *JHEP* **10** (2015) 036, [arXiv:1502.07352 \[hep-ph\]](#). 22, 24, 71
- [58] R. Franceschini, G. F. Giudice, J. F. Kamenik, M. McCullough, A. Pomarol, R. Rattazzi, M. Redi, F. Riva, A. Strumia, and R. Torre, “What is the  $\gamma\gamma$  resonance at 750 GeV?,” *JHEP* **03** (2016) 144, [arXiv:1512.04933 \[hep-ph\]](#). 23
- [59] A. Banerjee, G. Bhattacharyya, and T. S. Ray, “Improving Fine-tuning in Composite Higgs Models,” [arXiv:1703.08011 \[hep-ph\]](#). 23
- [60] D. Croon, V. Sanz, and E. R. M. Tarrant, “Reheating with a composite Higgs boson,” *Phys. Rev.* **D94** (2016) no. 4, 045010, [arXiv:1507.04653 \[hep-ph\]](#). 23
- [61] J. R. Espinosa, B. Gripaios, T. Konstandin, and F. Riva, “Electroweak Baryogenesis in Non-minimal Composite Higgs Models,” *JCAP* **1201** (2012) 012, [arXiv:1110.2876 \[hep-ph\]](#). 23
- [62] G. C. Branco, P. M. Ferreira, L. Lavoura, M. N. Rebelo, M. Sher, and J. P. Silva, “Theory and phenomenology of two-Higgs-doublet models,” *Phys. Rept.* **516** (2012) 1–102, [arXiv:1106.0034 \[hep-ph\]](#). 24
- [63] **ATLAS** Collaboration, M. Aaboud *et al.*, “Evidence for the associated production of the Higgs boson and a top quark pair with the ATLAS detector,” [arXiv:1712.08891 \[hep-ex\]](#). 25
- [64] **ATLAS** Collaboration, T. A. collaboration, “Measurements of Higgs boson properties in the diphoton decay channel with  $36.1 \text{ fb}^{-1}$   $pp$  collision data at the center-of-mass energy of 13 TeV with the ATLAS detector,”. 25
- [65] **CMS** Collaboration, C. Collaboration, “Measurements of properties of the Higgs boson in the diphoton decay channel with the full 2016 data set,”. 25
- [66] **CMS** Collaboration, C. Collaboration, “Observation of the SM scalar boson decaying to a pair of  $\tau$  leptons with the CMS experiment at the LHC,”. 25
- [67] **CMS** Collaboration, C. Collaboration, “Higgs to WW measurements with  $15.2 \text{ fb}^{-1}$  of 13 TeV proton-proton collisions,”. 25
- [68] **ATLAS** Collaboration, M. Aaboud *et al.*, “Measurement of the Higgs boson coupling properties in the  $H \rightarrow ZZ^* \rightarrow 4\ell$  decay channel at  $\sqrt{s} = 13 \text{ TeV}$  with the ATLAS detector,” [arXiv:1712.02304 \[hep-ex\]](#). 25

- [69] **CMS** Collaboration, C. Collaboration, “Measurements of properties of the Higgs boson decaying into four leptons in pp collisions at  $\sqrt{s} = 13$  TeV,”. 25
- [70] **ATLAS** Collaboration, M. Aaboud *et al.*, “Evidence for the  $H \rightarrow b\bar{b}$  decay with the ATLAS detector,” *JHEP* **12** (2017) 024, [arXiv:1708.03299](#) [[hep-ex](#)]. 25
- [71] **CMS** Collaboration, A. M. Sirunyan *et al.*, “Evidence for the Higgs boson decay to a bottom quark-antiquark pair,” [arXiv:1709.07497](#) [[hep-ex](#)]. 25
- [72] **ATLAS** Collaboration, T. A. collaboration, “Measurements of the Higgs boson production cross section via Vector Boson Fusion and associated  $WH$  production in the  $WW^* \rightarrow \ell\nu\ell\nu$  decay mode with the ATLAS detector at  $\sqrt{s} = 13$  TeV,”. 25
- [73] M. Gillioz, R. Grober, C. Grojean, M. Muhlleitner, and E. Salvioni, “Higgs Low-Energy Theorem (and its corrections) in Composite Models,” *JHEP* **10** (2012) 004, [arXiv:1206.7120](#) [[hep-ph](#)]. 25
- [74] **ATLAS** Collaboration, T. A. collaboration, “Search for Higgs boson production via weak boson fusion and decaying to  $b\bar{b}$  in association with a high-energy photon in the ATLAS detector,”. 25
- [75] **CMS** Collaboration, C. Collaboration, “Search for Higgs boson production in association with top quarks in multilepton final states at  $\sqrt{s} = 13$  TeV,”. 25
- [76] R. Lewis, C. Pica, and F. Sannino, “Light Asymmetric Dark Matter on the Lattice: SU(2) Technicolor with Two Fundamental Flavors,” *Phys. Rev.* **D85** (2012) 014504, [arXiv:1109.3513](#) [[hep-ph](#)]. 26, 46
- [77] T. Appelquist *et al.*, “Strongly interacting dynamics and the search for new physics at the LHC,” *Phys. Rev.* **D93** (2016) no. 11, 114514, [arXiv:1601.04027](#) [[hep-lat](#)]. 26
- [78] G. 't Hooft, “A Planar Diagram Theory for Strong Interactions,” *Nucl. Phys.* **B72** (1974) 461. 26, 49, 58
- [79] E. Witten, “Baryons in the  $1/n$  Expansion,” *Nucl. Phys.* **B160** (1979) 57–115. 26, 49, 58, 95
- [80] P. Batra and Z. Chacko, “A Composite Twin Higgs Model,” *Phys. Rev.* **D79** (2009) 095012, [arXiv:0811.0394](#) [[hep-ph](#)]. 27

- [81] C. Csaki, M. Geller, O. Telem, and A. Weiler, “The Flavor of the Composite Twin Higgs,” *JHEP* **09** (2016) 146, [arXiv:1512.03427 \[hep-ph\]](#). 27
- [82] A. H. Guth, “Inflationary universe: A possible solution to the horizon and flatness problems,” *Phys. Rev. D* **23** (Jan, 1981) 347–356.  
<https://link.aps.org/doi/10.1103/PhysRevD.23.347>. 30
- [83] **Planck** Collaboration, P. A. R. Ade *et al.*, “Planck 2015 results. XX. Constraints on inflation,” *Astron. Astrophys.* **594** (2016) A20, [arXiv:1502.02114 \[astro-ph.CO\]](#). 30, 42, 43, 46
- [84] D. H. Lyth, “What would we learn by detecting a gravitational wave signal in the cosmic microwave background anisotropy?,” *Phys. Rev. Lett.* **78** (1997) 1861–1863, [arXiv:hep-ph/9606387 \[hep-ph\]](#). 30
- [85] D. H. Lyth, “BICEP2, the curvature perturbation and supersymmetry,” *JCAP* **1411** (2014) no. 11, 003, [arXiv:1403.7323 \[hep-ph\]](#). 30
- [86] K. Freese, J. A. Frieman, and A. V. Olinto, “Natural inflation with pseudo - Nambu-Goldstone bosons,” *Phys. Rev. Lett.* **65** (1990) 3233–3236. 30
- [87] F. C. Adams, J. R. Bond, K. Freese, J. A. Frieman, and A. V. Olinto, “Natural inflation: Particle physics models, power law spectra for large scale structure, and constraints from COBE,” *Phys. Rev.* **D47** (1993) 426–455, [arXiv:hep-ph/9207245 \[hep-ph\]](#). 30
- [88] D. Croon and V. Sanz, “Saving Natural Inflation,” *JCAP* **1502** (2015) no. 02, 008, [arXiv:1411.7809 \[hep-ph\]](#). 30, 31
- [89] P. Svrcek and E. Witten, “Axions In String Theory,” *JHEP* **06** (2006) 051, [arXiv:hep-th/0605206 \[hep-th\]](#). 30
- [90] R. Kallosh, A. D. Linde, D. A. Linde, and L. Susskind, “Gravity and global symmetries,” *Phys. Rev.* **D52** (1995) 912–935, [arXiv:hep-th/9502069 \[hep-th\]](#). 30
- [91] M. Montero, A. M. Uranga, and I. Valenzuela, “Transplanckian axions!?, ” *JHEP* **08** (2015) 032, [arXiv:1503.03886 \[hep-th\]](#). 30
- [92] Z. Kenton and S. Thomas, “D-brane Potentials in the Warped Resolved Conifold and Natural Inflation,” *JHEP* **02** (2015) 127, [arXiv:1409.1221 \[hep-th\]](#). 30

- [93] N. Arkani-Hamed, H.-C. Cheng, P. Creminelli, and L. Randall, “Extra natural inflation,” *Phys. Rev. Lett.* **90** (2003) 221302, [arXiv:hep-th/0301218 \[hep-th\]](#). 31
- [94] A. D. Linde, “Hybrid inflation,” *Phys. Rev.* **D49** (1994) 748–754, [arXiv:astro-ph/9307002 \[astro-ph\]](#). 31
- [95] J. E. Kim, H. P. Nilles, and M. Peloso, “Completing natural inflation,” *JCAP* **0501** (2005) 005, [arXiv:hep-ph/0409138 \[hep-ph\]](#). 31
- [96] S. Dimopoulos, S. Kachru, J. McGreevy, and J. G. Wacker, “N-flation,” *JCAP* **0808** (2008) 003, [arXiv:hep-th/0507205 \[hep-th\]](#). 31
- [97] A. R. Liddle, A. Mazumdar, and F. E. Schunck, “Assisted inflation,” *Phys. Rev.* **D58** (1998) 061301, [arXiv:astro-ph/9804177 \[astro-ph\]](#). 31
- [98] E. J. Copeland, A. Mazumdar, and N. J. Nunes, “Generalized assisted inflation,” *Phys. Rev.* **D60** (1999) 083506, [arXiv:astro-ph/9904309 \[astro-ph\]](#). 31
- [99] E. Silverstein and A. Westphal, “Monodromy in the CMB: Gravity Waves and String Inflation,” *Phys. Rev.* **D78** (2008) 106003, [arXiv:0803.3085 \[hep-th\]](#). 31
- [100] N. Arkani-Hamed, H.-C. Cheng, P. Creminelli, and L. Randall, “Pseudonatural inflation,” *JCAP* **0307** (2003) 003, [arXiv:hep-th/0302034 \[hep-th\]](#). 31
- [101] C. Csaki, N. Kaloper, J. Serra, and J. Terning, “Inflation from Broken Scale Invariance,” *Phys. Rev. Lett.* **113** (2014) 161302, [arXiv:1406.5192 \[hep-th\]](#). 31
- [102] R. Contino, Y. Nomura, and A. Pomarol, “Higgs as a holographic pseudoGoldstone boson,” *Nucl. Phys.* **B671** (2003) 148–174, [arXiv:hep-ph/0306259 \[hep-ph\]](#). 31
- [103] G. von Gersdorff, E. Pontón, and R. Rosenfeld, “The Dynamical Composite Higgs,” *JHEP* **06** (2015) 119, [arXiv:1502.07340 \[hep-ph\]](#). 32, 58, 99
- [104] A. Pomarol and F. Riva, “The Composite Higgs and Light Resonance Connection,” *JHEP* **08** (2012) 135, [arXiv:1205.6434 \[hep-ph\]](#). 37
- [105] J. R. Ellis, K. Enqvist, D. V. Nanopoulos, and F. Zwirner, “Observables in Low-Energy Superstring Models,” *Mod. Phys. Lett.* **A1** (1986) 57. 43
- [106] R. Barbieri and G. F. Giudice, “Upper Bounds on Supersymmetric Particle Masses,” *Nucl. Phys.* **B306** (1988) 63–76. 43

- [107] J. R. Espinosa, C. Grojean, V. Sanz, and M. Trott, “NSUSY fits,” *JHEP* **12** (2012) 077, [arXiv:1207.7355 \[hep-ph\]](#). 44
- [108] J. Gasser and A. Zepeda, “Approaching the Chiral Limit in QCD,” *Nucl. Phys.* **B174** (1980) 445. 44
- [109] J. Gasser and H. Leutwyler, “Chiral Perturbation Theory to One Loop,” *Annals Phys.* **158** (1984) 142. 44
- [110] J. Gasser and H. Leutwyler, “Chiral Perturbation Theory: Expansions in the Mass of the Strange Quark,” *Nucl. Phys.* **B250** (1985) 465–516. 44
- [111] D. Baumann, D. Green, H. Lee, and R. A. Porto, “Signs of Analyticity in Single-Field Inflation,” *Phys. Rev.* **D93** (2016) no. 2, 023523, [arXiv:1502.07304 \[hep-th\]](#). 45
- [112] B. Bellazzini, L. Martucci, and R. Torre, “Symmetries, Sum Rules and Constraints on Effective Field Theories,” *JHEP* **09** (2014) 100, [arXiv:1405.2960 \[hep-th\]](#). 45
- [113] A. V. Manohar and V. Mateu, “Dispersion Relation Bounds for  $\pi\pi$  Scattering,” *Phys. Rev.* **D77** (2008) 094019, [arXiv:0801.3222 \[hep-ph\]](#). 45
- [114] V. Mateu, “Universal Bounds for  $SU(3)$  Low Energy Constants,” *Phys. Rev.* **D77** (2008) 094020, [arXiv:0801.3627 \[hep-ph\]](#). 45
- [115] A. Filipuzzi, J. Portoles, and P. Ruiz-Femenia, “Zeros of the  $W_L Z_L \rightarrow W_L Z_L$  Amplitude: Where Vector Resonances Stand,” *JHEP* **08** (2012) 080, [arXiv:1205.4682 \[hep-ph\]](#). 45
- [116] J. J. Sanz-Cillero, D.-L. Yao, and H.-Q. Zheng, “Positivity constraints on the low-energy constants of the chiral pion-nucleon Lagrangian,” *Eur. Phys. J.* **C74** (2014) 2763, [arXiv:1312.0664 \[hep-ph\]](#). 45
- [117] G. Ecker, J. Gasser, A. Pich, and E. de Rafael, “The Role of Resonances in Chiral Perturbation Theory,” *Nucl. Phys.* **B321** (1989) 311–342. 46
- [118] G. Ecker, J. Gasser, H. Leutwyler, A. Pich, and E. de Rafael, “Chiral Lagrangians for Massive Spin 1 Fields,” *Phys. Lett.* **B223** (1989) 425–432. 46
- [119] D. Baumann and D. Green, “Equilateral Non-Gaussianity and New Physics on the Horizon,” *JCAP* **1109** (2011) 014, [arXiv:1102.5343 \[hep-th\]](#). 47

- [120] D. Baumann, D. Green, and R. A. Porto, “B-modes and the Nature of Inflation,” *JCAP* **1501** (2015) no. 01, 016, [arXiv:1407.2621 \[hep-th\]](#). 47
- [121] G. ’t Hooft, “A Two-Dimensional Model for Mesons,” *Nucl. Phys.* **B75** (1974) 461–470. 49
- [122] S. Weinberg, “Precise relations between the spectra of vector and axial vector mesons,” *Phys. Rev. Lett.* **18** (1967) 507–509. 50
- [123] M. Knecht and E. de Rafael, “Patterns of spontaneous chiral symmetry breaking in the large  $N(c)$  limit of QCD - like theories,” *Phys. Lett.* **B424** (1998) 335–342, [arXiv:hep-ph/9712457 \[hep-ph\]](#). 50
- [124] A. Martin and V. Sanz, “Mass-Matching in Higgsless,” *JHEP* **01** (2010) 075, [arXiv:0907.3931 \[hep-ph\]](#). 51
- [125] J. Hirn, A. Martin, and V. Sanz, “Describing viable technicolor scenarios,” *Phys. Rev.* **D78** (2008) 075026, [arXiv:0807.2465 \[hep-ph\]](#). 51
- [126] J. Hirn, A. Martin, and V. Sanz, “Benchmarks for new strong interactions at the LHC,” *JHEP* **05** (2008) 084, [arXiv:0712.3783 \[hep-ph\]](#). 51
- [127] G. Cacciapaglia, C. Csaki, C. Grojean, and J. Terning, “Curing the Ills of Higgsless models: The S parameter and unitarity,” *Phys. Rev.* **D71** (2005) 035015, [arXiv:hep-ph/0409126 \[hep-ph\]](#). 51
- [128] K. Agashe, C. Csaki, C. Grojean, and M. Reece, “The S-parameter in holographic technicolor models,” *JHEP* **12** (2007) 003, [arXiv:0704.1821 \[hep-ph\]](#). 51
- [129] J. Hirn and V. Sanz, “A Negative S parameter from holographic technicolor,” *Phys. Rev. Lett.* **97** (2006) 121803, [arXiv:hep-ph/0606086 \[hep-ph\]](#). 51
- [130] J. Hirn and V. Sanz, “The Fifth dimension as an analogue computer for strong interactions at the LHC,” *JHEP* **03** (2007) 100, [arXiv:hep-ph/0612239 \[hep-ph\]](#). 51
- [131] N. Kaloper, A. Lawrence, and L. Sorbo, “An Ignoble Approach to Large Field Inflation,” *JCAP* **1103** (2011) 023, [arXiv:1101.0026 \[hep-th\]](#). 51
- [132] X. Calmet and V. Sanz, “Excursion into Quantum Gravity via Inflation,” *Phys. Lett.* **B737** (2014) 12–15, [arXiv:1403.5100 \[hep-ph\]](#). 51

- [133] W. H. Kinney and K. T. Mahanthappa, “Inflation at low scales: General analysis and a detailed model,” *Phys. Rev.* **D53** (1996) 5455–5467, [arXiv:hep-ph/9512241](#) [[hep-ph](#)]. 52
- [134] Y. Grossman and M. Neubert, “Neutrino masses and mixings in nonfactorizable geometry,” *Phys. Lett.* **B474** (2000) 361–371, [arXiv:hep-ph/9912408](#) [[hep-ph](#)]. 58
- [135] T. Gherghetta and A. Pomarol, “Bulk fields and supersymmetry in a slice of AdS,” *Nucl. Phys.* **B586** (2000) 141–162, [arXiv:hep-ph/0003129](#) [[hep-ph](#)]. 58
- [136] O. Matsedonskyi, G. Panico, and A. Wulzer, “Light Top Partners for a Light Composite Higgs,” *JHEP* **01** (2013) 164, [arXiv:1204.6333](#) [[hep-ph](#)]. 58, 67, 68, 95, 101
- [137] E. E. Jenkins, “Large N(c) baryons,” *Ann. Rev. Nucl. Part. Sci.* **48** (1998) 81–119, [arXiv:hep-ph/9803349](#) [[hep-ph](#)]. 58
- [138] G. Panico, M. Redi, A. Tesi, and A. Wulzer, “On the Tuning and the Mass of the Composite Higgs,” *JHEP* **03** (2013) 051, [arXiv:1210.7114](#) [[hep-ph](#)]. 58
- [139] K. Agashe and R. Contino, “The Minimal composite Higgs model and electroweak precision tests,” *Nucl. Phys.* **B742** (2006) 59–85, [arXiv:hep-ph/0510164](#) [[hep-ph](#)]. 58
- [140] G. Panico and A. Wulzer, “The Composite Nambu-Goldstone Higgs,” *Lect. Notes Phys.* **913** (2016) pp.1–316, [arXiv:1506.01961](#) [[hep-ph](#)]. 58
- [141] H.-C. Cheng, B. A. Dobrescu, and J. Gu, “Higgs Mass from Compositeness at a Multi-TeV Scale,” *JHEP* **08** (2014) 095, [arXiv:1311.5928](#) [[hep-ph](#)]. 58
- [142] J. Barnard, T. Gherghetta, T. S. Ray, and A. Spray, “The Unnatural Composite Higgs,” *JHEP* **01** (2015) 067, [arXiv:1409.7391](#) [[hep-ph](#)]. 58
- [143] H.-C. Cheng and J. Gu, “Top seesaw with a custodial symmetry, and the 126 GeV Higgs,” *JHEP* **10** (2014) 002, [arXiv:1406.6689](#) [[hep-ph](#)]. 58
- [144] S. De Curtis, M. Redi, and E. Vigiani, “Non Minimal Terms in Composite Higgs Models and in QCD,” *JHEP* **06** (2014) 071, [arXiv:1403.3116](#) [[hep-ph](#)]. 58
- [145] D. Marzocca, M. Serone, and J. Shu, “General Composite Higgs Models,” *JHEP* **08** (2012) 013, [arXiv:1205.0770](#) [[hep-ph](#)]. 58



- [146] C. Niehoff, P. Stangl, and D. M. Straub, “Direct and indirect signals of natural composite Higgs models,” *JHEP* **01** (2016) 119, [arXiv:1508.00569 \[hep-ph\]](#). 58
- [147] J. Barnard and M. White, “Collider constraints on tuning in composite Higgs models,” *JHEP* **10** (2015) 072, [arXiv:1507.02332 \[hep-ph\]](#). 58
- [148] G. Cacciapaglia, H. Cai, A. Deandrea, T. Flacke, S. J. Lee, and A. Parolini, “Composite scalars at the LHC: the Higgs, the Sextet and the Octet,” *JHEP* **11** (2015) 201, [arXiv:1507.02283 \[hep-ph\]](#). 58
- [149] A. Carmona and M. Chala, “Composite Dark Sectors,” *JHEP* **06** (2015) 105, [arXiv:1504.00332 \[hep-ph\]](#). 58
- [150] A. Thamm, R. Torre, and A. Wulzer, “Future tests of Higgs compositeness: direct vs indirect,” *JHEP* **07** (2015) 100, [arXiv:1502.01701 \[hep-ph\]](#). 58
- [151] S. Kanemura, K. Kaneta, N. Machida, and T. Shindou, “New resonance scale and fingerprint identification in minimal composite Higgs models,” *Phys. Rev.* **D91** (2015) 115016, [arXiv:1410.8413 \[hep-ph\]](#). 58
- [152] N. Vignaroli, “New W’ signals at the LHC,” *Phys. Rev.* **D89** (2014) no. 9, 095027, [arXiv:1404.5558 \[hep-ph\]](#). 58
- [153] M. Redi, V. Sanz, M. de Vries, and A. Weiler, “Strong Signatures of Right-Handed Compositeness,” *JHEP* **08** (2013) 008, [arXiv:1305.3818](#). 58
- [154] K. Agashe, A. Azatov, T. Han, Y. Li, Z.-G. Si, and L. Zhu, “LHC Signals for Coset Electroweak Gauge Bosons in Warped/Composite PGB Higgs Models,” *Phys. Rev.* **D81** (2010) 096002, [arXiv:0911.0059 \[hep-ph\]](#). 58
- [155] A. Carmona, M. Chala, and J. Santiago, “New Higgs Production Mechanism in Composite Higgs Models,” *JHEP* **07** (2012) 049, [arXiv:1205.2378 \[hep-ph\]](#). 58
- [156] M. Redi and A. Tesi, “Implications of a Light Higgs in Composite Models,” *JHEP* **10** (2012) 166, [arXiv:1205.0232 \[hep-ph\]](#). 58
- [157] R. Contino, D. Marzocca, D. Pappadopulo, and R. Rattazzi, “On the effect of resonances in composite Higgs phenomenology,” *JHEP* **10** (2011) 081, [arXiv:1109.1570 \[hep-ph\]](#). 58

- [158] M. Backovic, T. Flacke, J. H. Kim, and S. J. Lee, “Search Strategies for TeV Scale Fermionic Top Partners with Charge  $2/3$ ,” *JHEP* **04** (2016) 014, [arXiv:1507.06568 \[hep-ph\]](#). 58
- [159] A. Buckley, C. Englert, J. Ferrando, D. J. Miller, L. Moore, M. Russell, and C. D. White, “Global fit of top quark effective theory to data,” *Phys. Rev.* **D92** (2015) no. 9, 091501, [arXiv:1506.08845 \[hep-ph\]](#). 58
- [160] J. Serra, “Beyond the Minimal Top Partner Decay,” *JHEP* **09** (2015) 176, [arXiv:1506.05110 \[hep-ph\]](#). 58
- [161] S. Dawson and E. Furlan, “Yukawa Corrections to Higgs Production in Top Partner Models,” *Phys. Rev.* **D89** (2014) no. 1, 015012, [arXiv:1310.7593 \[hep-ph\]](#). 58
- [162] C. Grojean, O. Matsedonskyi, and G. Panico, “Light top partners and precision physics,” *JHEP* **10** (2013) 160, [arXiv:1306.4655 \[hep-ph\]](#). 58
- [163] M. Backović, T. Flacke, J. H. Kim, and S. J. Lee, “Boosted Event Topologies from TeV Scale Light Quark Composite Partners,” *JHEP* **04** (2015) 082, [arXiv:1410.8131 \[hep-ph\]](#). 58
- [164] E. Drueke, J. Nutter, R. Schwienhorst, N. Vignaroli, D. G. E. Walker, and J.-H. Yu, “Single Top Production as a Probe of Heavy Resonances,” *Phys. Rev.* **D91** (2015) no. 5, 054020, [arXiv:1409.7607 \[hep-ph\]](#). 58
- [165] J. Reuter and M. Tonini, “Top Partner Discovery in the  $T \rightarrow tZ$  channel at the LHC,” *JHEP* **01** (2015) 088, [arXiv:1409.6962 \[hep-ph\]](#). 58
- [166] O. Matsedonskyi, G. Panico, and A. Wulzer, “On the Interpretation of Top Partners Searches,” *JHEP* **12** (2014) 097, [arXiv:1409.0100 \[hep-ph\]](#). 58
- [167] B. Gripaios, T. Müller, M. A. Parker, and D. Sutherland, “Search Strategies for Top Partners in Composite Higgs models,” *JHEP* **08** (2014) 171, [arXiv:1406.5957 \[hep-ph\]](#). 58
- [168] C.-Y. Chen, S. Dawson, and I. M. Lewis, “Top Partners and Higgs Boson Production,” *Phys. Rev.* **D90** (2014) no. 3, 035016, [arXiv:1406.3349 \[hep-ph\]](#). 58
- [169] O. Matsedonskyi, G. Panico, and A. Wulzer, “Light Top Partners for a Light Composite Higgs,” *JHEP* **01** (2013) 164, [arXiv:1204.6333 \[hep-ph\]](#). 58

- [170] A. Banfi, A. Martin, and V. Sanz, “Probing top-partners in Higgs+jets,” *JHEP* **08** (2014) 053, [arXiv:1308.4771 \[hep-ph\]](#). 58
- [171] J. A. Aguilar-Saavedra, “Identifying top partners at LHC,” *JHEP* **11** (2009) 030, [arXiv:0907.3155 \[hep-ph\]](#). 58
- [172] J. A. Aguilar-Saavedra, R. Benbrik, S. Heinemeyer, and M. Pérez-Victoria, “Handbook of vectorlike quarks: Mixing and single production,” *Phys. Rev.* **D88** (2013) no. 9, 094010, [arXiv:1306.0572 \[hep-ph\]](#). 58
- [173] H. D. Kim, “Electroweak symmetry breaking from SUSY breaking with bosonic see-saw mechanism,” *Phys. Rev.* **D72** (2005) 055015, [arXiv:hep-ph/0501059 \[hep-ph\]](#). 58
- [174] R. Contino, L. Da Rold, and A. Pomarol, “Light custodians in natural composite Higgs models,” *Phys. Rev.* **D75** (2007) 055014, [arXiv:hep-ph/0612048 \[hep-ph\]](#). 59, 95
- [175] N. Craig, F. D’Eramo, P. Draper, S. Thomas, and H. Zhang, “The Hunt for the Rest of the Higgs Bosons,” *JHEP* **06** (2015) 137, [arXiv:1504.04630 \[hep-ph\]](#). 71
- [176] M. Carena, H. E. Haber, I. Low, N. R. Shah, and C. E. M. Wagner, “Alignment limit of the NMSSM Higgs sector,” *Phys. Rev.* **D93** (2016) no. 3, 035013, [arXiv:1510.09137 \[hep-ph\]](#). 71
- [177] G. Cacciapaglia, H. Cai, T. Flacke, S. J. Lee, A. Parolini, and H. Serôdio, “Anarchic Yukawas and top partial compositeness: the flavour of a successful marriage,” *JHEP* **06** (2015) 085, [arXiv:1501.03818 \[hep-ph\]](#). 71
- [178] B. Gripaios, M. Nardecchia, and S. A. Renner, “Composite leptoquarks and anomalies in  $B$ -meson decays,” *JHEP* **05** (2015) 006, [arXiv:1412.1791 \[hep-ph\]](#). 71
- [179] M. Redi, “Composite MFV and Beyond,” *Eur. Phys. J.* **C72** (2012) 2030, [arXiv:1203.4220 \[hep-ph\]](#). 71
- [180] C. Delaunay, C. Grojean, and G. Perez, “Modified Higgs Physics from Composite Light Flavors,” *JHEP* **09** (2013) 090, [arXiv:1303.5701 \[hep-ph\]](#). 71
- [181] M. Redi and A. Weiler, “Flavor and CP Invariant Composite Higgs Models,” *JHEP* **11** (2011) 108, [arXiv:1106.6357 \[hep-ph\]](#). 71

- [182] M. Drees and X. Tata, “Signals for heavy exotics at hadron colliders and supercolliders,” *Phys. Lett.* **B252** (1990) 695–702. 75
- [183] J. L. Hewett, B. Lillie, M. Masip, and T. G. Rizzo, “Signatures of long-lived gluinos in split supersymmetry,” *JHEP* **09** (2004) 070, [arXiv:hep-ph/0408248](#) [hep-ph]. 75
- [184] A. Arvanitaki, S. Dimopoulos, A. Pierce, S. Rajendran, and J. G. Wacker, “Stopping gluinos,” *Phys. Rev.* **D76** (2007) 055007, [arXiv:hep-ph/0506242](#) [hep-ph]. 75
- [185] M. Cirelli, N. Fornengo, and A. Strumia, “Minimal dark matter,” *Nucl. Phys.* **B753** (2006) 178–194, [arXiv:hep-ph/0512090](#) [hep-ph]. 75
- [186] M. J. Strassler and K. M. Zurek, “Echoes of a hidden valley at hadron colliders,” *Phys. Lett.* **B651** (2007) 374–379, [arXiv:hep-ph/0604261](#) [hep-ph]. 75
- [187] **ATLAS** Collaboration, S. Mehlhase, “Search for Stable Massive Particles with the ATLAS detector in proton-proton collisions at  $\sqrt{s}=13$  TeV,” *PoS ICHEP2016* (2017) 1119. 75
- [188] **CMS** Collaboration, V. Khachatryan *et al.*, “Search for long-lived charged particles in proton-proton collisions at  $\sqrt{s}=13$  TeV,” *Phys. Rev.* **D94** (2016) no. 11, 112004, [arXiv:1609.08382](#) [hep-ex]. 75
- [189] **ATLAS Collaboration** Collaboration, “Search for long-lived neutral particles decaying in the hadronic calorimeter of ATLAS at  $\sqrt{s}=13$  TeV in  $3.2\text{ fb}^{-1}$  of data,” Tech. Rep. ATLAS-CONF-2016-103, CERN, Geneva, Sep, 2016. <http://cds.cern.ch/record/2219571>. 75
- [190] **CMS** Collaboration, V. Khachatryan *et al.*, “Search for Long-Lived Neutral Particles Decaying to Quark-Antiquark Pairs in Proton-Proton Collisions at  $\sqrt{s}=8$  TeV,” *Phys. Rev.* **D91** (2015) no. 1, 012007, [arXiv:1411.6530](#) [hep-ex]. 75
- [191] **ATLAS Collaboration** Collaboration, “Search for long-lived charginos based on a disappearing-track signature in  $pp$  collisions at  $\sqrt{s}=13$  TeV with the ATLAS detector,” Tech. Rep. ATLAS-CONF-2017-017, CERN, Geneva, Apr, 2017. <https://cds.cern.ch/record/2258131>. 75

- [192] **CMS** Collaboration, V. Khachatryan *et al.*, “Search for disappearing tracks in proton-proton collisions at  $\sqrt{s} = 8$  TeV,” *JHEP* **01** (2015) 096, [arXiv:1411.6006 \[hep-ex\]](#). 75
- [193] J. Kang and M. A. Luty, “Macroscopic Strings and ‘Quirks’ at Colliders,” *JHEP* **11** (2009) 065, [arXiv:0805.4642 \[hep-ph\]](#). 75, 78, 81
- [194] G. D. Kribs, T. S. Roy, J. Terning, and K. M. Zurek, “Quirky Composite Dark Matter,” *Phys. Rev.* **D81** (2010) 095001, [arXiv:0909.2034 \[hep-ph\]](#). 75
- [195] H. Cai, H.-C. Cheng, and J. Terning, “A Quirky Little Higgs Model,” *JHEP* **05** (2009) 045, [arXiv:0812.0843 \[hep-ph\]](#). 75
- [196] G. Burdman, Z. Chacko, H.-S. Goh, and R. Harnik, “Folded supersymmetry and the LEP paradox,” *JHEP* **02** (2007) 009, [arXiv:hep-ph/0609152 \[hep-ph\]](#). 75
- [197] G. Burdman, Z. Chacko, H.-S. Goh, R. Harnik, and C. A. Krenke, “The Quirky Collider Signals of Folded Supersymmetry,” *Phys. Rev.* **D78** (2008) 075028, [arXiv:0805.4667 \[hep-ph\]](#). 75
- [198] N. Craig, A. Katz, M. Strassler, and R. Sundrum, “Naturalness in the Dark at the LHC,” *JHEP* **07** (2015) 105, [arXiv:1501.05310 \[hep-ph\]](#). 75, 105
- [199] N. Craig, S. Knapen, P. Longhi, and M. Strassler, “The Vector-like Twin Higgs,” *JHEP* **07** (2016) 002, [arXiv:1601.07181 \[hep-ph\]](#). 75, 105
- [200] **D0** Collaboration, V. M. Abazov *et al.*, “Search for New Fermions (‘Quirks’) at the Fermilab Tevatron Collider,” *Phys. Rev. Lett.* **105** (2010) 211803, [arXiv:1008.3547 \[hep-ex\]](#). 76
- [201] M. Farina and M. Low, “Constraining Quirky Tracks with Conventional Searches,” [arXiv:1703.00912 \[hep-ph\]](#). 76, 82, 89
- [202] T. Sjostrand and *et. al.*, “An Introduction to PYTHIA 8.2,” *Comput. Phys. Commun.* **191** (2015) 159–177, [arXiv:1410.3012 \[hep-ph\]](#). 77, 81
- [203] M. Luscher and P. Weisz, “Quark confinement and the bosonic string,” *JHEP* **07** (2002) 049, [arXiv:hep-lat/0207003 \[hep-lat\]](#). 77
- [204] C. J. Morningstar and M. J. Peardon, “The Glueball spectrum from an anisotropic lattice study,” *Phys. Rev.* **D60** (1999) 034509, [arXiv:hep-lat/9901004 \[hep-lat\]](#). 81

- [205] J. Alwall and et. al., “The automated computation of tree-level and next-to-leading order differential cross sections, and their matching to parton shower simulations,” *JHEP* **07** (2014) 079, [arXiv:1405.0301 \[hep-ph\]](#). 81
- [206] M. Buchkremer, G. Cacciapaglia, A. Deandrea, and L. Panizzi, “Model Independent Framework for Searches of Top Partners,” *Nucl. Phys.* **B876** (2013) 376–417, [arXiv:1305.4172 \[hep-ph\]](#). 81
- [207] T. Sjostrand, S. Mrenna, and P. Z. Skands, “PYTHIA 6.4 Physics and Manual,” *JHEP* **05** (2006) 026, [arXiv:hep-ph/0603175 \[hep-ph\]](#). 81
- [208] “The Expected Performance of the ATLAS Inner Detector,” Tech. Rep. ATL-PHYS-PUB-2009-002. ATL-COM-PHYS-2008-105, CERN, Geneva, Aug, 2008. <https://cds.cern.ch/record/1118445>. 81
- [209] **ATLAS** Collaboration, G. Aad *et al.*, “Performance of the ATLAS muon trigger in pp collisions at  $\sqrt{s} = 8$  TeV,” *Eur. Phys. J.* **C75** (2015) 120, [arXiv:1408.3179 \[hep-ex\]](#). 82
- [210] “2015 start-up trigger menu and initial performance assessment of the ATLAS trigger using Run-2 data,” Tech. Rep. ATL-DAQ-PUB-2016-001, CERN, Geneva, Mar, 2016. <https://cds.cern.ch/record/2136007>. 82
- [211] M. Shochet, L. Tompkins, V. Cavaliere, P. Giannetti, A. Annovi, and G. Volpi, “Fast TracKer (FTK) Technical Design Report,” Tech. Rep. CERN-LHCC-2013-007. ATLAS-TDR-021, Jun, 2013. <https://cds.cern.ch/record/1552953>. ATLAS Fast Tracker Technical Design Report. 82
- [212] D. Contardo, M. Klute, J. Mans, L. Silvestris, and J. Butler, “Technical Proposal for the Phase-II Upgrade of the CMS Detector,” Tech. Rep. CERN-LHCC-2015-010. LHCC-P-008. CMS-TDR-15-02, Geneva, Jun, 2015. <https://cds.cern.ch/record/2020886>. Upgrade Project Leader Deputies: Lucia Silvestris (INFN-Bari), Jeremy Mans (University of Minnesota) Additional contacts: [Lucia.Silvestris@cern.ch](mailto:Lucia.Silvestris@cern.ch), [Jeremy.Mans@cern.ch](mailto:Jeremy.Mans@cern.ch). 82
- [213] Y. Gershtein, “CMS Hardware Track Trigger: New Opportunities for Long-Lived Particle Searches at the HL-LHC,” [arXiv:1705.04321 \[hep-ph\]](#). 82

- [214] “Early Inner Detector Tracking Performance in the 2015 data at  $\sqrt{s} = 13$  TeV,” Tech. Rep. ATL-PHYS-PUB-2015-051, CERN, Geneva, Dec, 2015.  
<http://cds.cern.ch/record/2110140>. 86
- [215] S. Knapen, S. Pagan Griso, M. Papucci, and D. J. Robinson, “Triggering Soft Bombs at the LHC,” [arXiv:1612.00850 \[hep-ph\]](#). 86
- [216] **Particle Data Group** Collaboration, C. Patrignani *et al.*, “Review of Particle Physics,” *Chin. Phys.* **C40** (2016) no. 10, 100001. 87, 91
- [217] M. Farina and M. Low. Private communication. 90
- [218] M. Golterman and Y. Shamir, “Effective potential in ultraviolet completions for composite Higgs models,” [arXiv:1707.06033 \[hep-ph\]](#). 93
- [219] G. F. Giudice, C. Grojean, A. Pomarol, and R. Rattazzi, “The Strongly-Interacting Light Higgs,” *JHEP* **06** (2007) 045, [arXiv:hep-ph/0703164 \[hep-ph\]](#). 95, 100
- [220] D. Liu, A. Pomarol, R. Rattazzi, and F. Riva, “Patterns of Strong Coupling for LHC Searches,” *JHEP* **11** (2016) 141, [arXiv:1603.03064 \[hep-ph\]](#). 95
- [221] J. Galloway, J. A. Evans, M. A. Luty, and R. A. Tacchi, “Minimal Conformal Technicolor and Precision Electroweak Tests,” *JHEP* **10** (2010) 086, [arXiv:1001.1361 \[hep-ph\]](#). 97
- [222] A. Hietanen, R. Lewis, C. Pica, and F. Sannino, “Fundamental Composite Higgs Dynamics on the Lattice: SU(2) with Two Flavors,” *JHEP* **07** (2014) 116, [arXiv:1404.2794 \[hep-lat\]](#). 97
- [223] N. Arkani-Hamed, A. G. Cohen, E. Katz, and A. E. Nelson, “The Littlest Higgs,” *JHEP* **07** (2002) 034, [arXiv:hep-ph/0206021 \[hep-ph\]](#). 99
- [224] L. Vecchi, “The Natural Composite Higgs,” [arXiv:1304.4579 \[hep-ph\]](#). 99
- [225] A. Pomarol and J. Serra, “Top Quark Compositeness: Feasibility and Implications,” *Phys. Rev.* **D78** (2008) 074026, [arXiv:0806.3247 \[hep-ph\]](#). 100
- [226] B. Batell and T. Gherghetta, “Warped phenomenology in the holographic basis,” *Phys. Rev.* **D77** (2008) 045002, [arXiv:0710.1838 \[hep-ph\]](#). 100